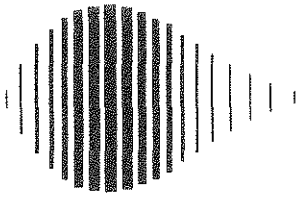

NATIONAL CENTER FOR EARTHQUAKE
ENGINEERING RESEARCH
State University of New York at Buffalo

A STUDY OF RADIATION DAMPING AND SOIL-STRUCTURE INTERACTION EFFECTS IN THE CENTRIFUGE

by

Karen Weissman

Supervised by: Jean H. Prevost

Department of Civil Engineering and Operations Research
Princeton University
Princeton, New Jersey 08544

Technical Report NCEER-88-0013

May 24, 1988

This research was conducted at Princeton University and was partially supported by the National Science Foundation under Grant No. ECE 86-07591.

NOTICE

This report was prepared by Princeton University as a result of research sponsored by the National Center for Earthquake Engineering Research (NCEER). Neither NCEER, associates of NCEER, its sponsors, Princeton University, or any person acting on their behalf:

a. makes any warranty, express or implied, with respect to the use of any information, apparatus, method, or process disclosed in this report or that such use may not infringe upon privately owned rights; or

b. assumes any liabilities of whatsoever kind with respect to the use of, or for damages resulting from the use of, any information, apparatus, method or process disclosed in this report.

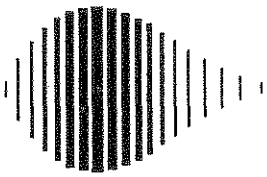

A STUDY OF RADIATION DAMPING AND SOIL-STRUCTURE INTERACTION EFFECTS IN THE CENTRIFUGE

by

Karen Weissman[1]

Supervised by Jean H. Prevost[2]

May 24, 1988

Technical Report NCEER-88-0013

NCEER Contract Numbers 86-2032 and 87-1312

NSF Master Contract Number ECE 86-07591

1 Graduate Student, Department of Civil Engineering and Operations Research, Princeton University

2 Professor, Department of Civil Engineering and Operations Research, Princeton University

NATIONAL CENTER FOR EARTHQUAKE ENGINEERING RESEARCH
State University of New York at Buffalo
Red Jacket Quadrangle, Buffalo, NY 14261

PREFACE

The National Center for Earthquake Engineering Research (NCEER) is devoted to the expansion and dissemination of knowledge about earthquakes, the improvement of earthquake-resistant design, and the implementation of seismic hazard mitigation procedures to minimize loss of lives and property. The emphasis is on structures and lifelines that are found in zones of moderate to high seismicity throughout the United States.

NCEER's research is being carried out in an integrated and coordinated manner following a structured program. The current research program comprises four main areas:

- Existing and New Structures
- Secondary and Protective Systems
- Lifeline Systems
- Disaster Research and Planning

This technical report pertains to Program 1, Existing and New Structures, and more specifically to geotechnical studies, soils and soil-structure interaction.

The long term goal of research in Existing and New Structures is to develop seismic hazard mitigation procedures through rational probabilistic risk assessment for damage or collapse of structures, mainly existing buildings, in regions of moderate to high seismicity. The work relies on improved definitions of seismicity and site response, experimental and analytical evaluations of systems response, and more accurate assessment of risk factors. This technology will be incorporated in expert systems tools and improved code formats for existing and new structures. Methods of retrofit will also be developed. When this work is completed, it should be possible to characterize and quantify societal impact of seismic risk in various geographical regions and large municipalities. Toward this goal, the program has been divided into five components, as shown in the figure below:

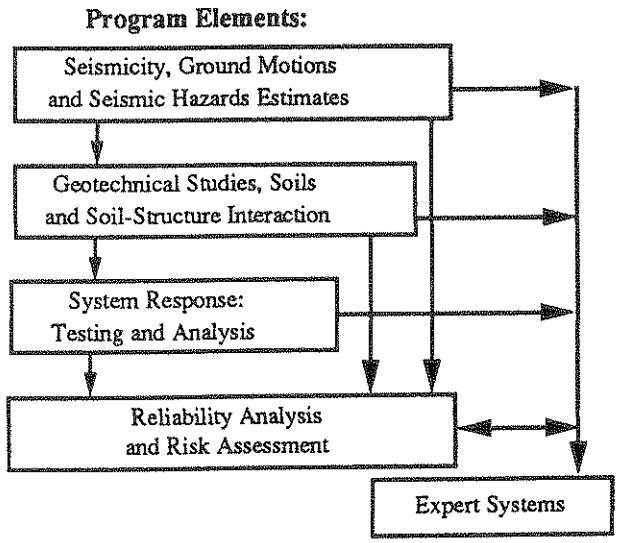

Tasks:

Earthquake Hazards Estimates,
Ground Motion Estimates,
New Ground Motion Instrumentation,
Earthquake & Ground Motion Data Base.

Site Response Estimates,
Large Ground Deformation Estimates,
Soil-Structure Interaction.

Typical Structures and Critical Structural Components:
Testing and Analysis;
Modern Analytical Tools.

Vulnerability Analysis,
Reliability Analysis,
Risk Assessment,
Code Upgrading.

Architectural and Structural Design,
Evaluation of Existing Buildings.

Geotechnical studies, soils and soil-structure interaction constitute one of the important areas of research in Existing and New Structures. Current research activities include the following:

1. Development of linear and nonlinear site response estimates.
2. Development of liquefaction and large ground deformation estimates.
3. Investigation of soil-structure interaction phenomena.
4. Development of computational methods.
5. Incorporation of local soil effects and soil-structure interaction into existing codes.

The ultimate goal of projects in this area is to develop methods of engineering estimation of large soil deformations, site response, and the effect that the interaction of structures and soils have on the resistance of structures against earthquakes.

This study represents one step in a sequence of investigations carried out by NCEER in the field of soil-structure interaction. The authors present the results of an extensive series of centrifuge tests on radiation damping and soil-structure interaction. The data generated from these tests will be applied to existing and newly developed analytical models.

ABSTRACT

This report describes the experimental phase of an ongoing research project on dynamic soil-structure interaction effects. The details of an in depth experimental study of radiation damping and dynamic soil-structure interaction performed in the Princeton University Geotechnical Centrifuge are reported. The experiments were designed to create a data pool which demonstrates the influence of the frequencies of the structure, the foundation embedment and the foundation shape on radiation damping and soil-structure interaction effects for a structure on a finite layer of soil during an earthquake. A total of 37 test cases are examined which include structures with surface and embedded circular, square, rectangular and strip footings and a variety of natural frequencies. The results are presented in the form of plots and qualitative observations. At this stage, the emphasis is on the experiments themselves and the wealth of data they provide. The data is meant for use in the validation of existing and newly developed analytical models. This work is currently in progress at Princeton University and will be reported subsequently.

TABLE OF CONTENTS

LIST OF TABLES

LIST OF ILLUSTRATIONS

SECTION 1

INTRODUCTION

This report contains the details of an in depth experimental study of radiation damping and dynamic soil-structure interaction performed in the Princeton University Geotechnical Centrifuge. The repeatability in the simulated earthquakes demonstrated in an earlier report [1] is exploited in order to examine the response of various types of structures to the same earthquake. The simulated earthquake is generated using the hammer-exciter plate method [1]. Standing waves which could occur due to the confinement of the model container are absorbed by lining the walls with Duxseal. This method of standing wave attenuation was developed by Coe [4] and Coe, Prevost and Scanlan [5] and its effectiveness was further demonstrated in centrifuge experiments performed by the authors [1].

As elastic theory dictates, if a structure is built on a shallow layer over bedrock, radiation damping does not occur unless the natural frequencies of the structure are greater than the fundamental frequency of the site. With this in mind, the experiments were designed to create a data pool which demonstrates the influence of

1. the frequencies of the structure
2. the foundation embedment, and
3. the foundation shape

on radiation damping and soil-structure interaction effects for a structure on a finite layer of soil during an earthquake. This report presents the results of the experiments in the form of plots and qualitative observations. The emphasis is on the experiments themselves and the wealth of data they provide. All the tests described herein were performed in a centrifuge at a centrifugal acceleration of 100g; thus the model is constructed to $1/100^{th}$ of the prototype scale. To emphasize that the model really represents a system that is 100 times larger, all measurements in this report are given in prototype scale unless otherwise indicated.

SECTION 2

EXPERIMENTAL SETUP

In all of the following experiments the model system consists of a single building-like structure on a horizontal soil stratum over "bedrock". The "bedrock" in the model is actually the exciter plate which provides the source of excitation. Previous experiments reported in Reference [1] have demonstrated that the same simulated earthquake can be repeatedly generated. Therefore, by keeping the soil depth constant the earthquake input to the structure can be kept constant in the following experiments. This way the responses of a variety of independently tested structures may be directly compared as they are subjected to the same earthquake (i.e. the same amplitudes and frequencies of shaking). The soil deposit is a 27.08ft layer of Monterey-0 sand. The horizontal accelerations at various points in the model soil deposit for the simulated earthquake are shown in Figure 2-1. This represents the free field response as the structure has not yet been added to the system.

Similar structures are used in all of the experiments. They consist of a rigid base supporting a stem and a top mass. All components are made out of brass and, in all cases, the base is massive with respect to the superstructure. To vary the natural frequency of the superstructure the top mass can be moved up and down along the stem. Figure 2-2 depicts the dimensions of the structures. The 16.40ft dimension of the base represents the diameter in the case of a circular footing and the width in the cases of square, rectangular and strip footings. In all cases, the superstructure remains the same (except for the position of the top mass along the stem).

Each structure can be viewed as having two translational degrees of freedom, one associated with the horizontal motion of the superstructure and the other associated with the horizontal motion of the base. In order to explore the dependence of radiation damping on the frequencies of the structure relative to the frequency of the soil layer, it is desirable to vary at least one of these two frequencies above and below

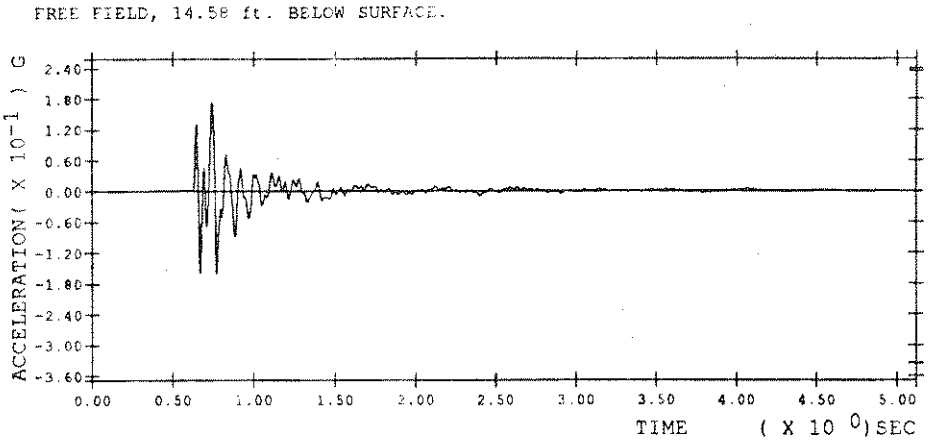

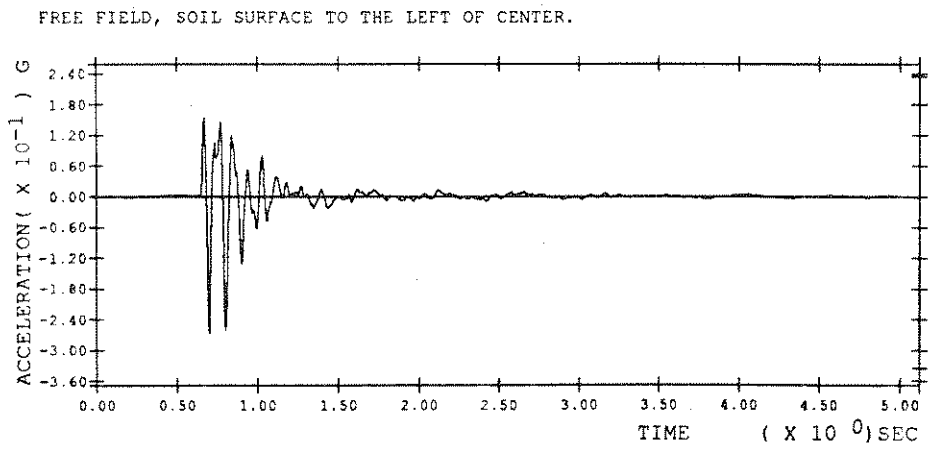

FIGURE 2-1: Horizontal Acceleration of Free Field Soil Deposit.

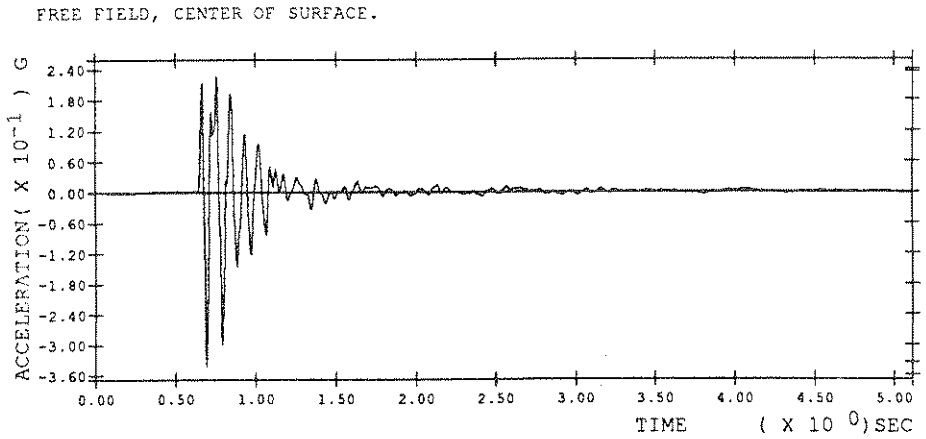

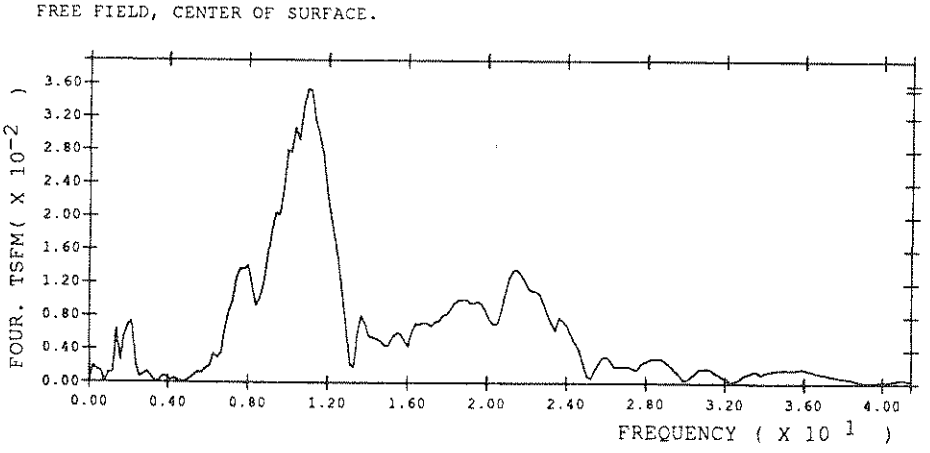

FIGURE 2-1: Horizontal Acceleration of Free Field Soil Deposit. (Cont'd)

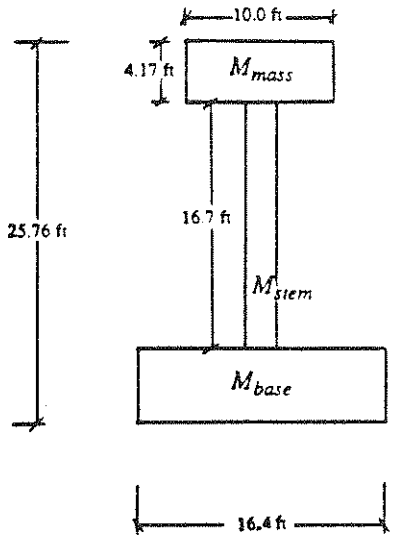

$$M_{base} = 1.71\times10^{4}\ \frac{lb}{ft/sec^2}$$

$$M_{mass} = 5.37\times10^{3}\ \frac{lb}{ft/sec^2}$$

$$M_{stem} = 9.33\times10^{2}\ \frac{lb}{ft/sec^2}$$

(scaled to prototype)

FIGURE 2-2: Dimensions of Structure.

the fundamental frequency of the soil layer (which remained constant). The structure is designed so that its fundamental frequency which is associated with the superstructure (henceforth denoted f_{str}) could be varied while the higher order frequency associated with the base (f_b) remains the same. It is, therefore, necessary to determine approximate values of f_{str} and f_{soil}. These values only need to be exact enough to provide, *a priori*, an appropriate range of values of f_{str} which span the value of f_{soil}. This is done as follows:

f_{str} - The fixed base natural frequency of the structure is determined experimentally from a measurement of the free vibration acceleration of the top mass while the base is clamped. A material damping ratio (ξ) is also estimated from this free vibration response

$$\xi = \frac{a_n - a_{n+m}}{2\pi m a_{n+m}} \times 100\%$$

where a_n and a_{n+m} are the amplitudes of the n^{th} and the $n+m^{th}$ cycles of acceleration respectively. Table 2-I shows the results of these fixed base experiments for a variety of positions of the top mass. Each of these configurations is used in at least one of the experiments to be described in the next three sections.

TABLE 2-I
FIXED BASE FREQUENCIES AND DAMPING RATIOS

HEIGHT OF TOP MASS (ft.)	f_{str} (Hz.)	ξ (% of critical)
18.75	1.95	0.37
12.50	2.98	0.32
9.90	3.12	0.80
9.38	4.05	0.53
7.81	4.69	0.24
6.25	5.27	0.36

f_{soil} - The cutoff frequency above which radiation damping will occur is determined by the fundamental frequency of the site in the horizontal direction. This is because the dynamic excitation provided by the exciter plate consists primarily of vertically incident shear waves and, since the

bottom-heavy structure is not inclined towards rocking, it can be assumed that the structure will respond to these shear waves predominantly in the swaying mode. This value of f_{str} is calculated form the formula

$$f_{soil} = \frac{V_s}{4d} = 4.90Hz$$

where V_s is the shear wave velocity in the soil at a depth equal to half the cross sectional dimension of the base of the structure (531ft/sec) and d equals the depth of the layer. A shear column model such as the one presented in Reference [3] would account for the variation of shear wave velocity with depth in the calculation, giving an average value of f_{str} for the stratum. However, the accuracy of this method is beyond the accuracy to which the shear modulus is known as a function of depth, so the extra effort involved in such a calculation is not worth while in this case. It should be noted that the rigid base is associated with a higher order structural frequency and should act almost independently of the fundamental mode regardless of the value of f_{str}. It is, therefore, not necessary to have an *a priori* estimate of f_b as the value does not change and is most likely greater than f_{soil}. Hence radiation damping is expected to occur at the base for all cases tested.

Uniaxial accelerometers are used to measure the response at various points in the system. Figure 2-3 shows the configuration of these transducers. There are horizontally oriented accelerometers placed at the soil surface, 14.5ft below the surface, the base of the structure and the mass of the structure. Vertically oriented accelerometers are placed on opposite ends of the base to detect rocking as well as vertical motion. The accelerometers in the soil are enclosed in cases to prevent erroneous readings due to the pressure of the sand. The output is recorded on a NORLAND 3001 digital processing oscilloscope and stored on the MicroVAX for future analysis.

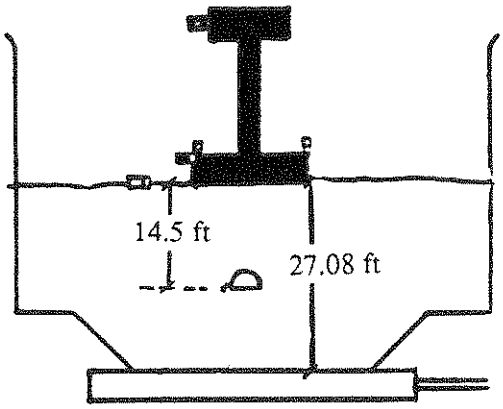

FIGURE 2-3: Accelerometer Configuration for Soil-Structure System.

Table 2-II is summary of the 37 tests cases studied.

TABLE 2-II
SUMMARY OF TEST CASES

FOOTING SHAPE	SURFACE/ EMBEDDED	FREQUENCY OF SUPERSTRUCTURE (Hz)	FIGURE
Circular	Surface	1.95	3-2
"	"	4.05	3-3
"	"	4.69	3-4
"	"	5.27	3-5
"	Embedded	1.95	4-1
"	"	2.98	4-2
"	"	3.12	4-3
"	"	4.69	4-4
"	"	5.27	4-5
Square	Surface	1.95	5-1
"	"	2.98	5-2
"	"	3.12	5-3
"	"	4.69	5-4
"	"	5.27	5-5
"	Embedded	1.95	5-6
"	"	2.98	5-7
"	"	3.12	5-8
"	"	4.69	5-9
"	"	5.27	5-10
Rectangular (L/W=2)	Surface	1.95	5-11
"	"	2.98	5-12
"	"	4.69	5-13
"	Embedded	1.95	5-14
"	"	2.98	5-15
"	"	4.69	5-16
Rectangular (L/W=4)	Surface	1.95	5-17
"	"	2.98	5-18
"	"	4.69	5-19
"	Embedded	1.95	5-20
"	"	2.98	5-21
"	"	4.69	5-22
Strip (L/W=8)	Surface	1.95	5-23
"	"	2.98	5-24
"	"	4.69	5-25
"	Embedded	1.95	5-26
"	"	2.98	5-27
"	"	4.69	5-28

The next three sections, in which the results of these tests are described, are organized as follows. First, the response of a structure with a surface footing is examined in detail, particularly for the influence of f_{str} and f_b on radiation damping and soil-structure interaction effects. Figure 2-4 shows a schematic diagram of a typical structure with a surface footing, where f_{str} is dependent on the height of the top mass above the base (h). Next, the response of a similar structure with an embedded footing is presented for comparison. Figure 2-5: shows a schematic diagram of a typical structure with an embedded footing. Lastly, responses of structures with surface and embedded foundations of various shapes are discussed.

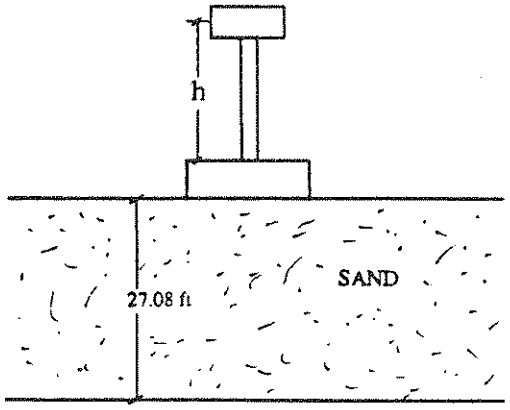

**FIGURE 2-4: Schematic of Structure with Surface Footing.
Frequency of Superstructure Varies with Height of Top Mass (h).**

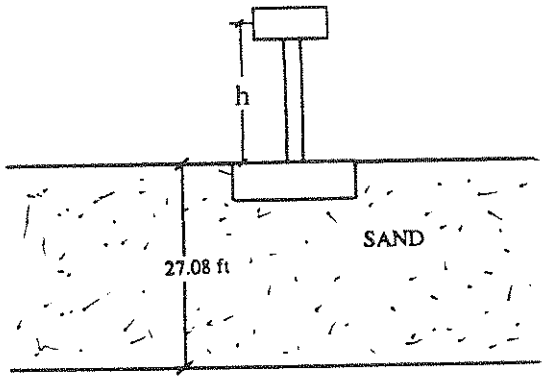

FIGURE 2-5: Schematic of Structure with Embedded Footing.

SECTION 3

STRUCTURE WITH A SURFACE FOOTING

In the first set of experiments, the structure with a circular base is placed on the surface of the soil deposit. The height of the mass is moved down or up to induce or inhibit radiation damping respectively. Four values of f_{str} were tested:

(a) $1.66\text{Hz} < f_{soil}$

(b) $4.05\text{Hz} < f_{soil}$

(c) $4.69\text{Hz} \approx f_{soil}$

(d) $5.27\text{Hz} > f_{soil}$.

Case (a) represents a situation where we anticipate no radiation damping. Case (d) represents a situation where radiation damping is expected to occur. Cases (b) and 4(c) fall in between these two extremes. In all cases, radiation damping is expected to occur at the base. Figures 3-1 through 3-5 show the accelerations recorded at various points in the soil-structure system along with their Fast Fourier Transforms. Many observations can be made from looking at this first set of results. First of all, it should be noted that the earthquake at 14.58 ft below the soil surface is similar for each case and, therefore, provides a consistent datum to which the structural response may be compared. Figure 3-1 shows the absolute acceleration of the top mass plotted with the earthquake recorded below the soil surface for cases (a) through (d). It can be seen from this comparison that in case (d) the response of the top mass dies out with the earthquake excitation while in case (a) the top mass is still accelerating after the earthquake has finished. This implies that for case (a) energy is trapped in the structure and not allowed to radiate away, thus radiation damping is small of nonexistent. Figures 3-1(b), (c) and (d) show that as f_{str} is increased above f_{soil} the amount of radiation damping increases. The concept derived from linear elastic theory that f_{soil} is a cut-off frequency perhaps suggests a more drastic jump between the occurrence and nonoccurrence of radiation damping than actually exists.

From Figures 3-2 through 3-5 it can also be seen that the response of the top mass to the strong motion part of the earthquake varies in frequency much more than amplitude. This motion is damped out within about the first second of the earthquake for all four values of f_{str}.

In contrast to the top mass, the horizontal motion of the base is very similar for all four frequency values and dies out with the input earthquake. The Fast Fourier Transforms of these signals indicate that the base is responding with a dominant frequency of about 7.82Hz which is above the fundamental frequency of the soil layer. Thus, the heavy base is essentially acting independently of the superstructure and radiation damping occurs for this degree of freedom regardless of the height of the top mass.

The vertical accelerations recorded at opposite ends of the base are also quite similar for all four values of f_{str}. The signals on the right and left side are out-of-phase indicating that some rocking does occur. However, the vertical accelerations die out with the earthquake indicating that rocking does not contribute to the trapped energy observed in the superstructure when $f_{str} > f_{soil}$. The amplitudes of the two vertical accelerations are slightly unequal indicating that some purely vertical motion exists as well.

Finally, in addition to these observations on the soil-structure system, an important conclusion can be drawn about the ability of the bounded model to represent a layer of infinite extent. The fact that radiation damping can be observed in the centrifuge model means that the Duxseal lining the containment walls is indeed preventing waves from being reflected back into the system. This fact is crucial to the study of soil-structure interaction in the centrifuge.

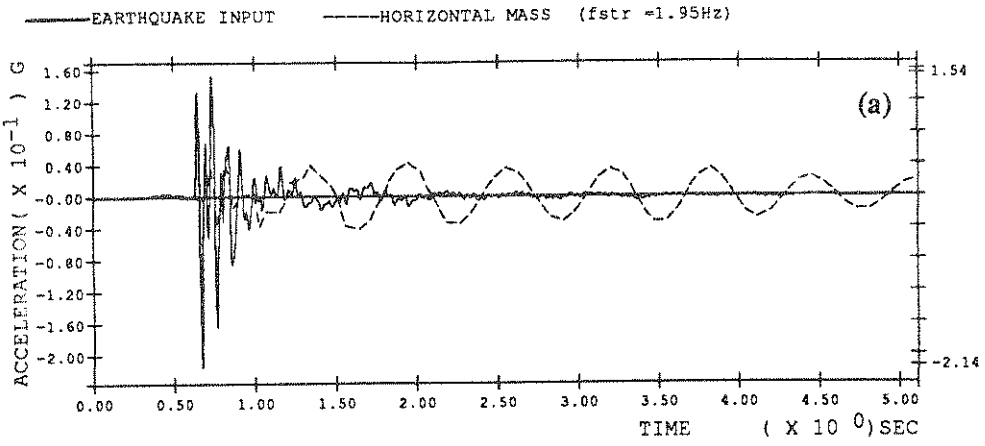

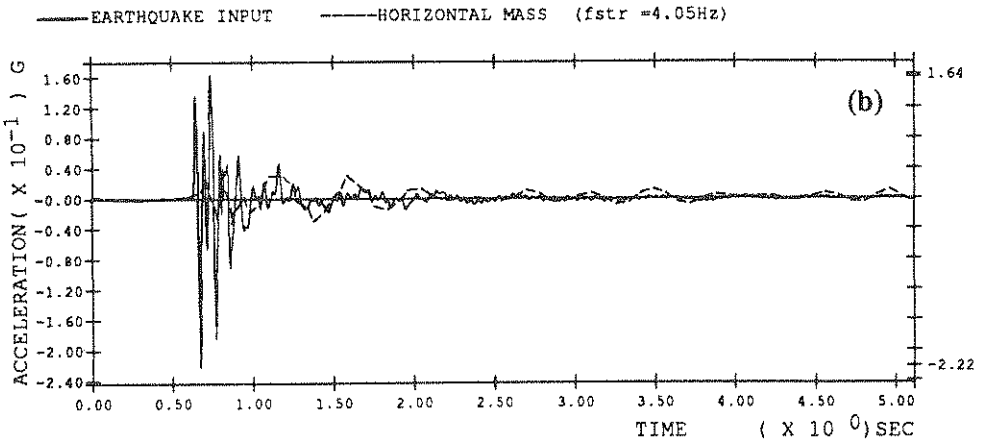

FIGURE 3-1: Horizontal Acceleration of Top Mass Plotted Against Earthquake Input For Structure with Surface Circular Footing.

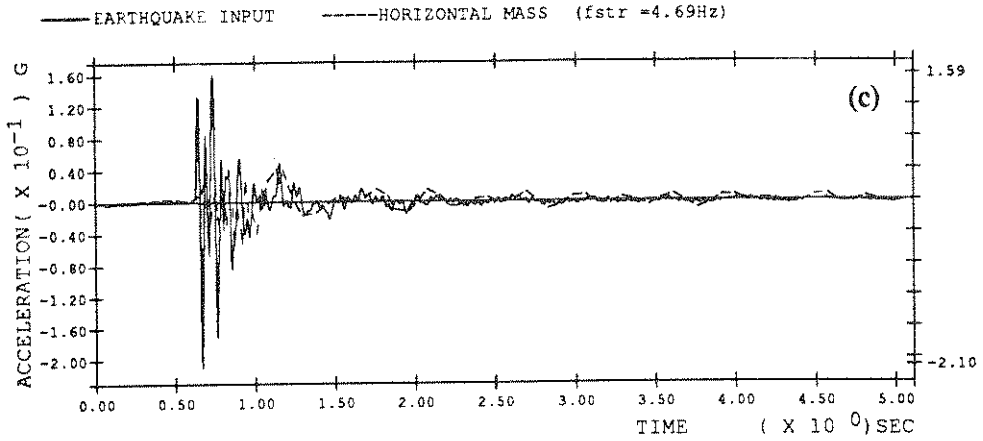

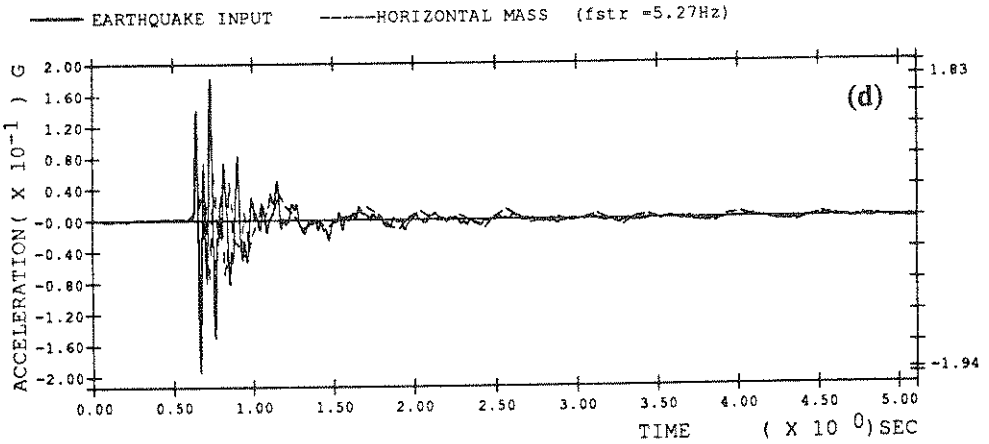

FIGURE 3-1: Horizontal Acceleration of Top Mass Plotted Against Earthquake Input For Structure with Surface Circular Footing. (Cont'd)

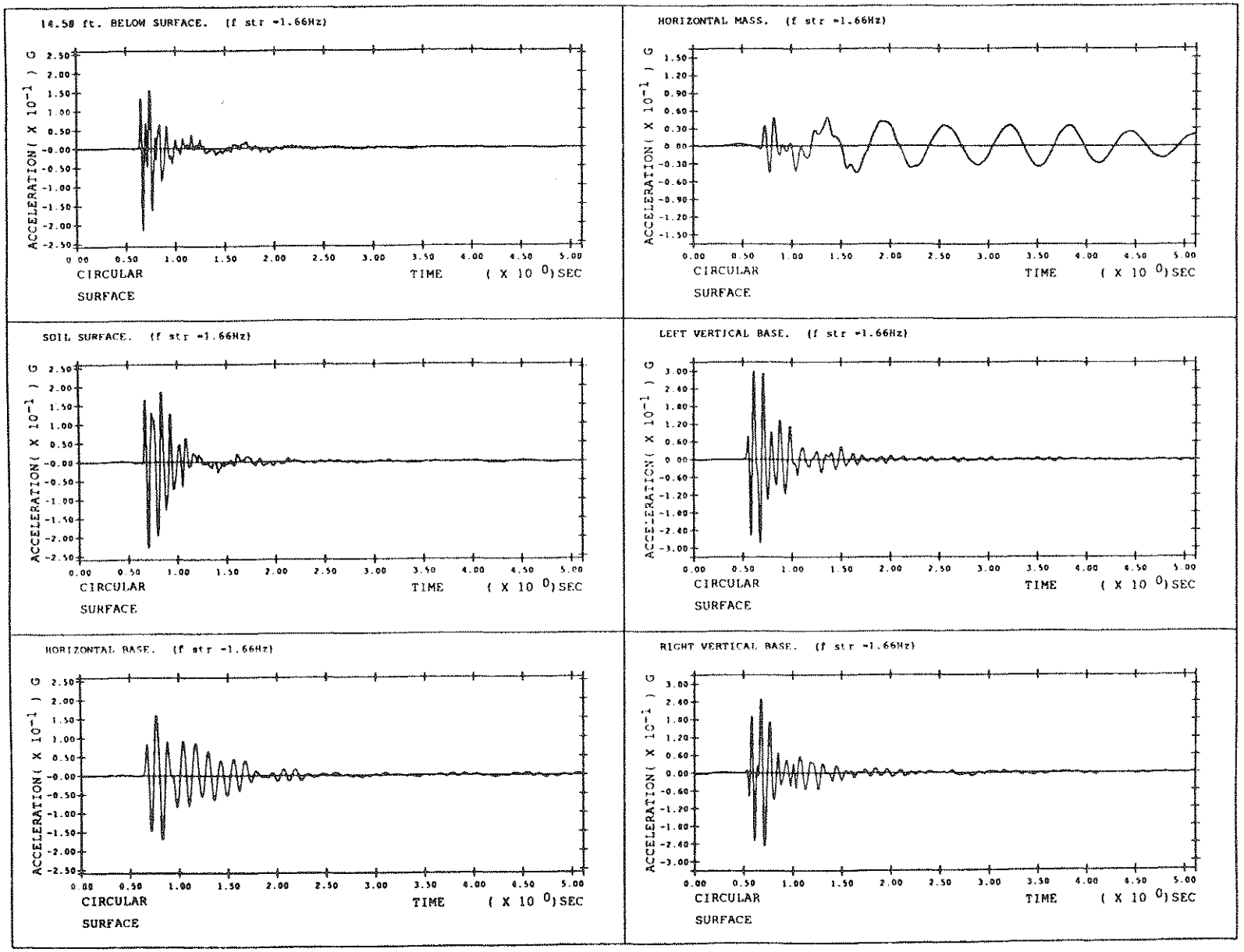

FIGURE 3-2 System with Surface Circular Footing (f_{str} = 1.66Hz)

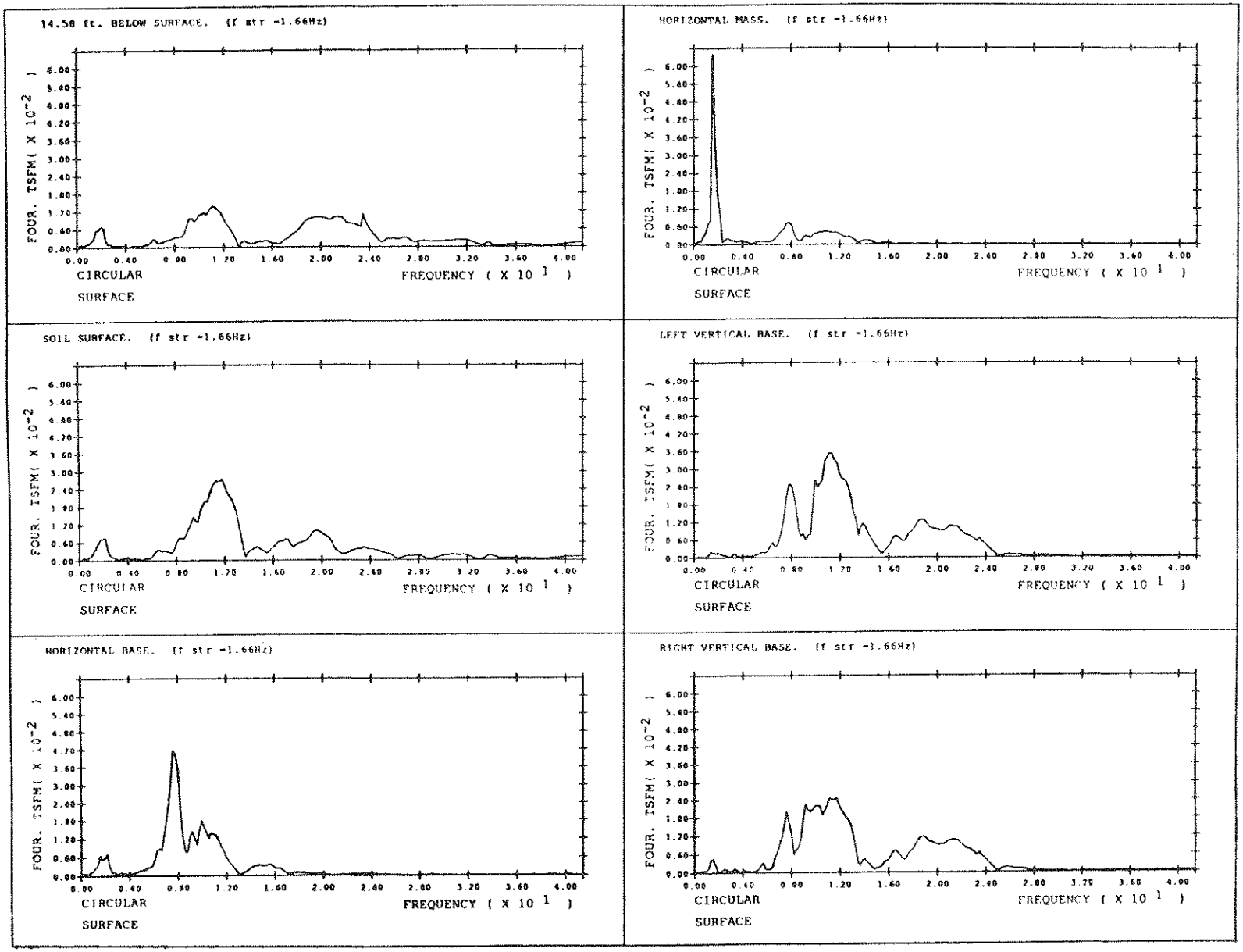

FIGURE 3-2 System with Surface Circular Footing (f_{str} = 1.66Hz) (cont'd)

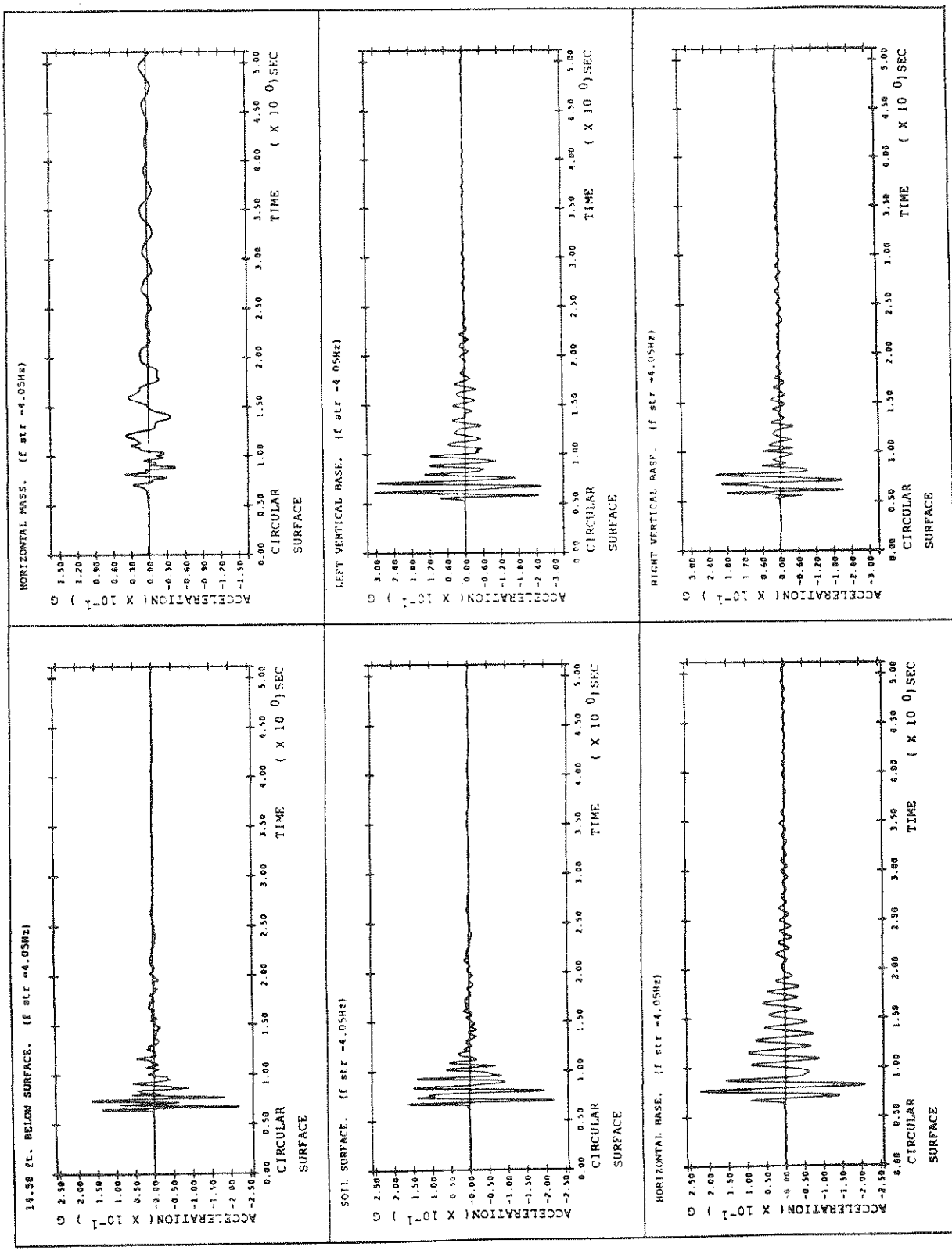

FIGURE 3-3 System with Surface Circular Footing (f_{str} = 4.05Hz)

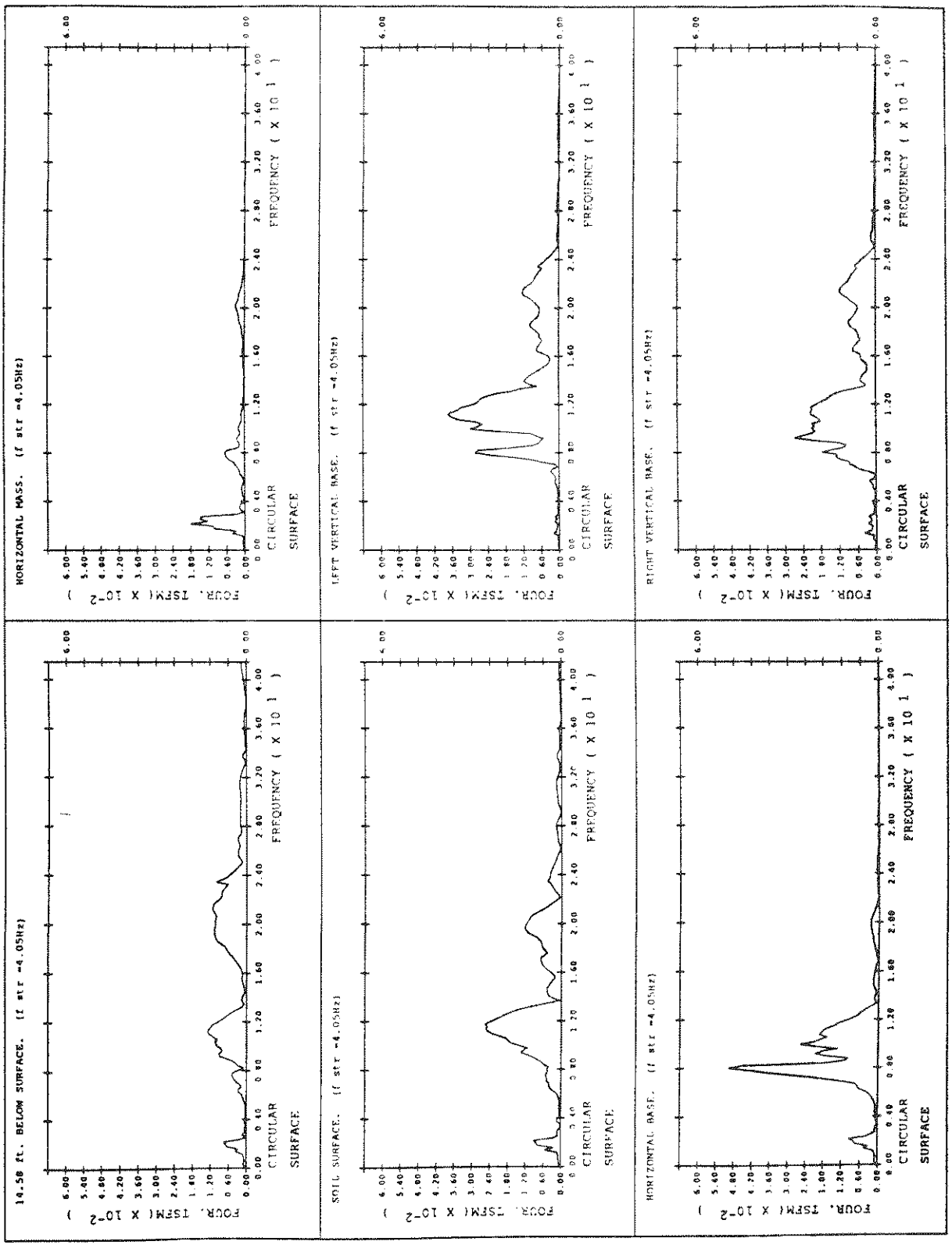

FIGURE 3-3 System with Surface Circular Footing (f_{str} = 4.05Hz) (cont'd)

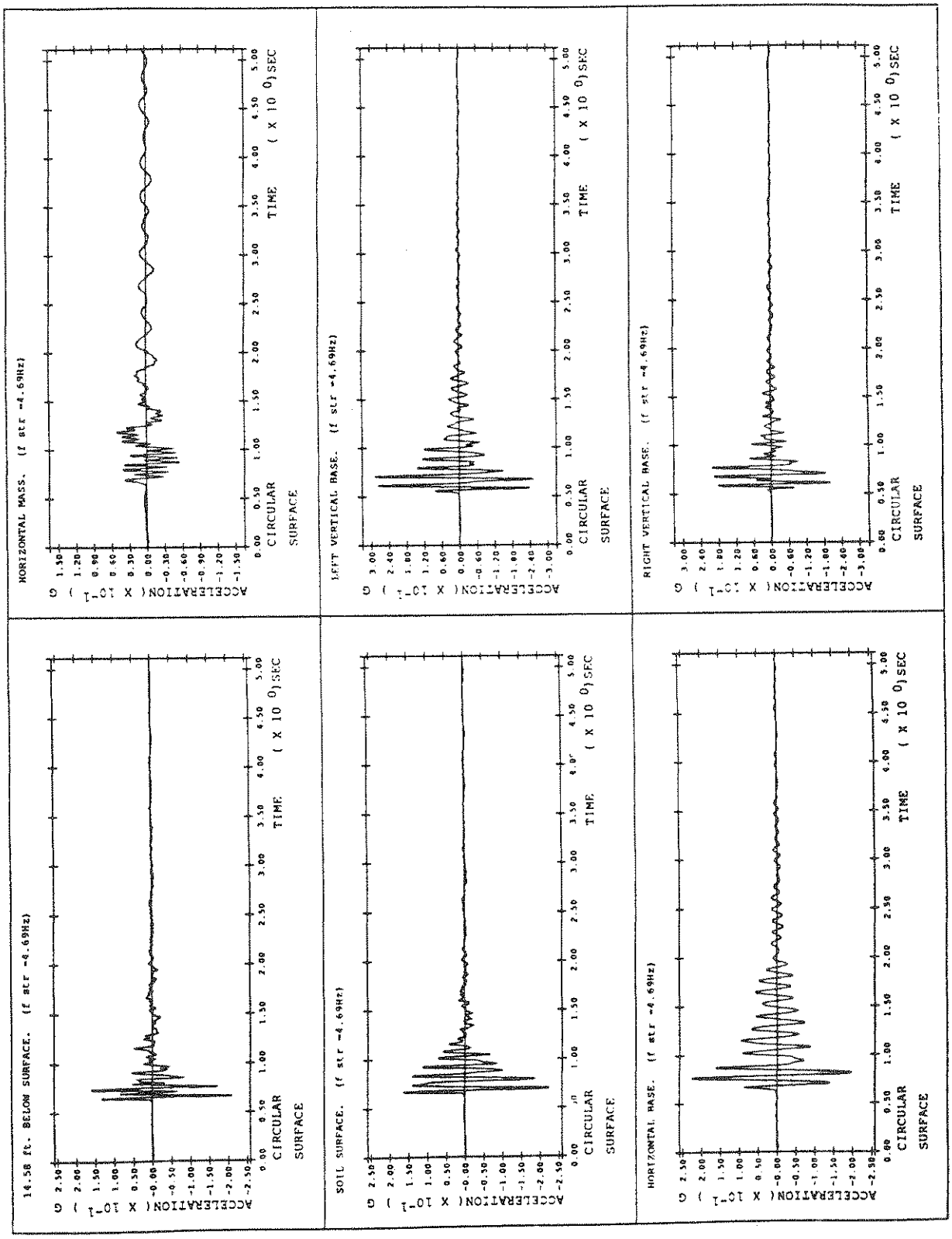

FIGURE 3-4 System with Surface Circular Footing (f_{str} = 4.69Hz)

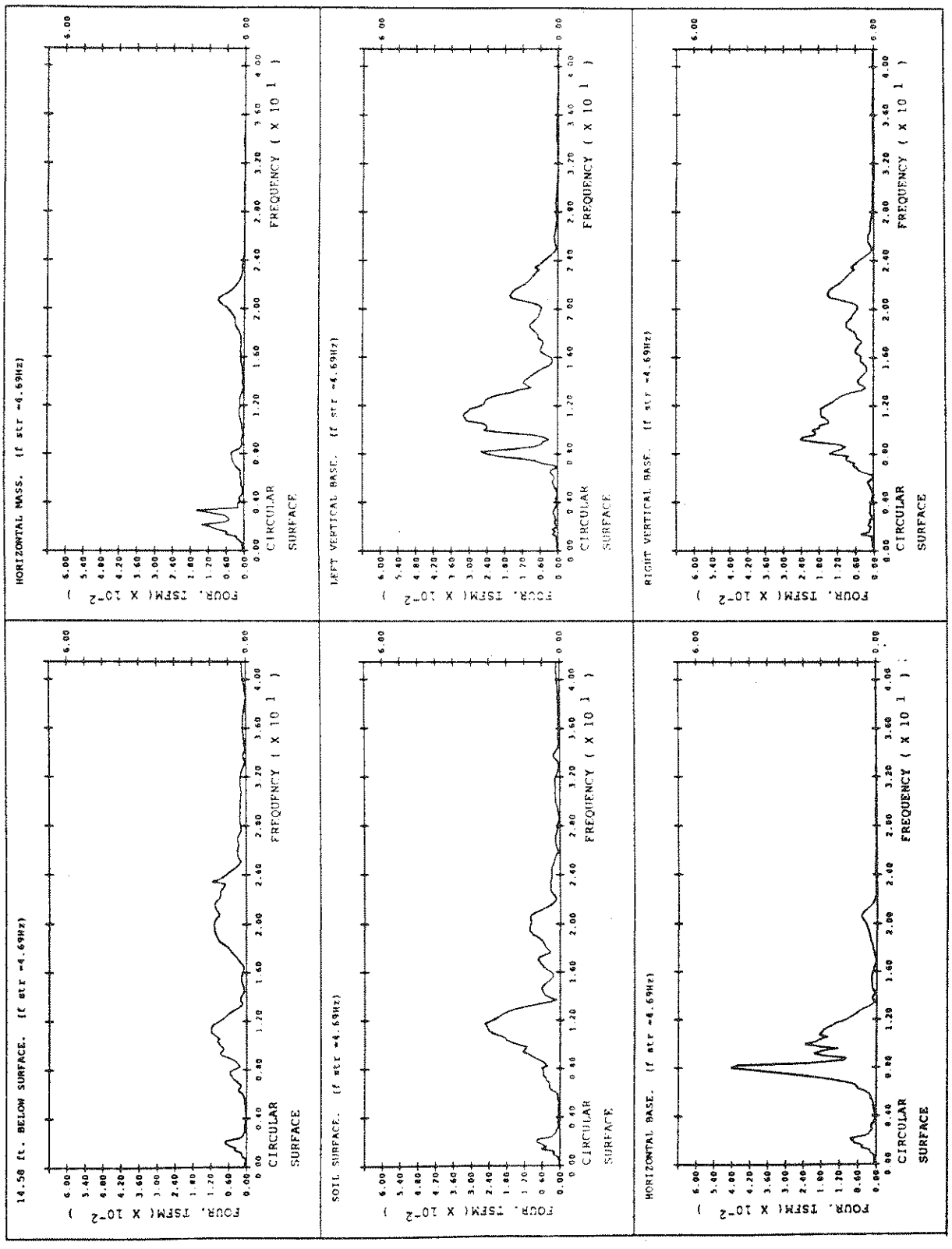

FIGURE 3-4 System with Surface Circular Footing (f_{str} = 4.69Hz)(cont'd)

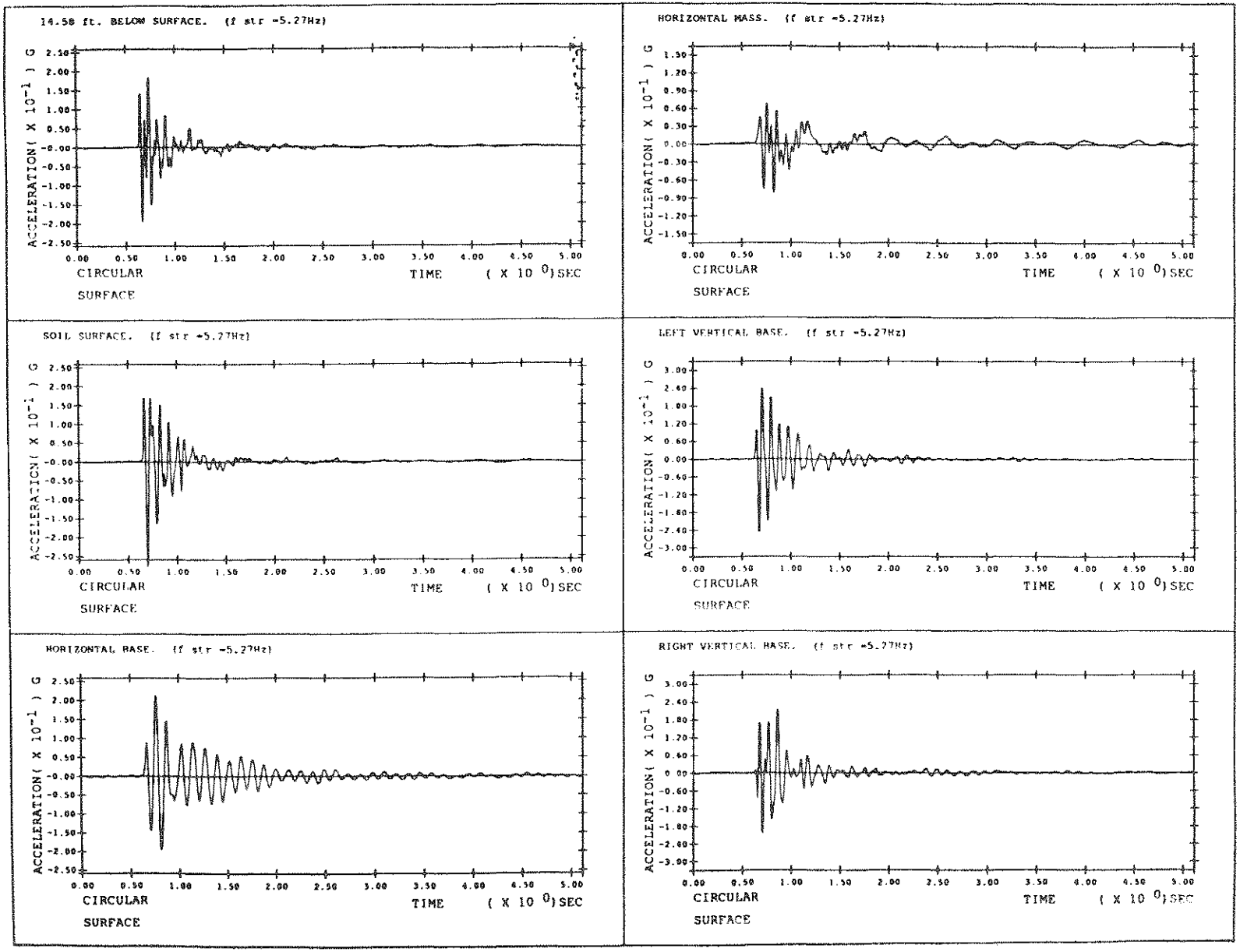

FIGURE 3-5 System with Surface Circular Footing (f_{str} = 5.27Hz)

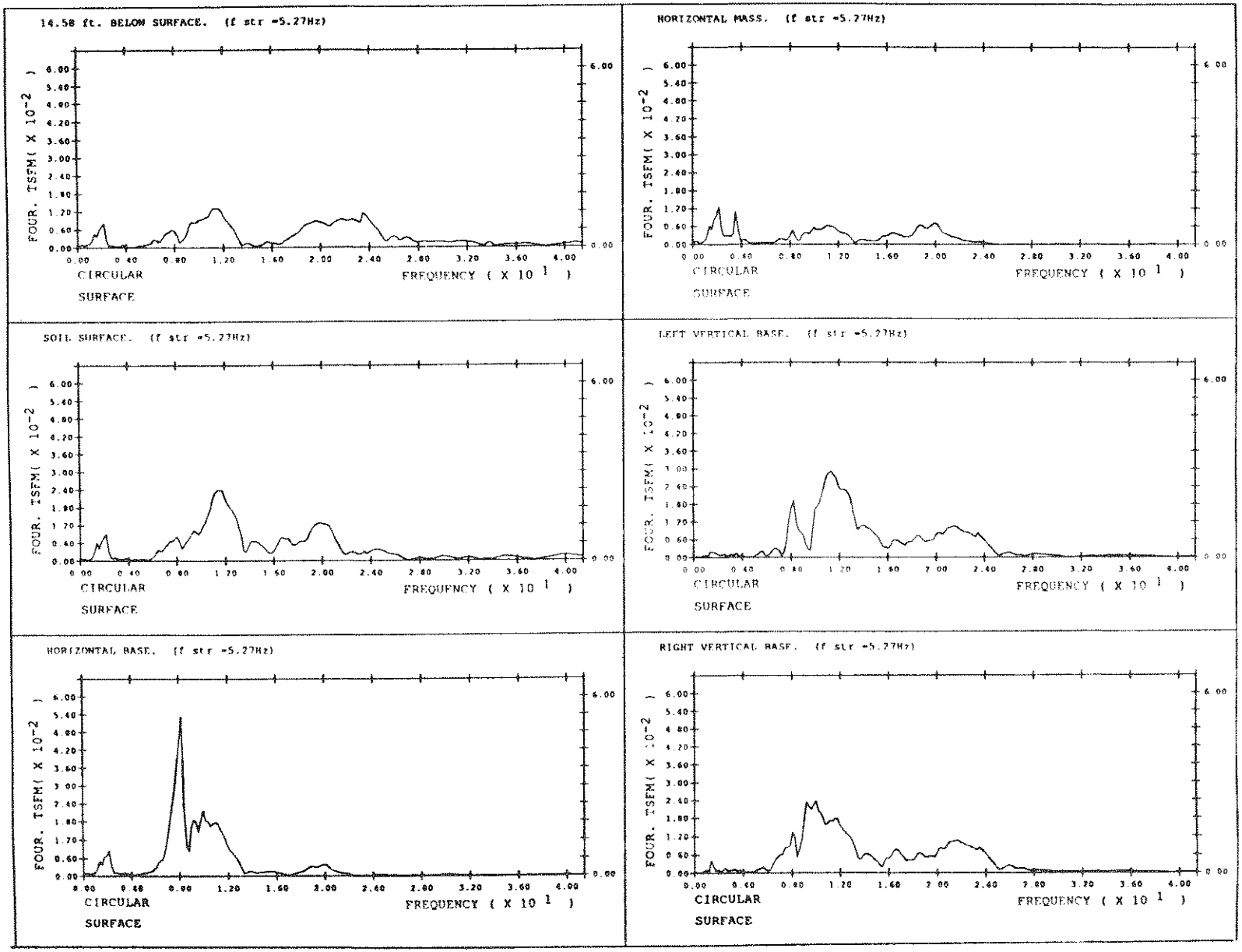

FIGURE 3-5 System with Surface Circular Footing (f_{str} = 5.27Hz) (cont'd)

SECTION 4

EFFECTS OF EMBEDMENT

In the next set of experiments the structure with the circular footing used in Section 3 is embedded up to the top of the base (see Figure 2-5). The depth of embedment, therefore, is 4.89ft. Sand is now glued to the side of the base as well as the bottom to ensure bonding between the side walls of the footing and the soil. Based on the results of the first set of tests it was decided that f_{str} should be increased more gradually in order to get a broader picture of the behavior of the structure (previously three out of the four cases had values of f_{str} close to or above f_{soil}). The new range of frequencies is as follows:

$$1.66\text{Hz} < f_{soil}$$

$$2.98\text{Hz} < f_{soil}$$

$$3.12\text{Hz} < f_{soil}$$

$$4.69\text{Hz} \approx f_{soil}$$

$$5.27\text{Hz} > f_{soil}.$$

Figures 4-1 through 4-5 show the accelerations and Fast Fourier Transforms for each of the cases. The earthquake input is the same as it was for the surface structure experiments so direct comparisons of the structural response can be made between the two systems.

The horizontal motion of the top mass shows the same general trends of radiation damping as the surface structure. The new range of f_{str} better illustrates the gradual increase in radiation damping as f_{str} is increased above f_{soil}. The amplitude and frequency content of the end of the signal (after two seconds) is similar for the embedded and the surface structures. The response to the strong motion, however, varies in amplitude as well as frequency for the embedded structure as opposed to the surface structure whose strong motion response varies only in frequency content as f_{str} is increased. The Fast Fourier Transform of the free field motion at the surface (shown back in Figure 2-1) has dominant peaks at

around 11Hz and 21Hz. Assuming this free field motion approximates the earthquake input at the base of the structure, it can be concluded that the embedded structure sees resonance effects from these peaks as f_{str} is varied whereas the surface structure does not.

The horizontal motion of the base behaves somewhat differently for the embedded case as well. First, the dominant frequency of the response, as seen from the Fast Fourier Transforms, is slightly larger for the embedded structures (10Hz) than for the surface structures (7.8Hz). Thus the stiffness at the base-soil level is larger for the embedded structure. Second, the damping associated with this peak frequency is also larger for the embedded structure. The third difference is that the base and the mass no longer act completely independently as they did for the surface structures. This can be seen most obviously when f_{str} = 1.66Hz (Figure 4-1) where the horizontal acceleration of the base exhibits a ringing at the end of the signal which vibrates at the same frequency as the ringing of the superstructure.

The vertical motions on opposite sides of the base are similar for all five values of f_{str} and are again out-of-phase and of unequal amplitude. However, the vertical accelerations are smaller for the embedded structure than the surface structure. This is quite reasonable as the embedment provides some resistance to rocking, and the bonding of the sides of the foundation to the soil restricts vertical motion.

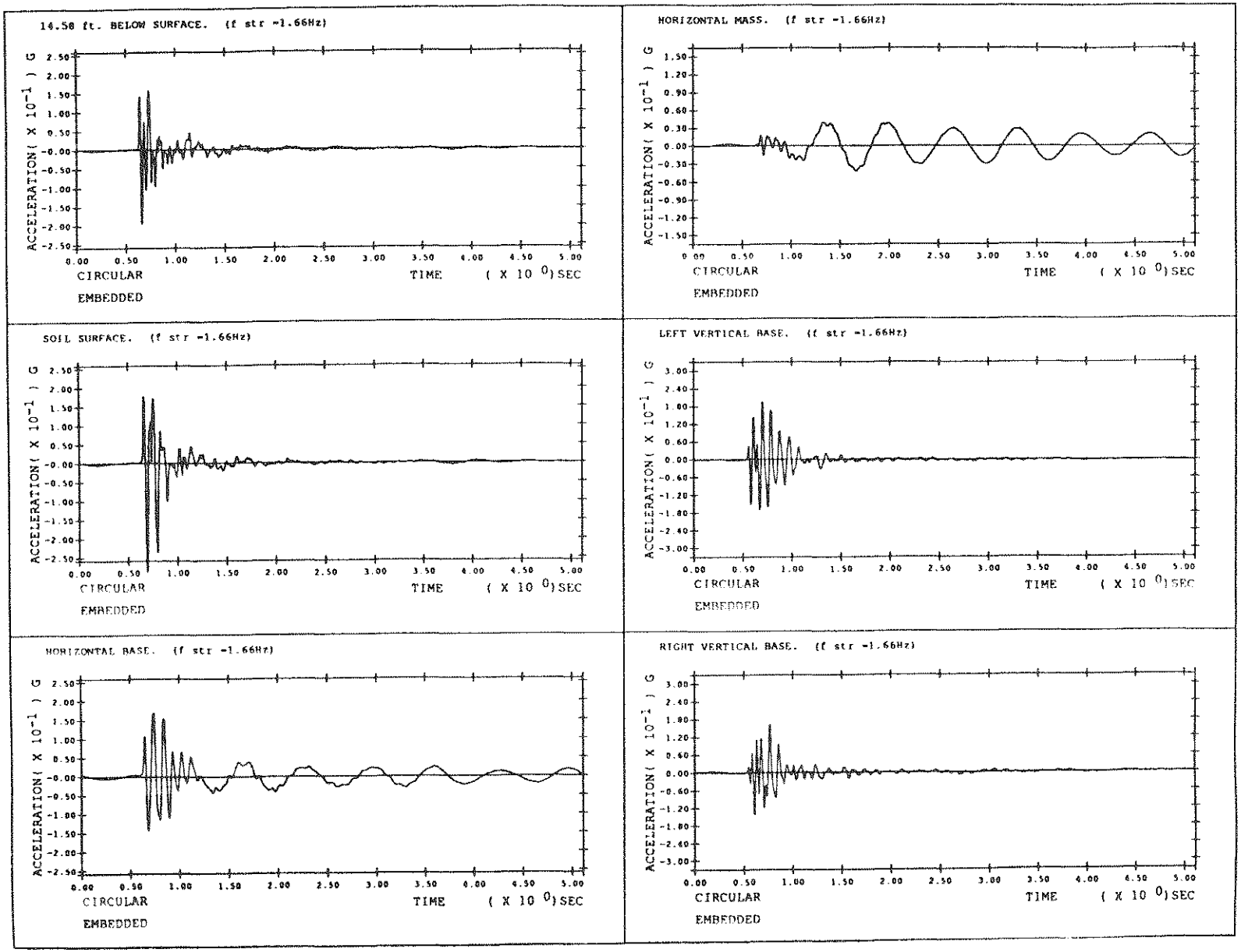

FIGURE 4-1 System with Embedded Circular Footing (f_{str} = 1.66Hz)

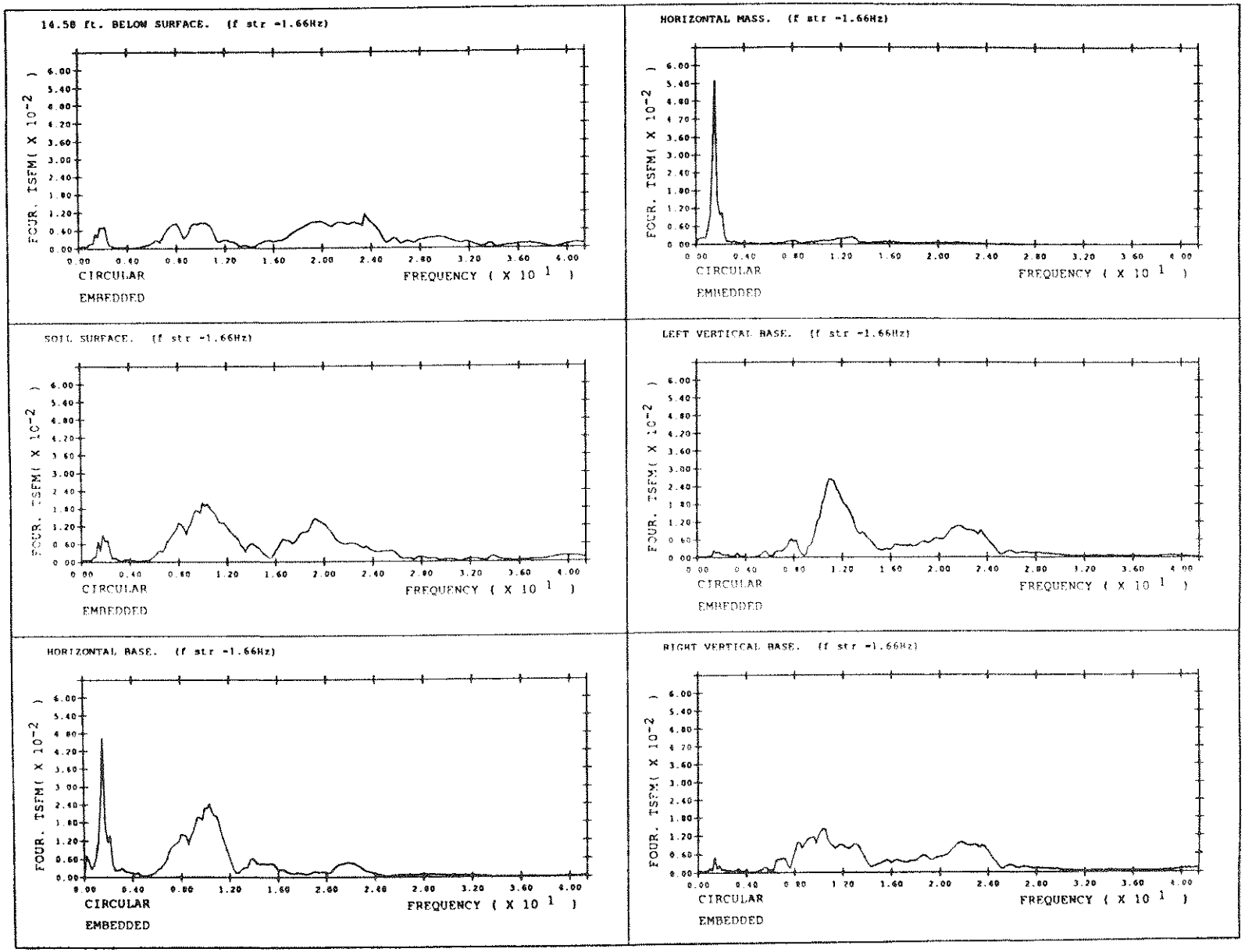

FIGURE 4-1 System with Embedded Circular Footing (f_{str} = 1.66Hz) (cont'd)

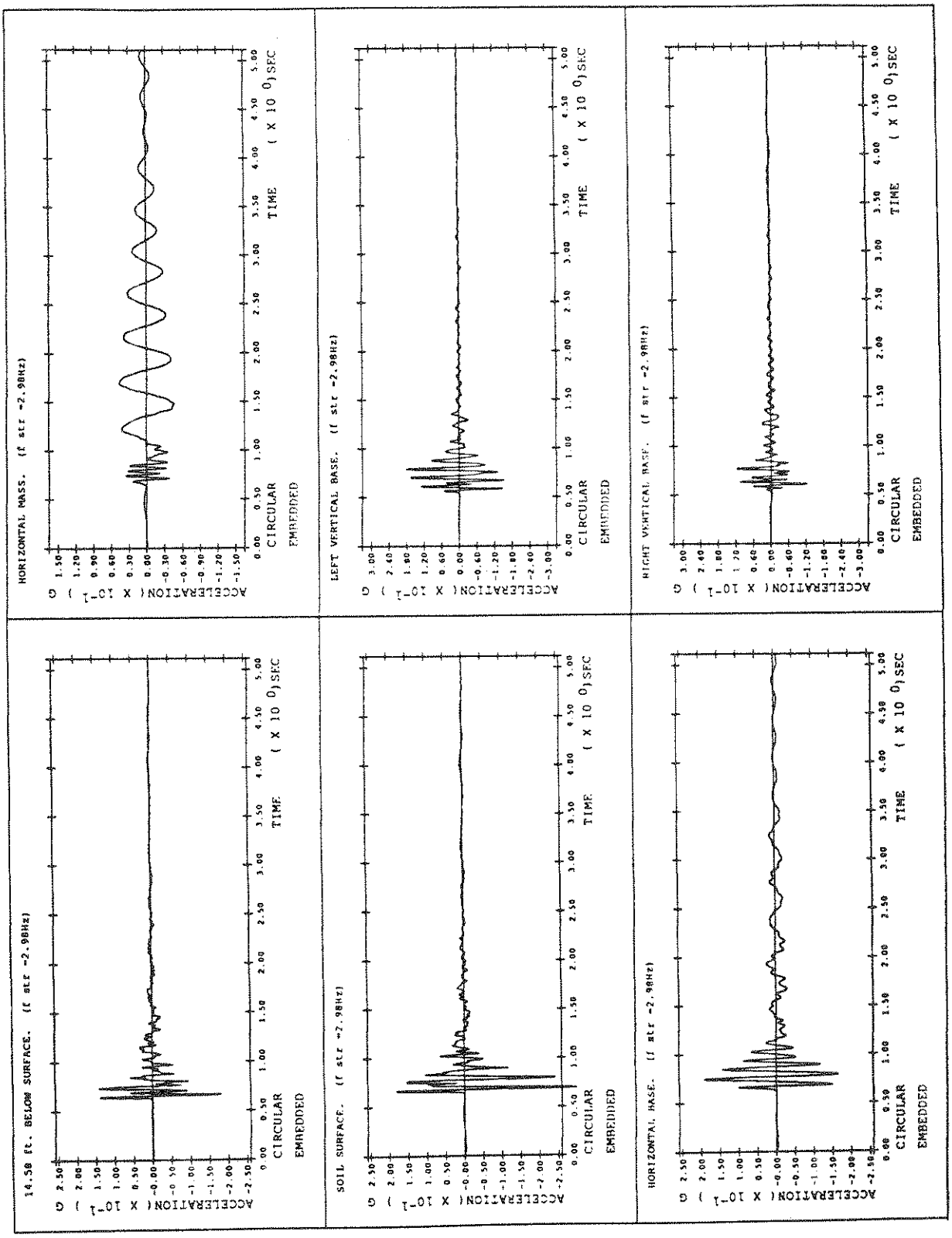

FIGURE 4-2 System with Embedded Circular Footing (f_{str} = 2.98Hz)

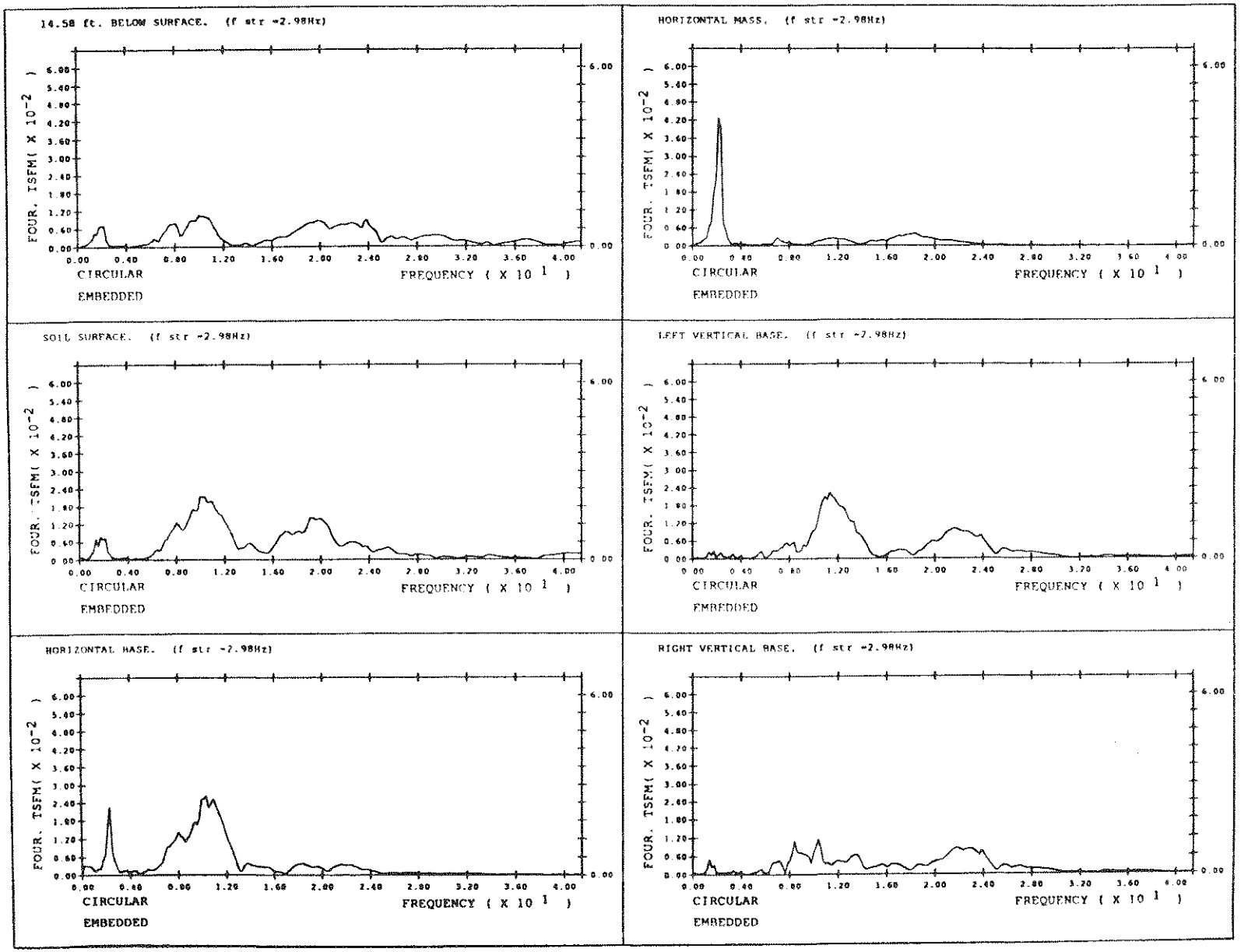

FIGURE 4-2 System with Embedded Circular Footing (f_{str} = 2.98Hz) (cont'd)

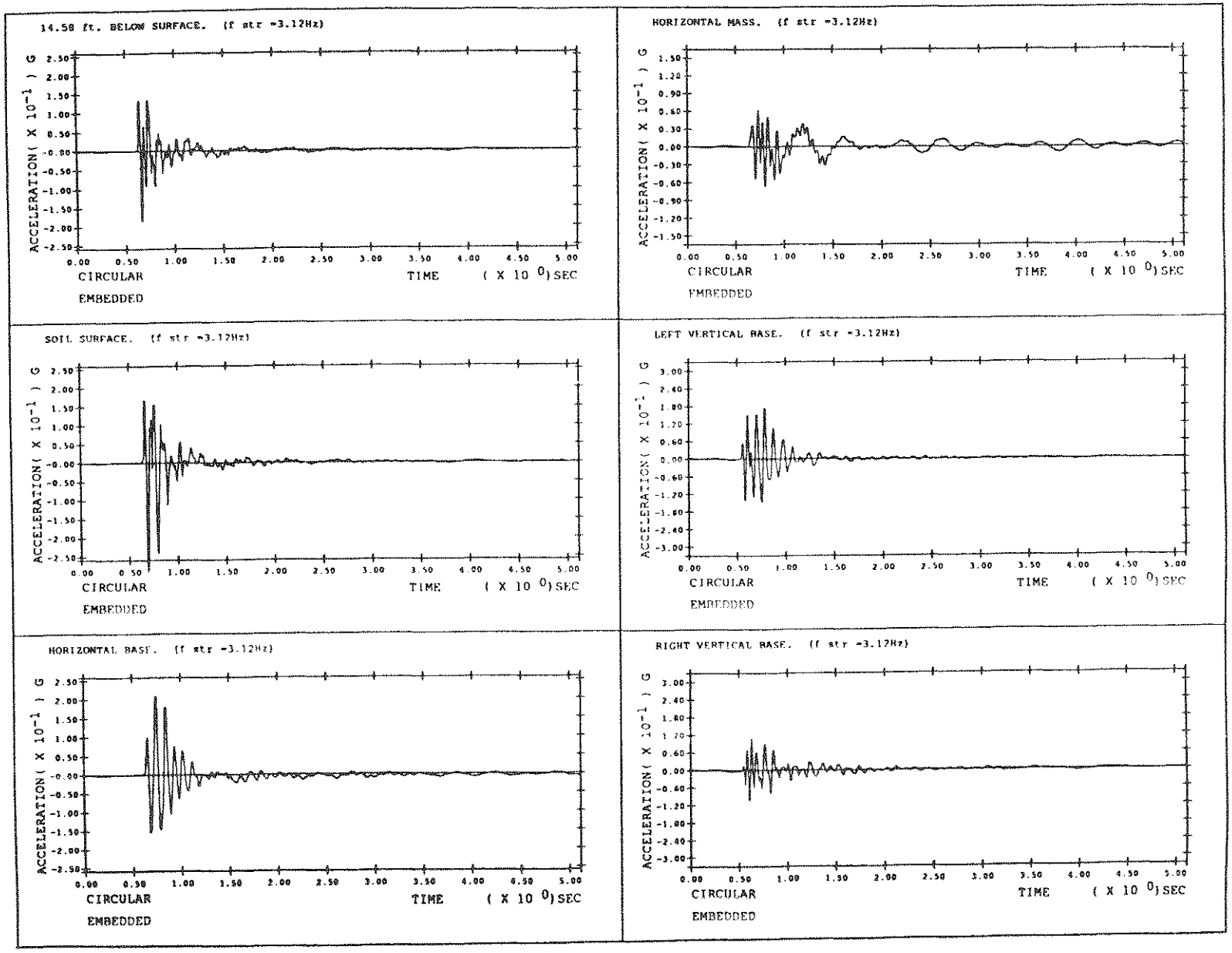

FIGURE 4-3 System with Embedded Circular Footing (f_{str} = 3.12Hz)

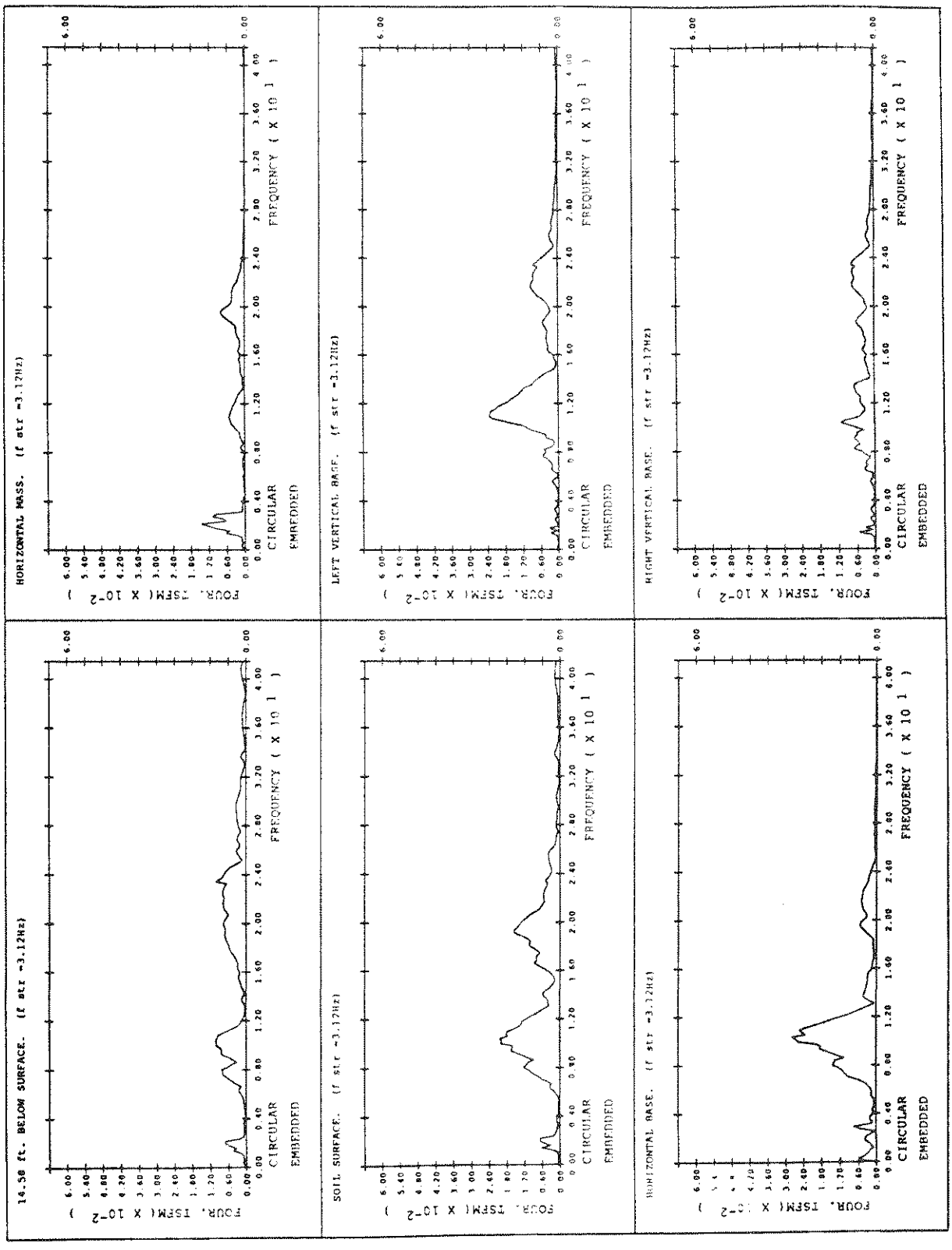

FIGURE 4-3 System with Embedded Circular Footing (f_{str} = 3.12Hz) (cont'd)

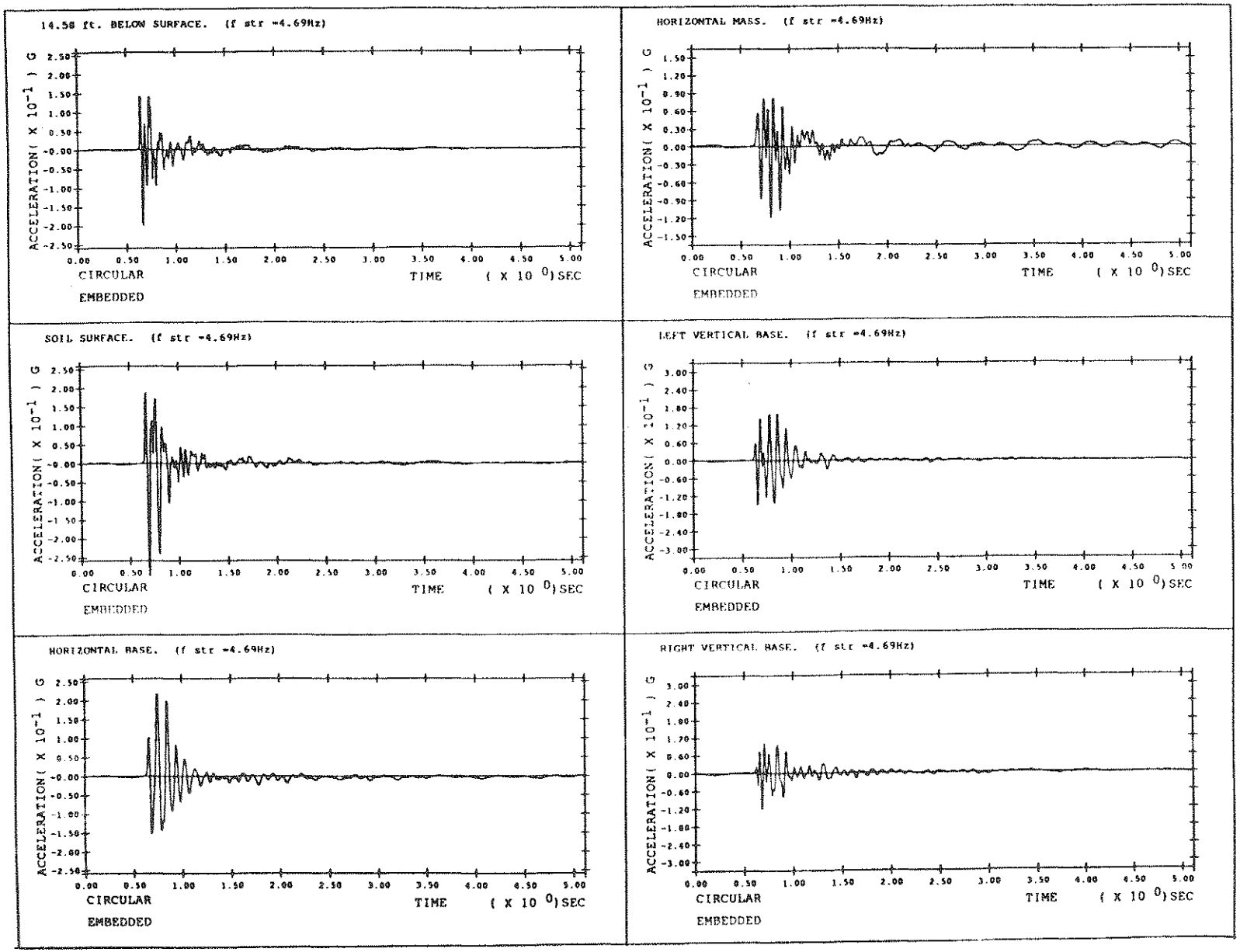

FIGURE 4-4 System with Embedded Circular Footing (f_{str} = 4.69Hz)

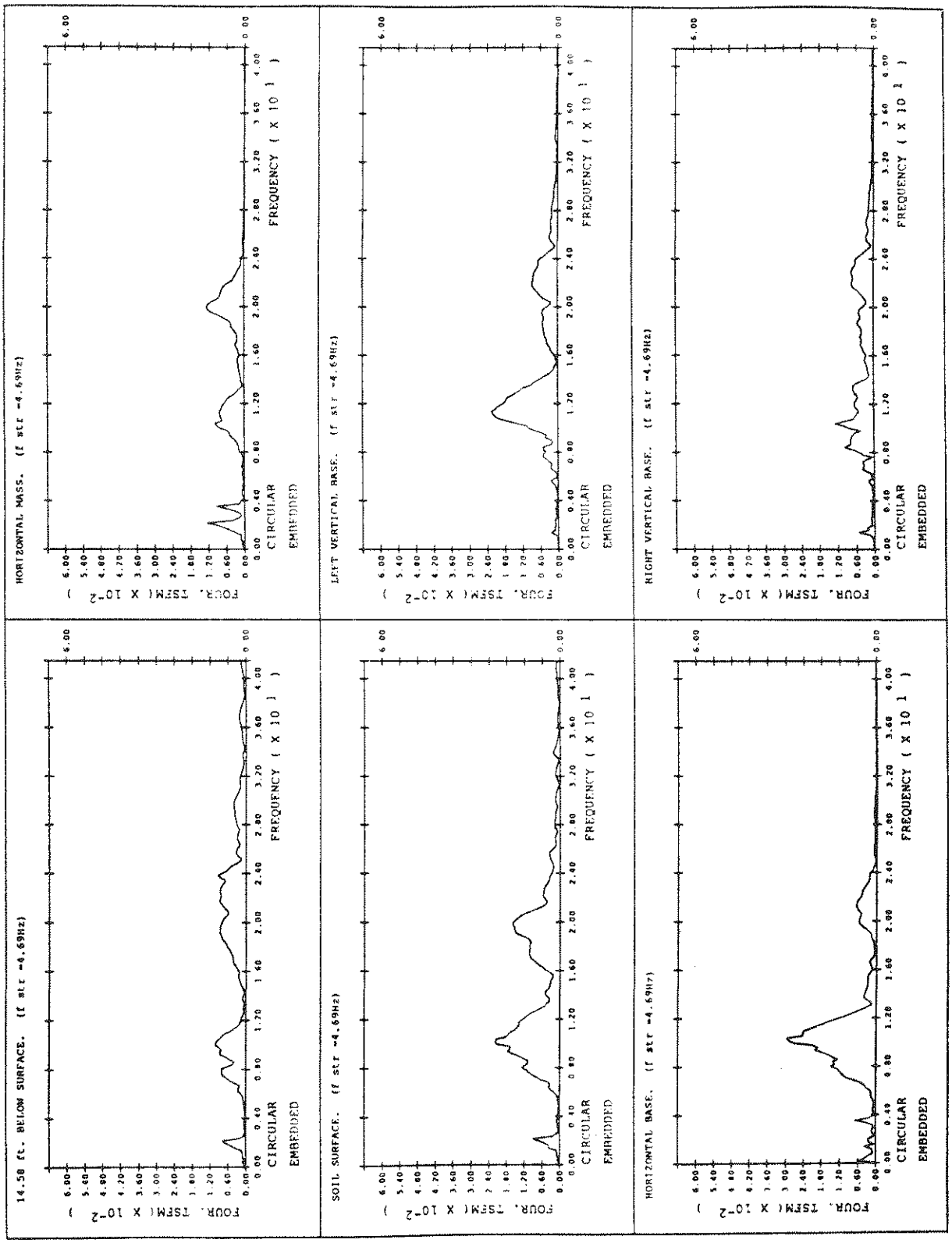

FIGURE 4-4 System with Embedded Circular Footing (f_{str} = 4.69Hz) (cont'd)

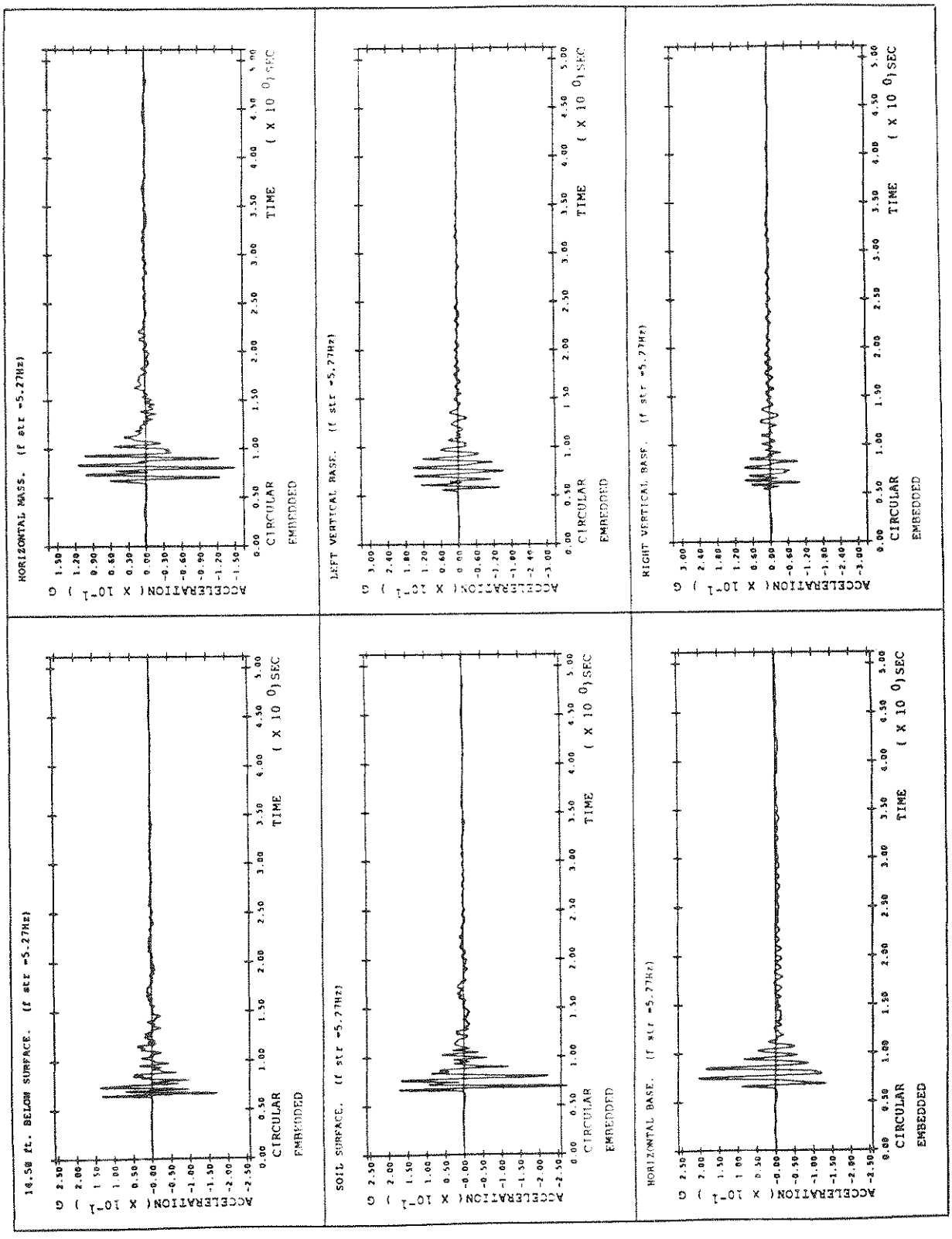

FIGURE 4-5 System with Embedded Circular Footing (f_{str} = 5.27Hz)

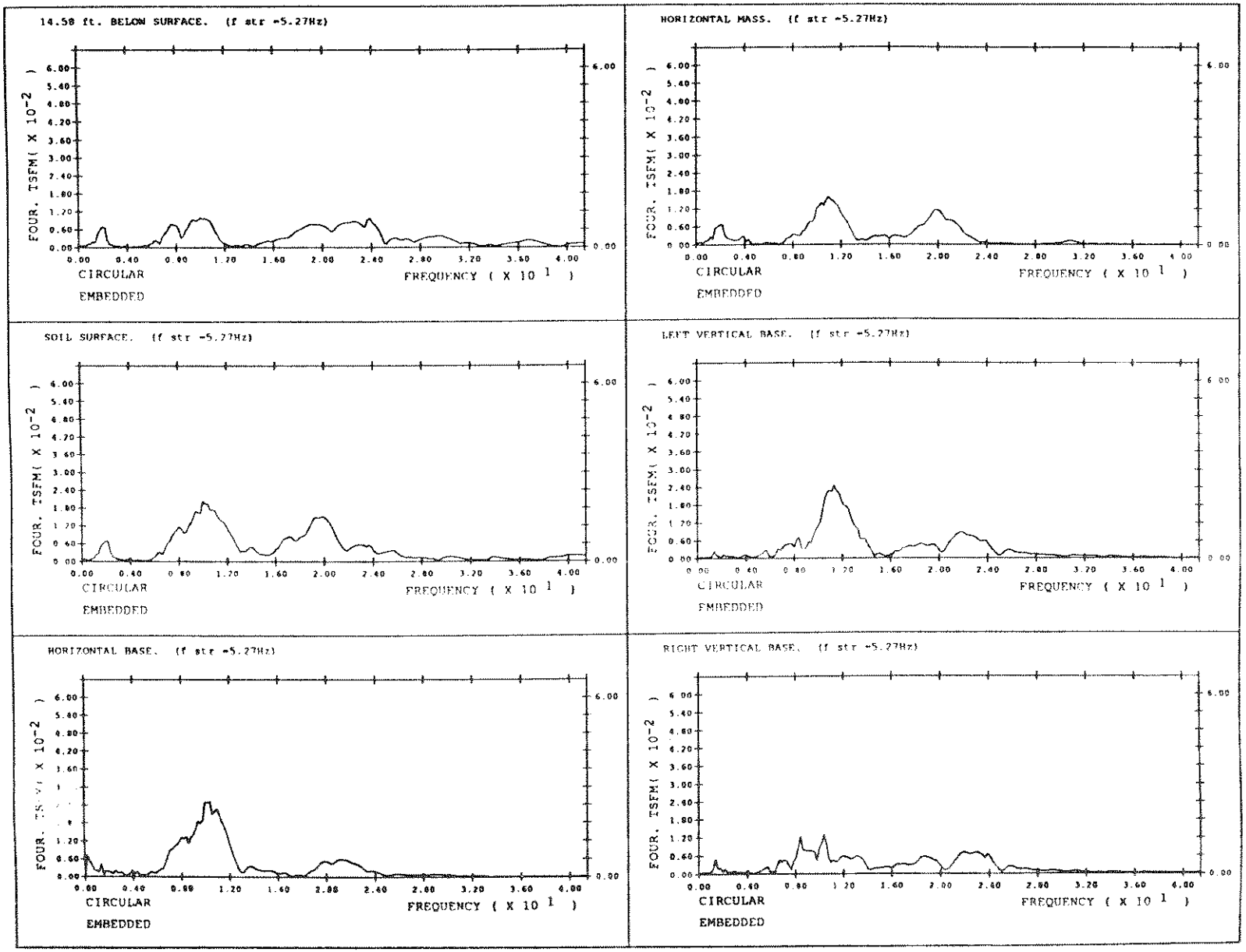

FIGURE 4-5 System with Embedded Circular Footing (f_{str} = 5.27Hz) (cont'd)

SECTION 5

EFFECTS OF FOUNDATION SHAPE

In order to establish the effects of foundation shape on radiation damping and soil-structure interaction, the experiments described in the preceding two sections are repeated for four additional foundation shapes. The additional shapes are a square, a rectangle with an aspect ratio of 2, a rectangle with an aspect ratio of 4, and a strip (a long rectangle with an aspect ratio of 8). The same adjustable superstructure was used in each case. The square and rectangular footings have half widths equal to the radius of the circular foundation (8.20 ft). However, because of the limited dimensions of the model container, the halfwidth of the strip footing must be reduced in order to obtain a large aspect ratio. In this section the results of the surface and embedded tests are presented simultaneously for each foundation. For the square footing, the entire range of frequencies presented in section 4 are tested. For the two rectangular and the strip footings the tests are performed only for values of f_{str} = 1.66Hz, 2.98Hz and 4.69Hz.

5.1 Square

The accelerations of various points of the system with a square footing are shown in Figures 5-1 through 5-5 and 5-6 through 5-10 for the surface and embedded cases respectively. The response of the top mass in these figures demonstrates the same relationship between radiation damping and f_{str} that is evident for the structure with a circular footing. For $f_{str} < f_{soil}$ energy is still trapped in the structure after the earthquake ends (e.g. Figures 5-1 and 5-6 HORIZONTAL MASS) whereas for $f_{str} > f_{soil}$ this energy is being radiated away (e.g. Figures 5-5 and 5-10 HORIZONTAL MASS). For both the surface and embedded structures there is a high frequency component of the response of the top mass that becomes more pronounced as f_{str} increases. As can be seen from the Fast Fourier Transforms of the horizontal acceleration, this frequency is about 21Hz for the surface case and about 11Hz for the embedded case. The fact

that the same structure responds to the same earthquake at two such distinctly different frequencies when the embedment is varied implies that soil-structure interaction is, to some degree, a function of foundation embedment. However, for the circular footing such a difference in the frequency of the response was not noticed; peaks at both 11Hz and 21Hz tended to appear in both cases (Figures 3-2, 3-3, 4-4 and 4-5 HORIZONTAL MASS). In general the results show that embedment affects the frequency content of the response of the top mass more for the structure with the square base and affects the peak amplitude of the response more for the structure with the circular base. These observations are most likely results of the difference in the foundation mass as well as the foundation shape.

For both the surface and embedded cases, the horizontal acceleration of the base is unaffected by the changes in the natural frequency of the superstructure. The dominant frequency of the base response is slightly higher for the embedded structure ($\approx$ 11Hz) than for the surface structure ($\approx$ 8Hz). Thus, embedment increases the horizontal stiffness at the base-soil interface. The peak amplitude and the damping at the base are slightly larger for the embedded case.

The vertical accelerations of the base are once again out-of-phase and unequal in amplitude signifying a combination of rocking and vertical motion. The difference in amplitude between the vertical motions on either side is slight for the surface structure but fairly large for the embedded structure.

5.2 Rectangular (Length/Width =2)

The response accelerations of the system with a surface and an embedded rectangular footing with an aspect ratio of 2 are shown in Figures 5-11 through 5-13 and 5-14 through 5-16. The output at the top mass indicates that the amount of radiation damping reflects changes in f_{str} much as it did in the previous tests with the circular and square footings.

The horizontal acceleration at the base is distinctly larger for the embedded structure than for the surface

structure. The peak amplitude differs by almost 100%. The peak frequency of the base acceleration for the embedded structure (≈ 11Hz) is once again slightly larger than for the surface structure (≈ 8Hz). The vertical accelerations of the base follow the same trends as the vertical accelerations of the square base.

5.3 Rectangular (Length/Width=4)

Figures 5-17 through 5-19 and 5-20 through 5-22 show the results of the tests performed on structures with a rectangular base with an aspect ratio of 4. The amplitude and frequency content of the horizontal acceleration of the top mass are generally comparable for the surface and embedded cases. Higher frequencies are not damped more heavily for the embedded structure as they are for the square footing and to a lesser extent for the other rectangular footing.

The horizontal acceleration at the base is quite low for this rectangular footing, especially for the surface case. This is most likely due to the fact that the base is now very large. Again, the frequency content is slightly higher and the damping is slightly larger for the response of the embedded base. The two vertical accelerations are out-of-phase, but are now very close in amplitude for each case of embedment and all values of f_{str}. It should be noted that the vertical accelerations decrease for the embedded structure while the horizontal base accelerations increase.

5.4 Strip (Length/Width=8)

The results for the strip footing are shown in Figures 5-23 through 5-25 and 5-26 through 5-28. The halfwidth of this footing was decreased by a factor of two in order to achieve a larger aspect ratio (halfwidth = 4.10ft). Thus the footing is narrower and less massive than the preceding rectangular footing and more rocking motion is likely to occur. This tendency is borne out in the large peak response of the top mass in Figure 5-23 which corresponds to the surface structure with f_{str} = 1.66Hz. The vertical accelerations in this figure are comparable in absolute amplitude to the vertical accelerations of the other

footing shapes. However, the vertical acceleration represents the tangential motion measured at a distance r from the center of rotation of the structure. Since r is roughly equal to the halfwidth of the footing, the rocking of the structure with the strip footing is actually twice as large because the footing width was decreased by a factor of 2. When the structure is embedded, the soil offers a greater resistance to rocking and the peak amplitudes of the horizontal motion at the top mass and the vertical motions at opposite sides of the base are smaller (Figure 5-26). Otherwise, the same trends of radiation damping are noticed for the response of the superstructure on the strip footing.

The peak horizontal response of the base is larger and has more damping and a higher dominant frequency for the embedded structure. The vertical motions are out-of-phase as they were before.

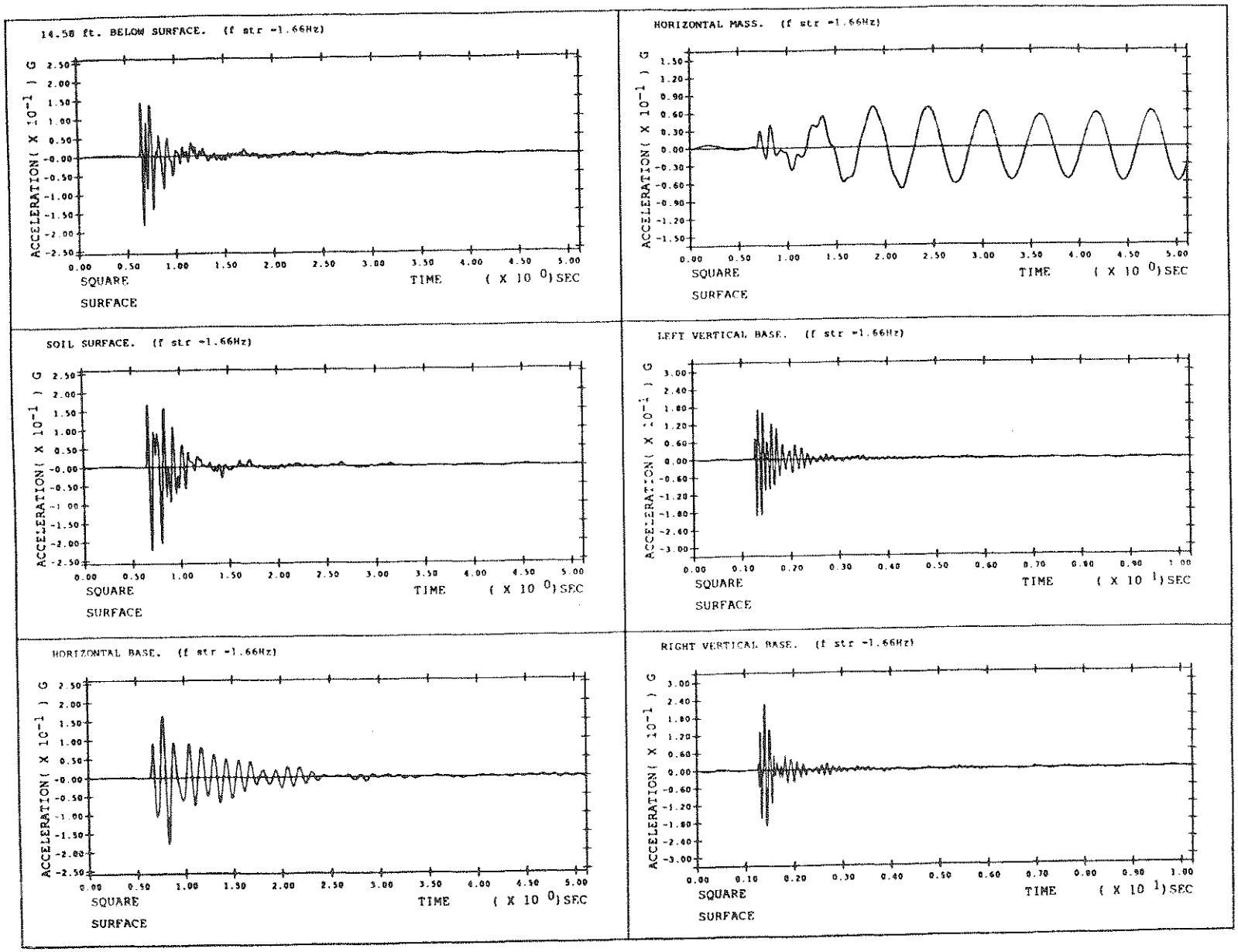

FIGURE 5-1 System with Surface Square Footing (f_{str} = 1.66Hz)

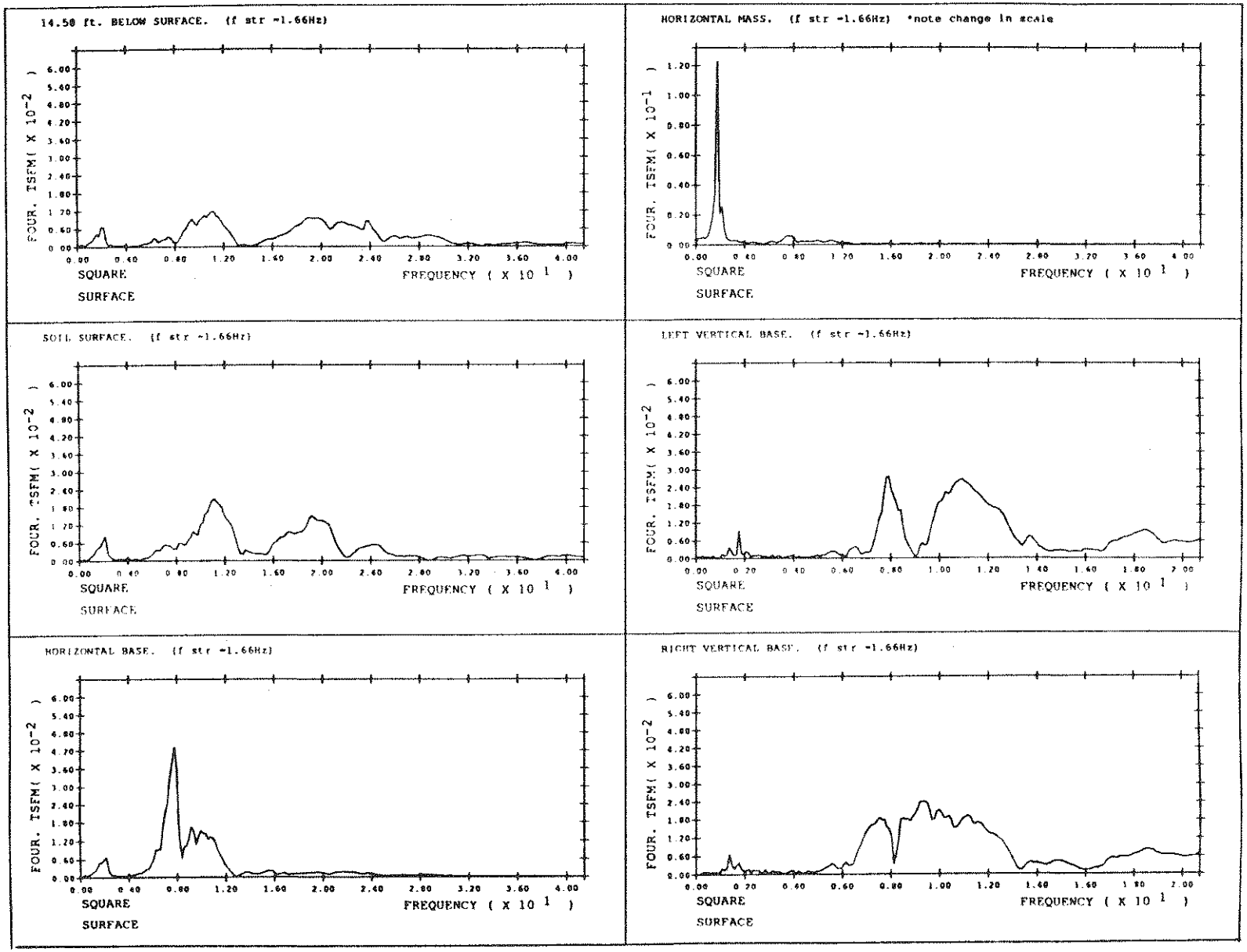

FIGURE 5-1 System with Surface Square Footing (f_{str} = 1.66Hz) (cont'd)

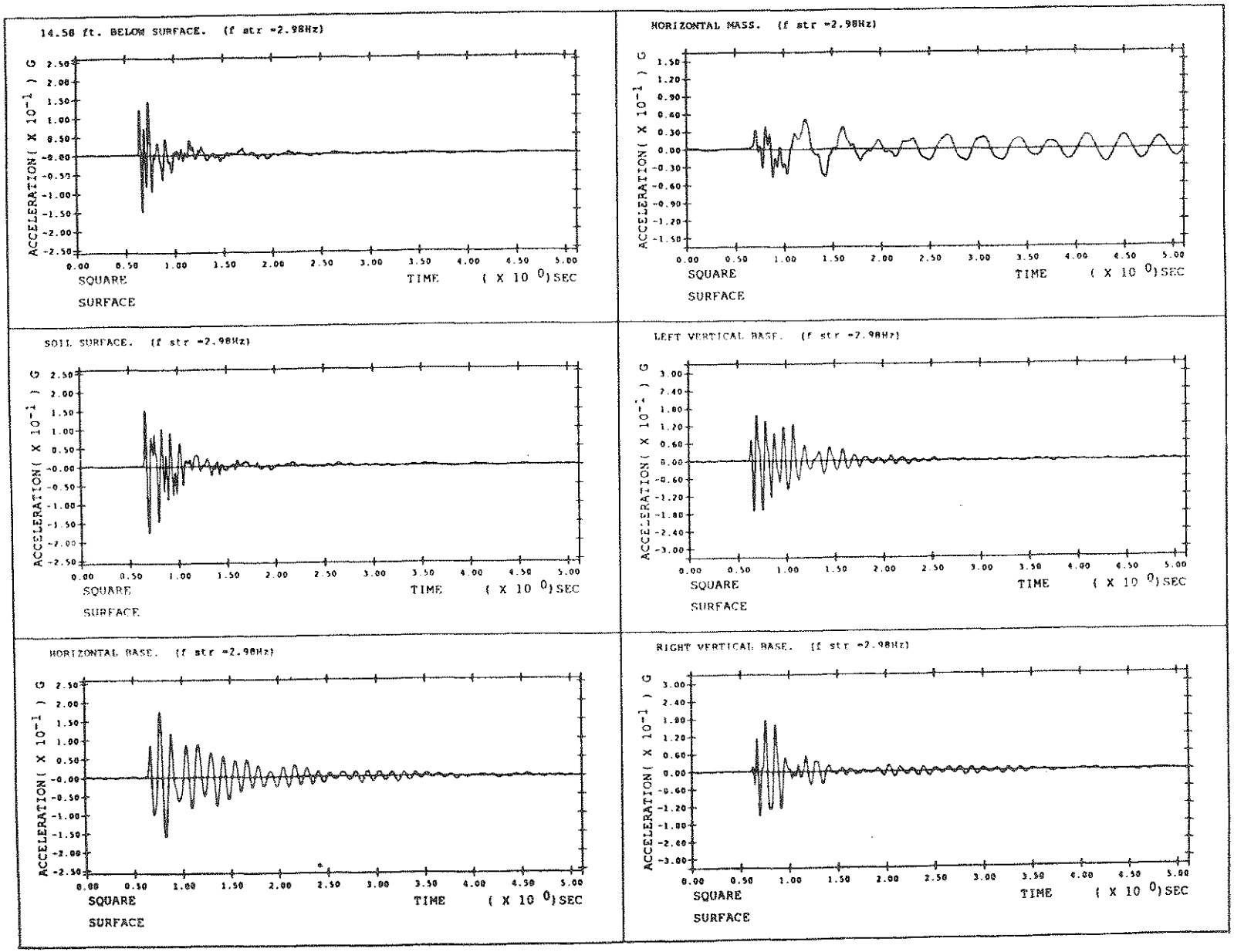

FIGURE 5-2 System with Surface Square Footing (f_{str} = 2.98Hz)

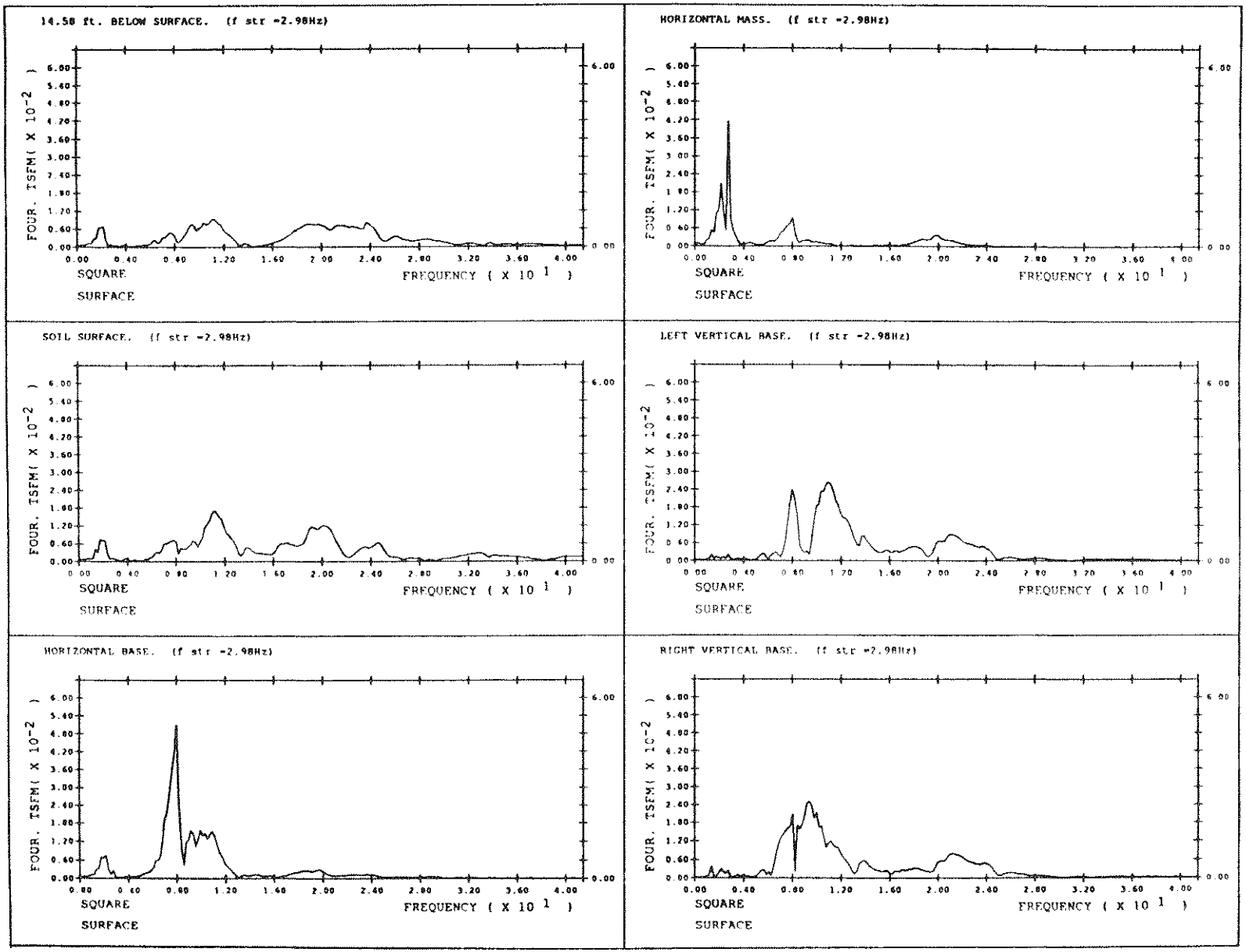

FIGURE 5-2 System with Surface Square Footing (f_{str} = 2.98Hz) (cont'd)

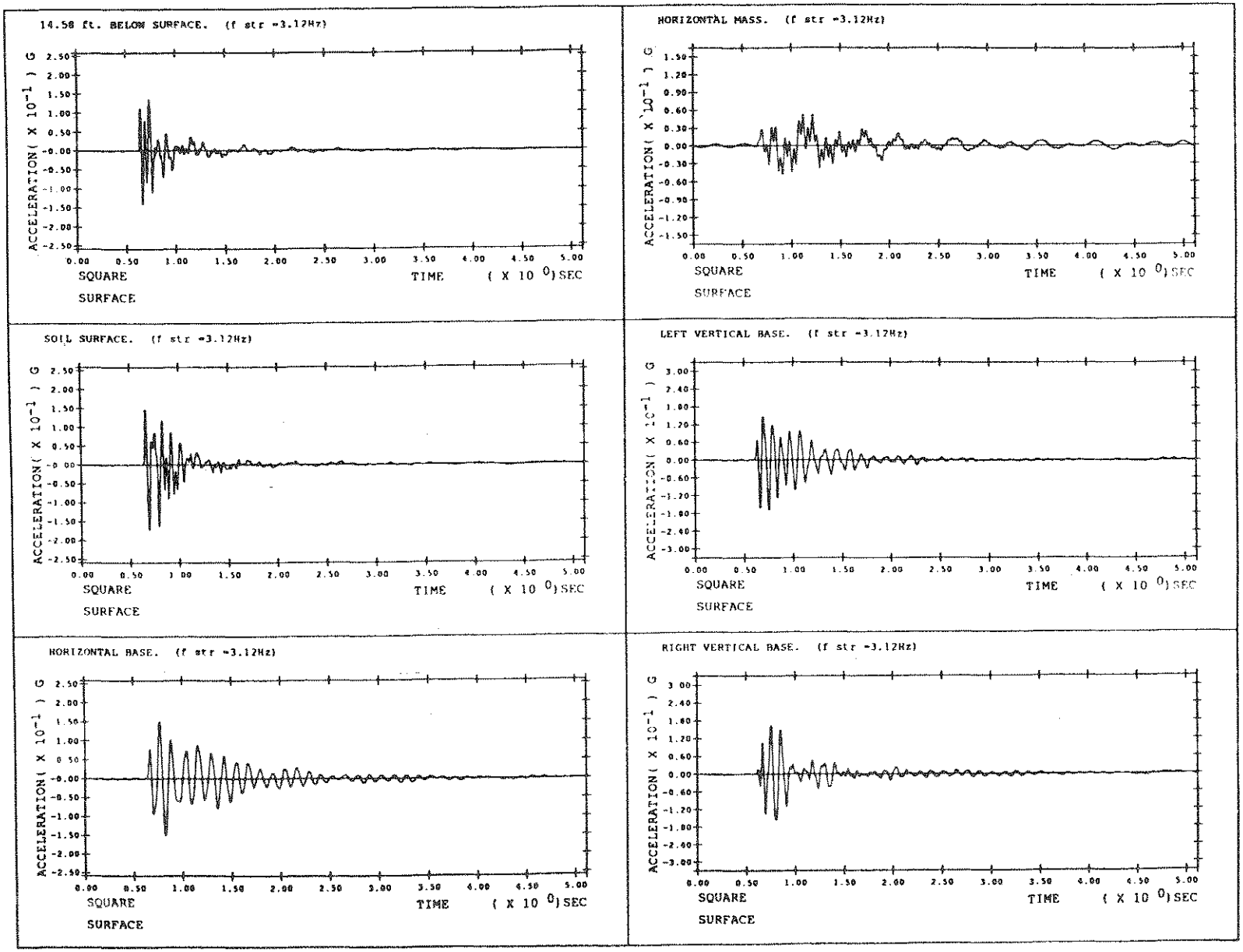

FIGURE 5-3 System with Surface Square Footing (f_{str} = 3.12Hz)

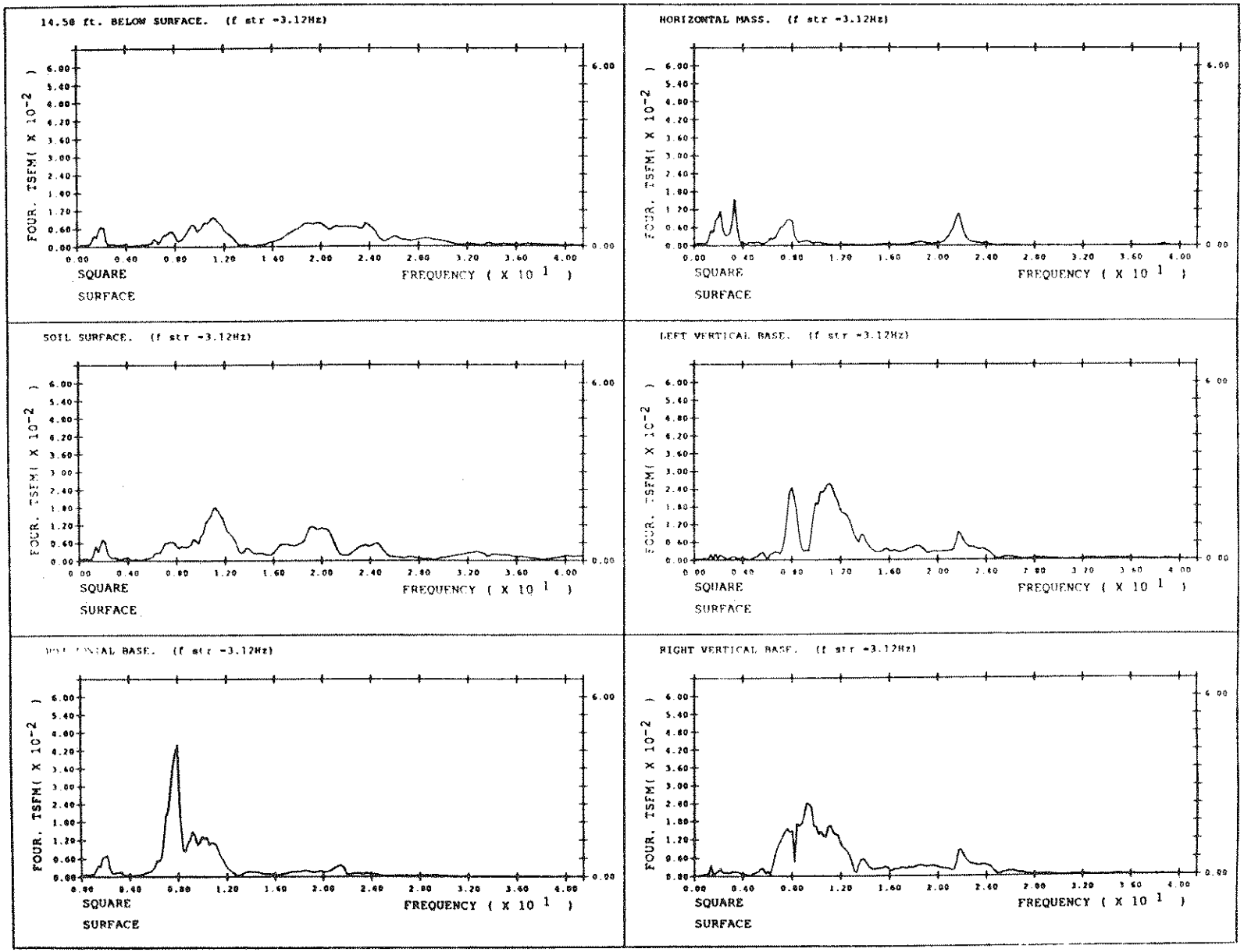

FIGURE 5-3 System with Surface Square Footing (f_{str} = 3.12Hz) (cont'd)

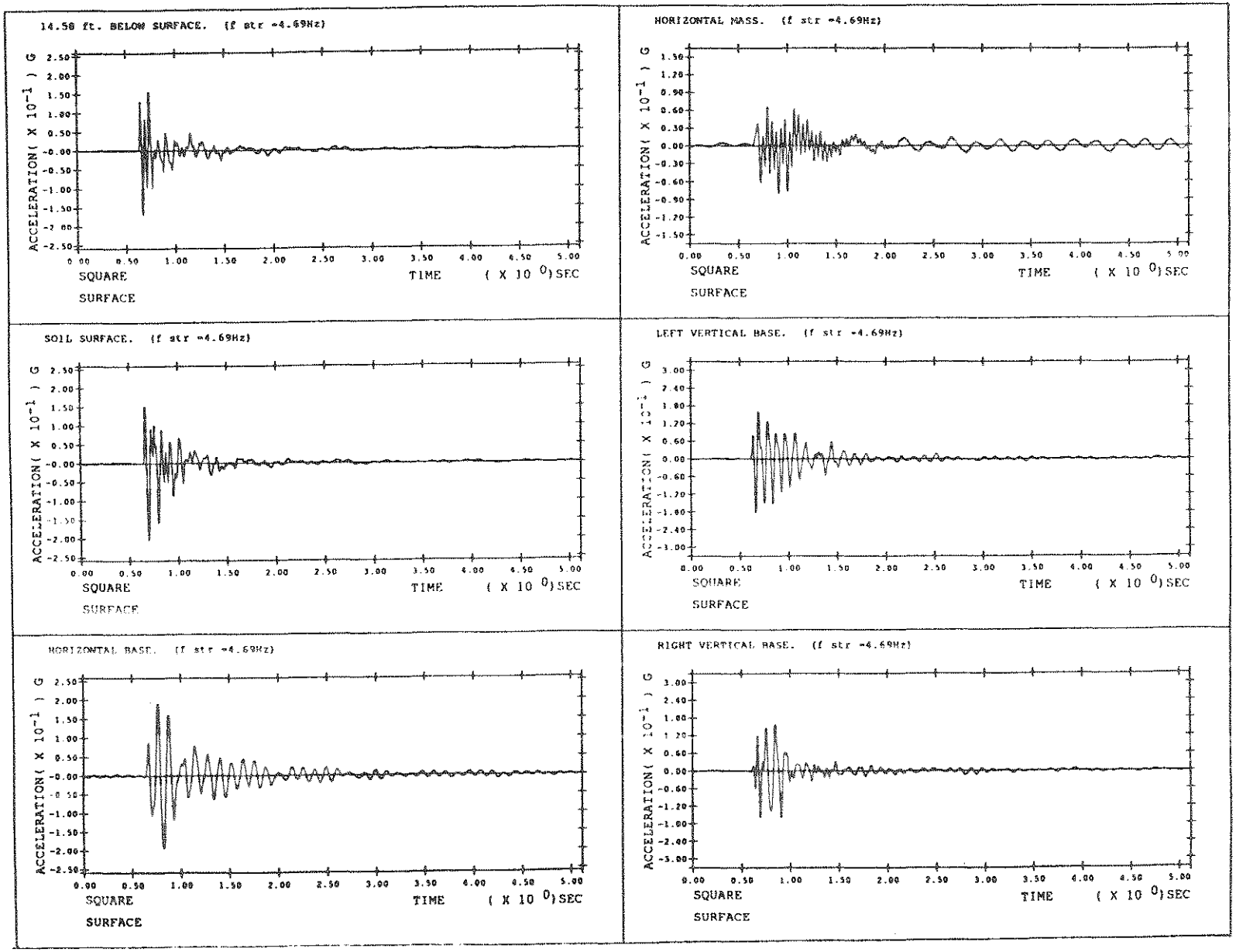

FIGURE 5-4 System with Surface Square Footing (f_{str} = 4.69Hz)

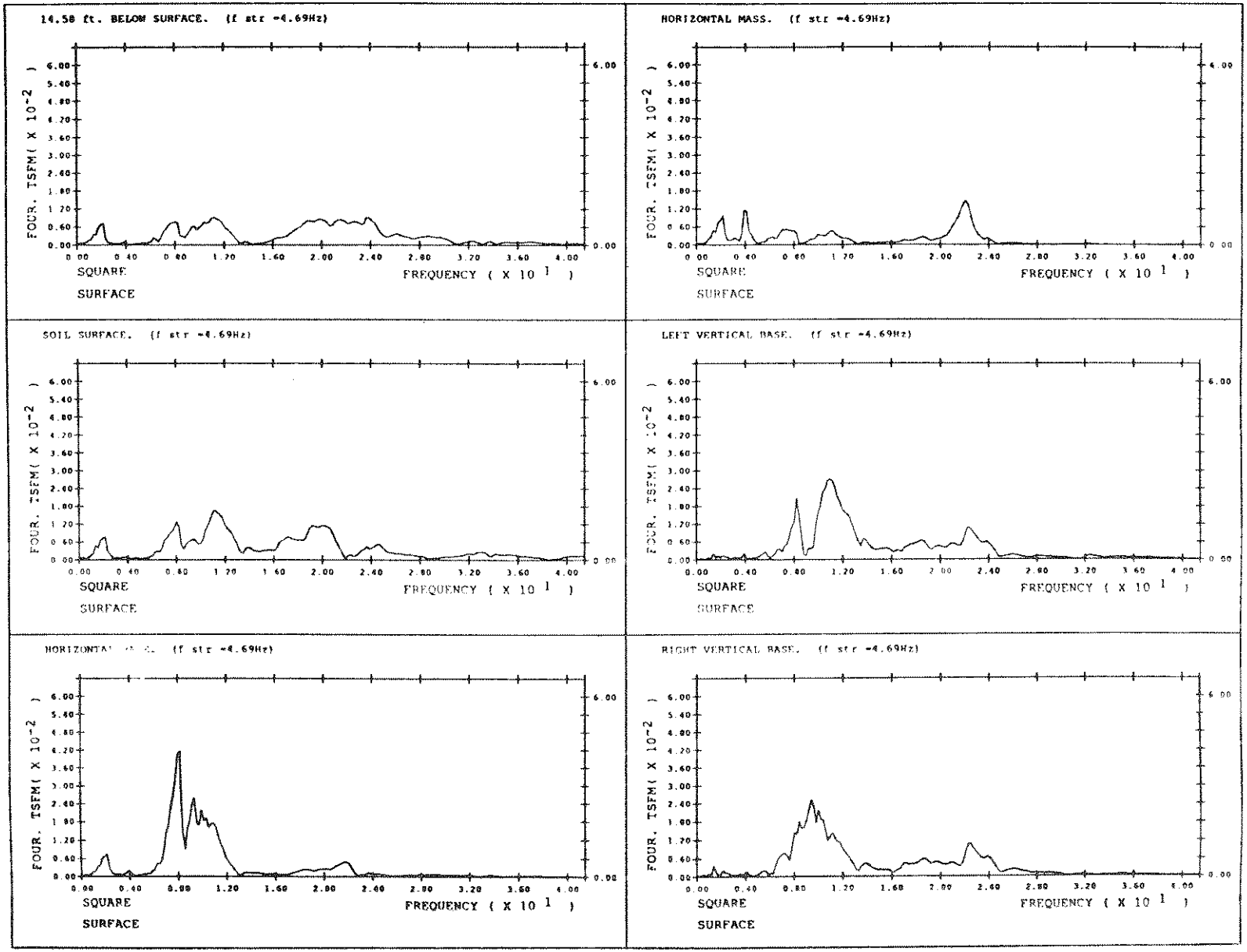

FIGURE 5-4 System with Surface Square Footing (f_{str} = 4.69Hz) (cont'd)

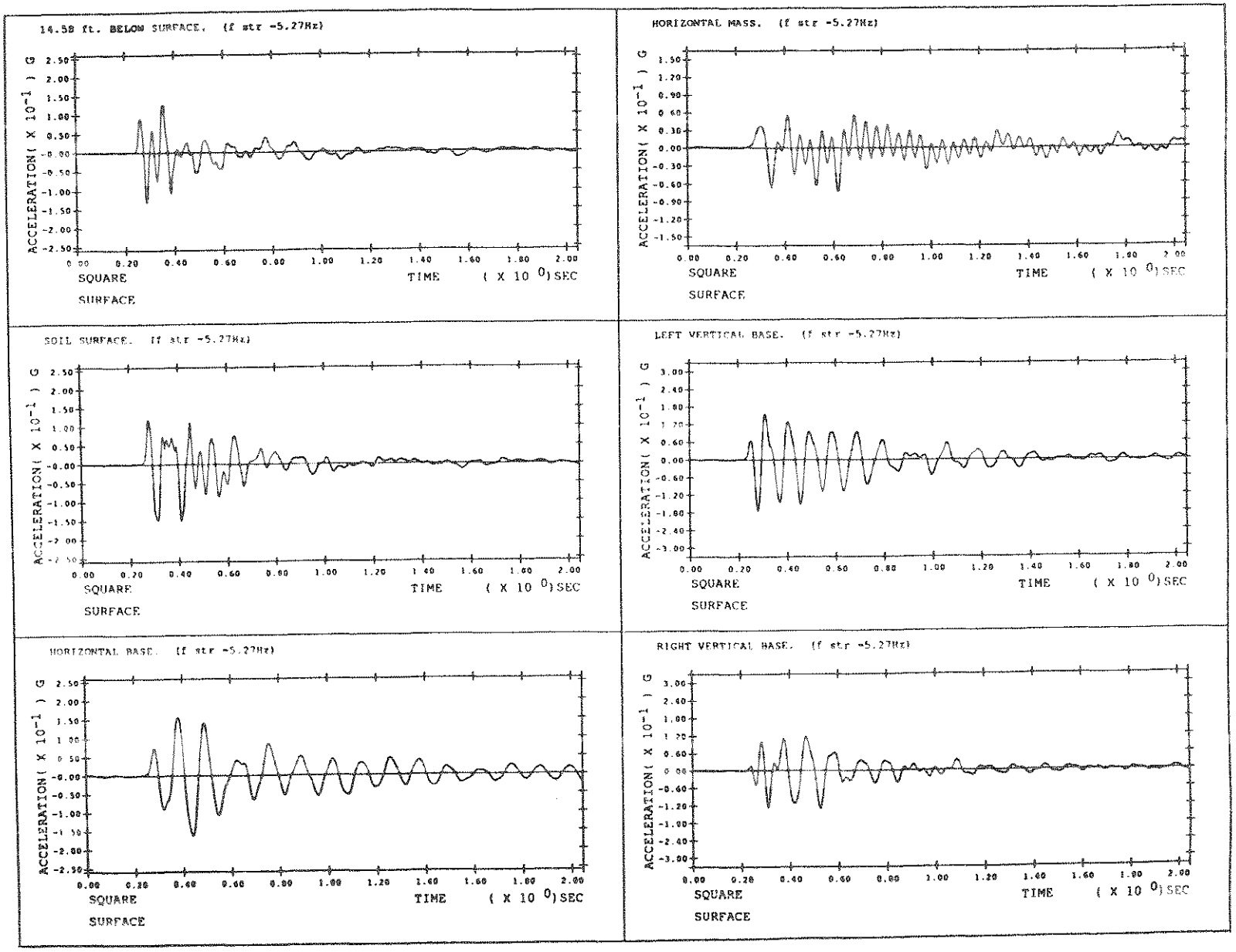

FIGURE 5-5 System with Surface Square Footing (f_{str} = 5.27Hz)

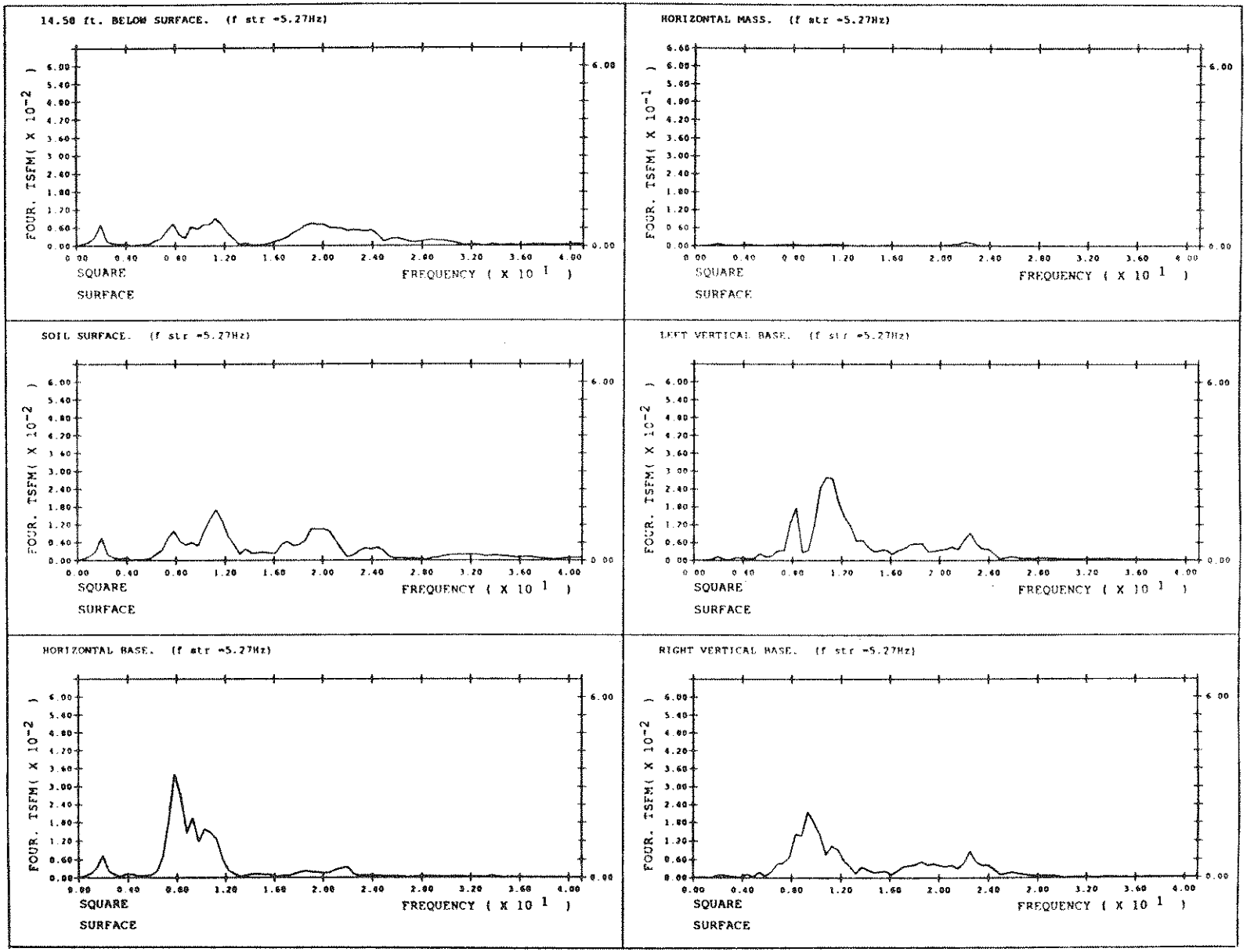

FIGURE 5-5 System with Surface Square Footing (f_{str} = 5.27Hz) (cont'd)

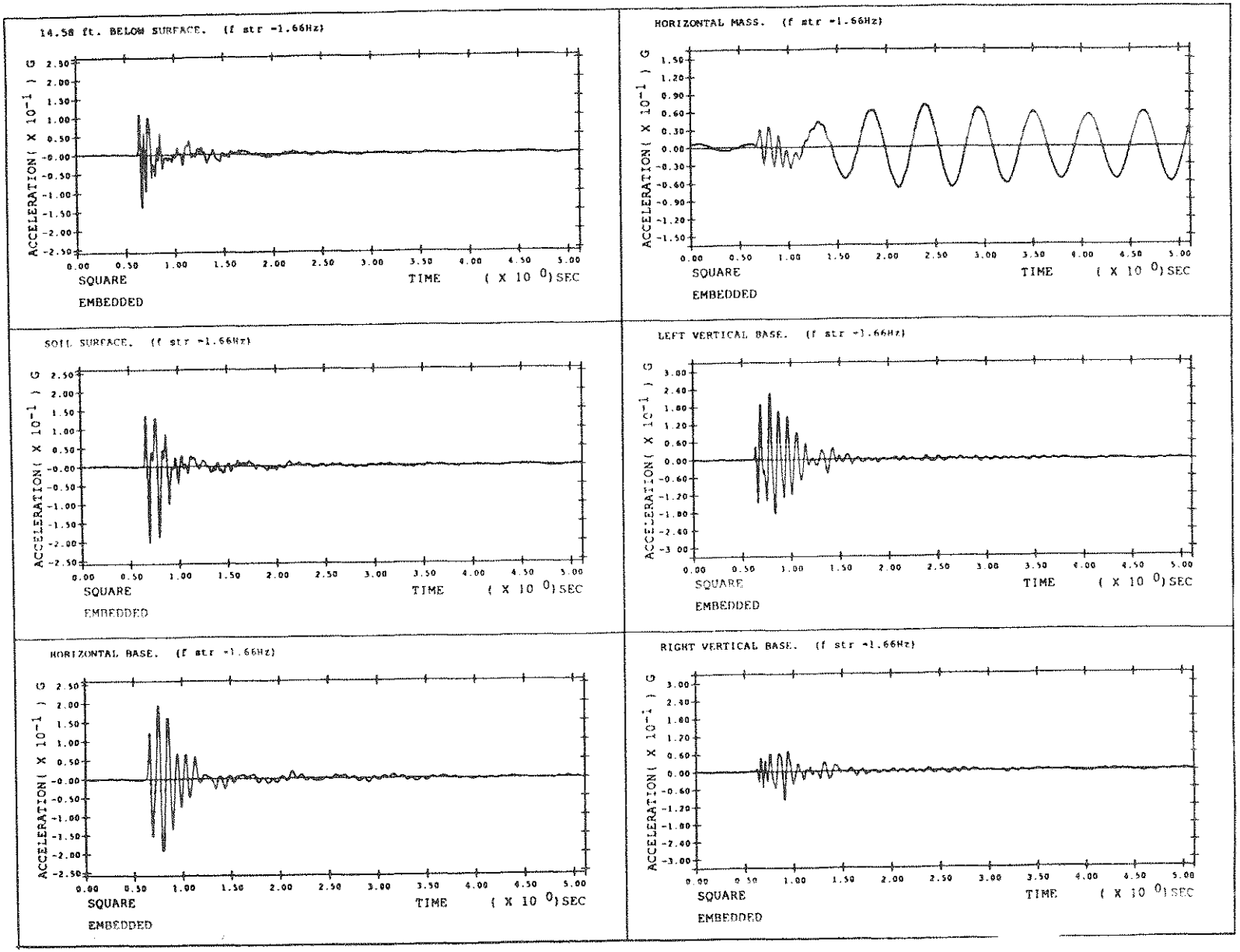

FIGURE 5-6 System with Embedded Square Footing (f_{str} = 1.66Hz)

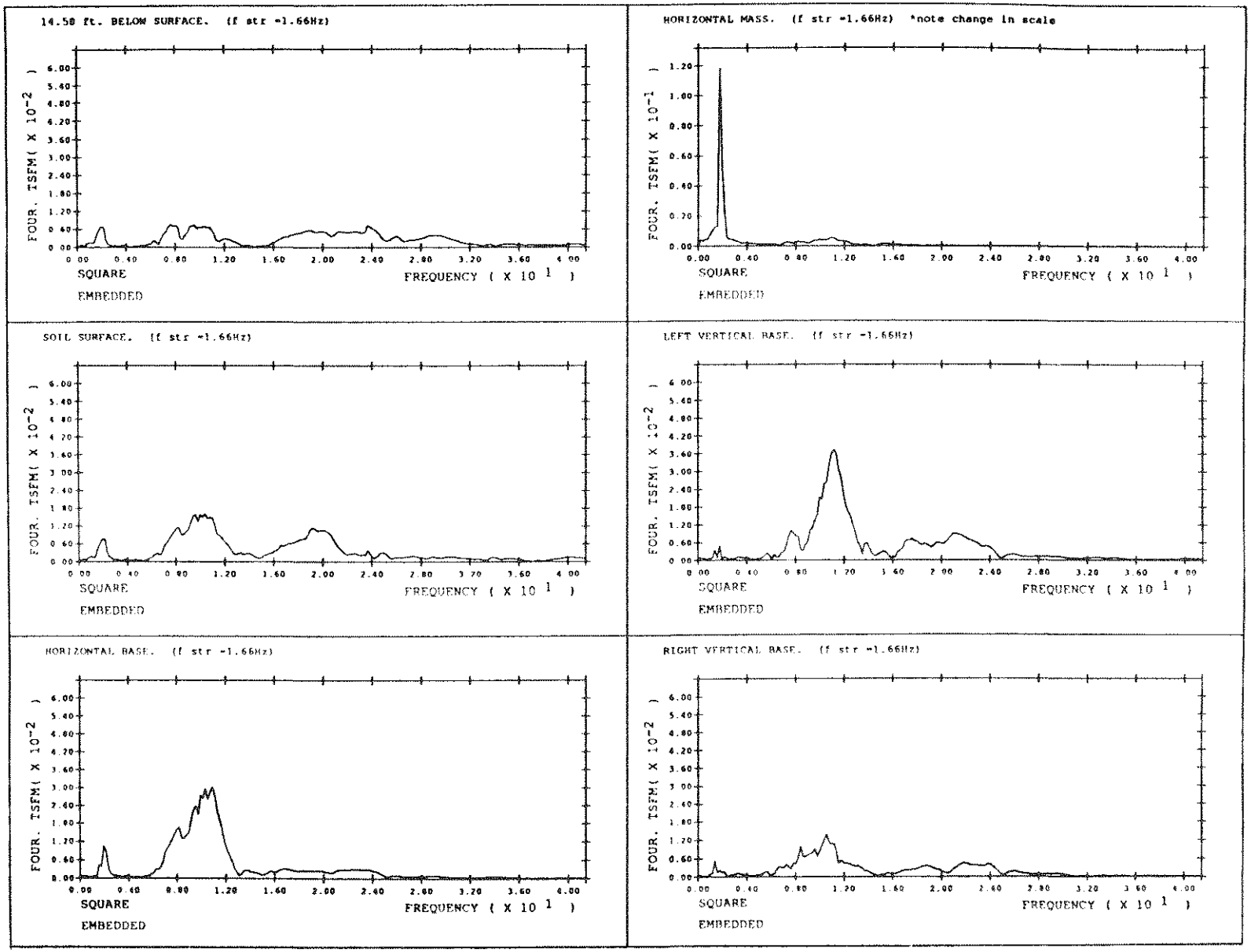

FIGURE 5-6 System with Embedded Square Footing (f_{str} = 1.66Hz) (cont'd)

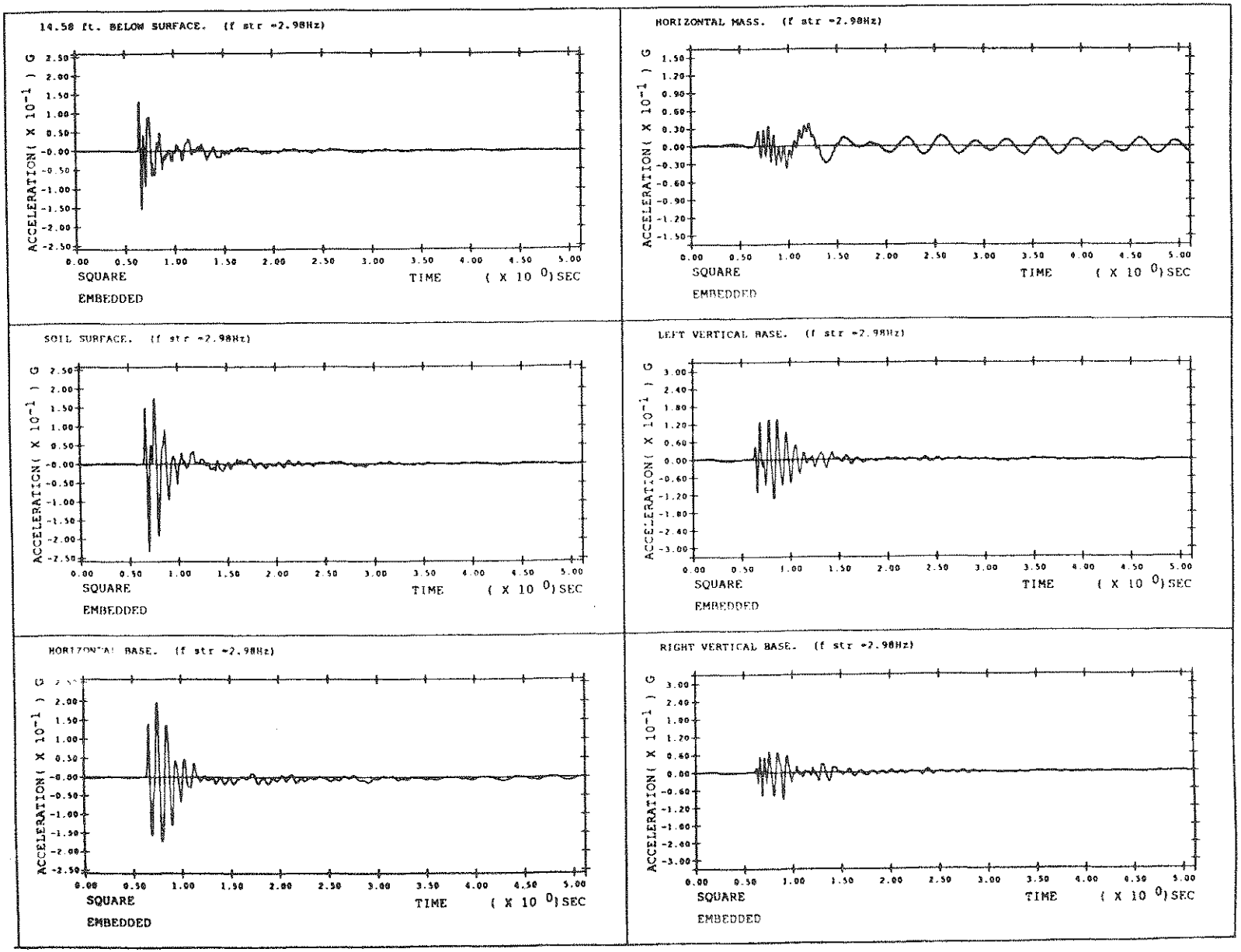

FIGURE 5-7 System with Embedded Square Footing (f_{str} = 2.98Hz)

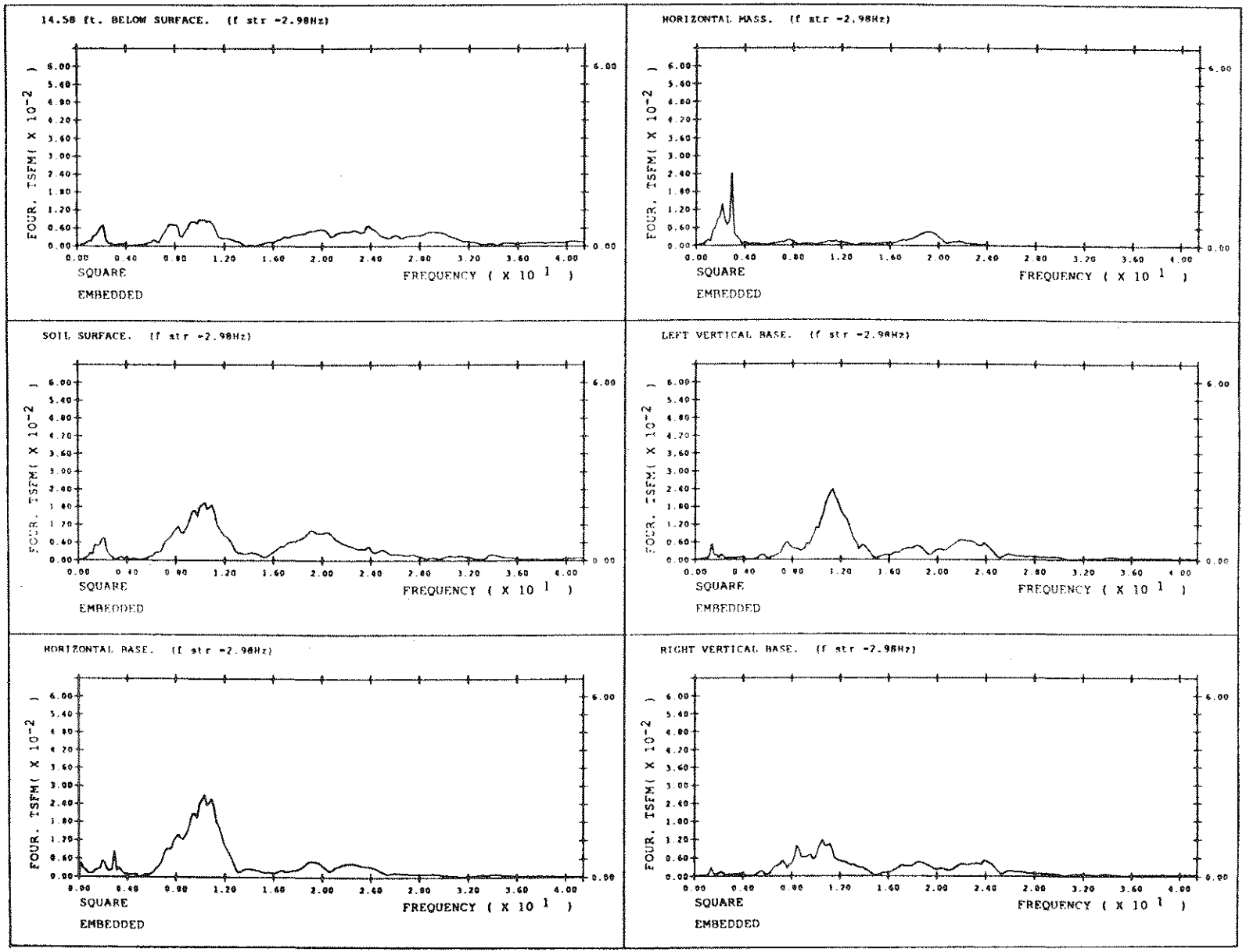

FIGURE 5-7 System with Embedded Square Footing (f_{str} = 2.98Hz) (cont'd)

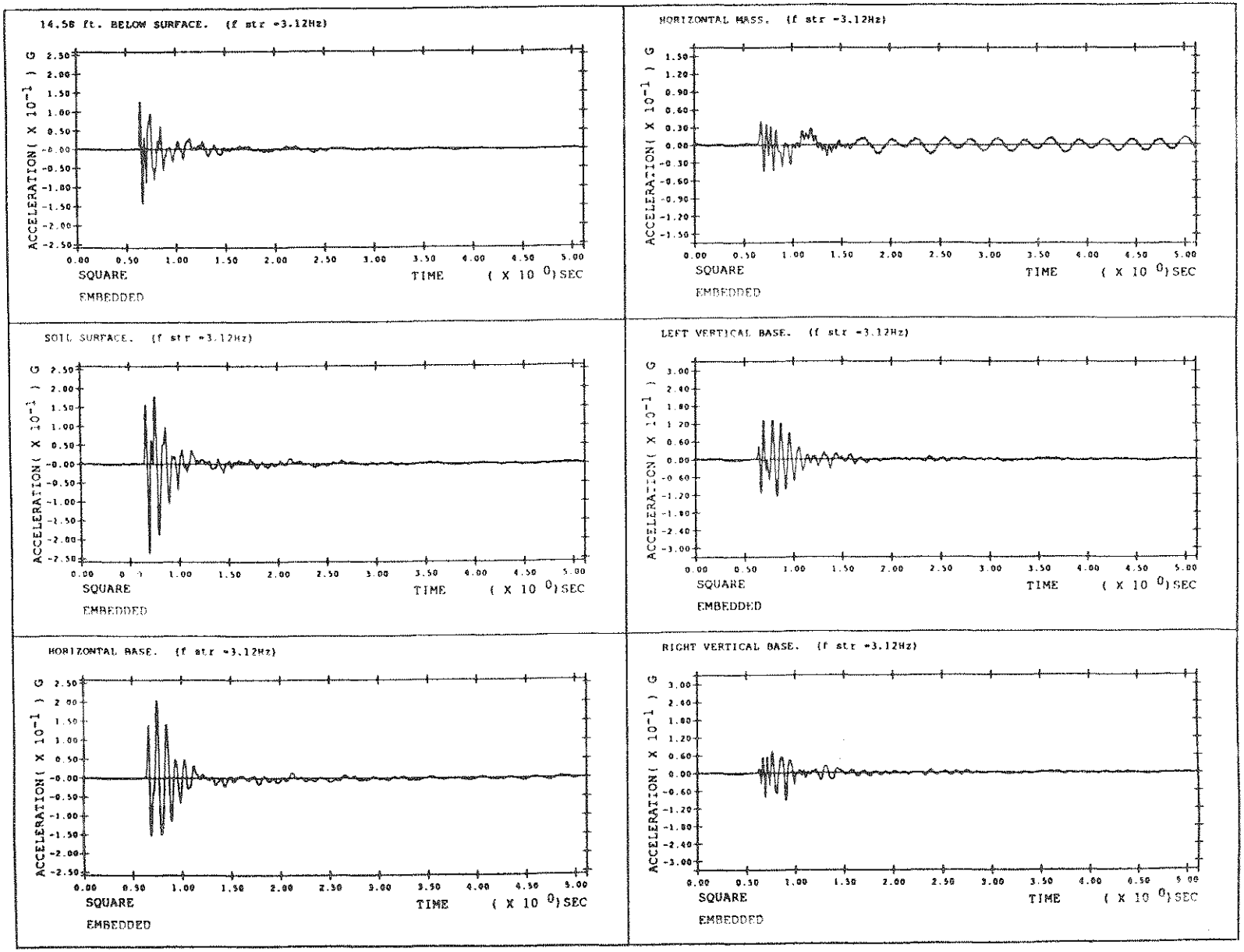

FIGURE 5-8 System with Embedded Square Footing (f_{str} = 3.12Hz)

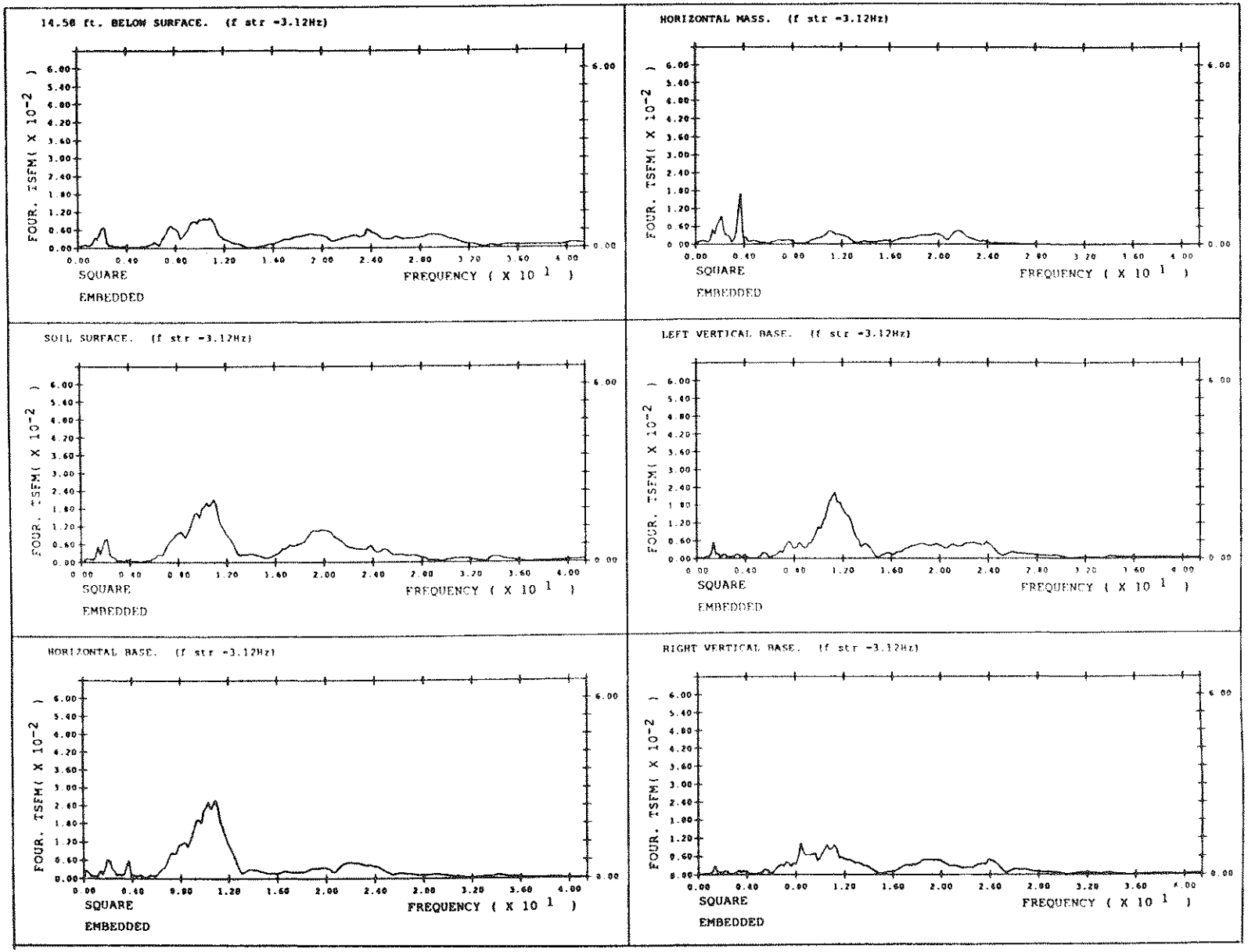

FIGURE 5-8 System with Embedded Square Footing (f_{str} = 3.12Hz) (cont'd)

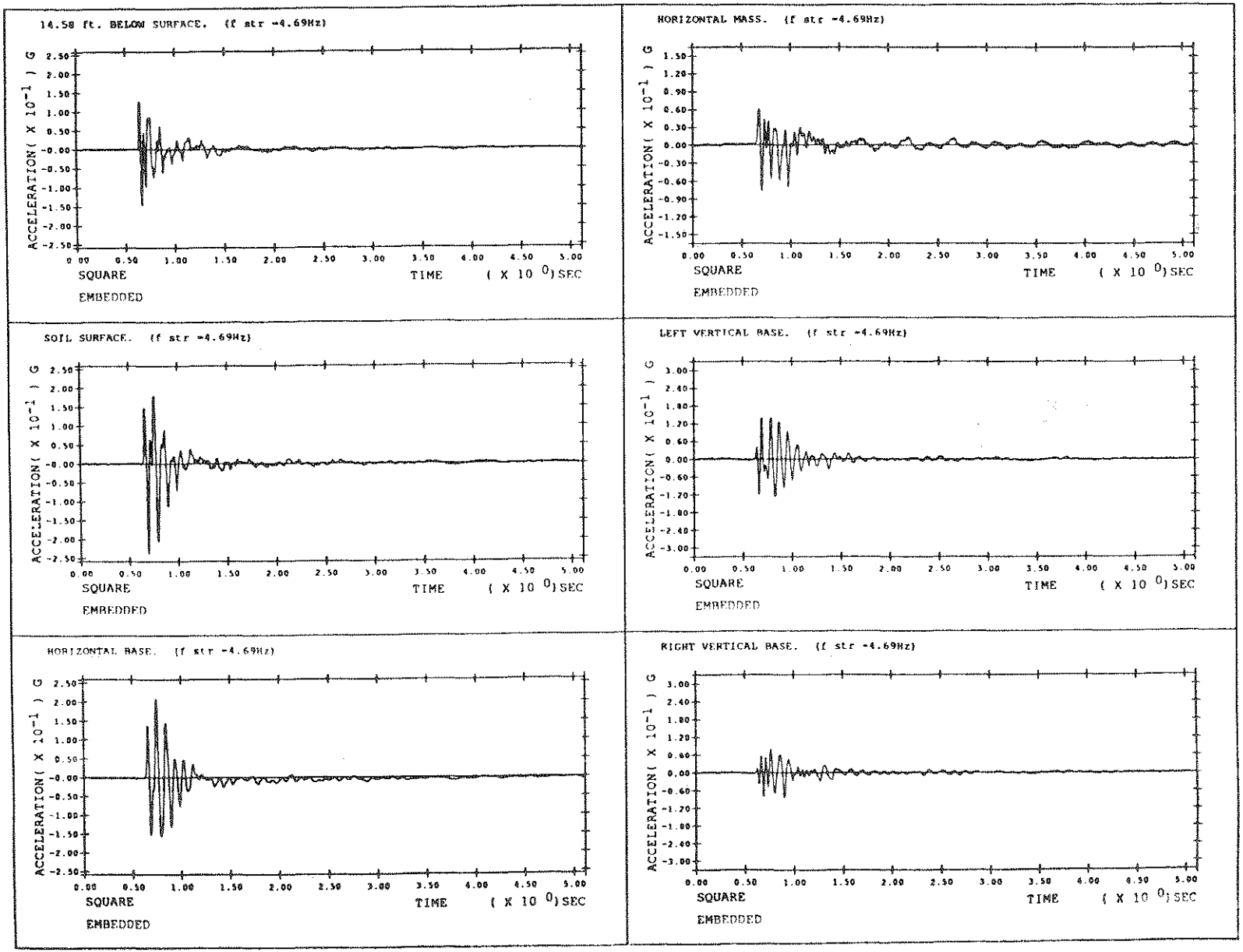

FIGURE 5-9 System with Embedded Square Footing (f_{str} = 4.69Hz)

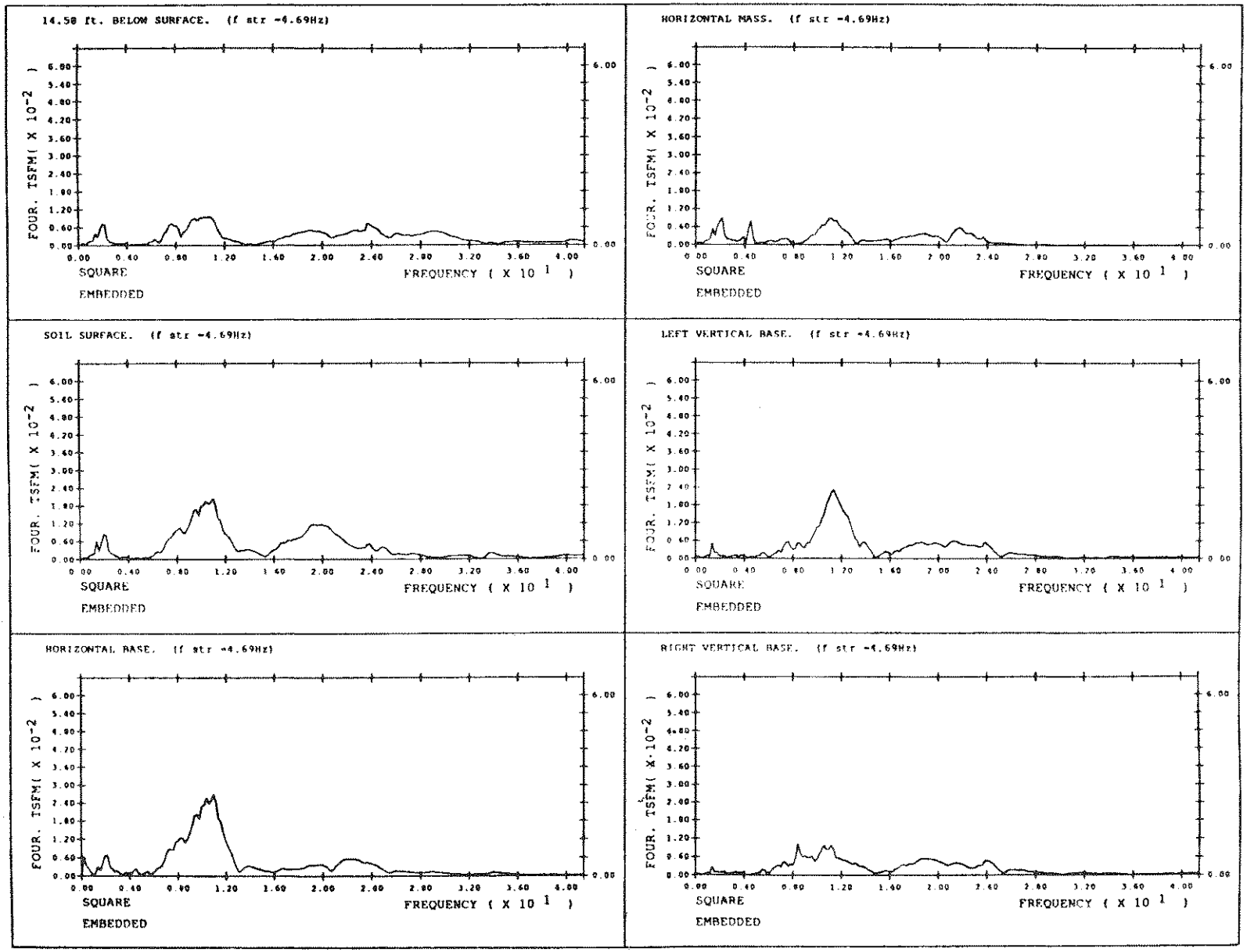

FIGURE 5-9 System with Embedded Square Footing (f_{str} = 4.69Hz) (cont'd)

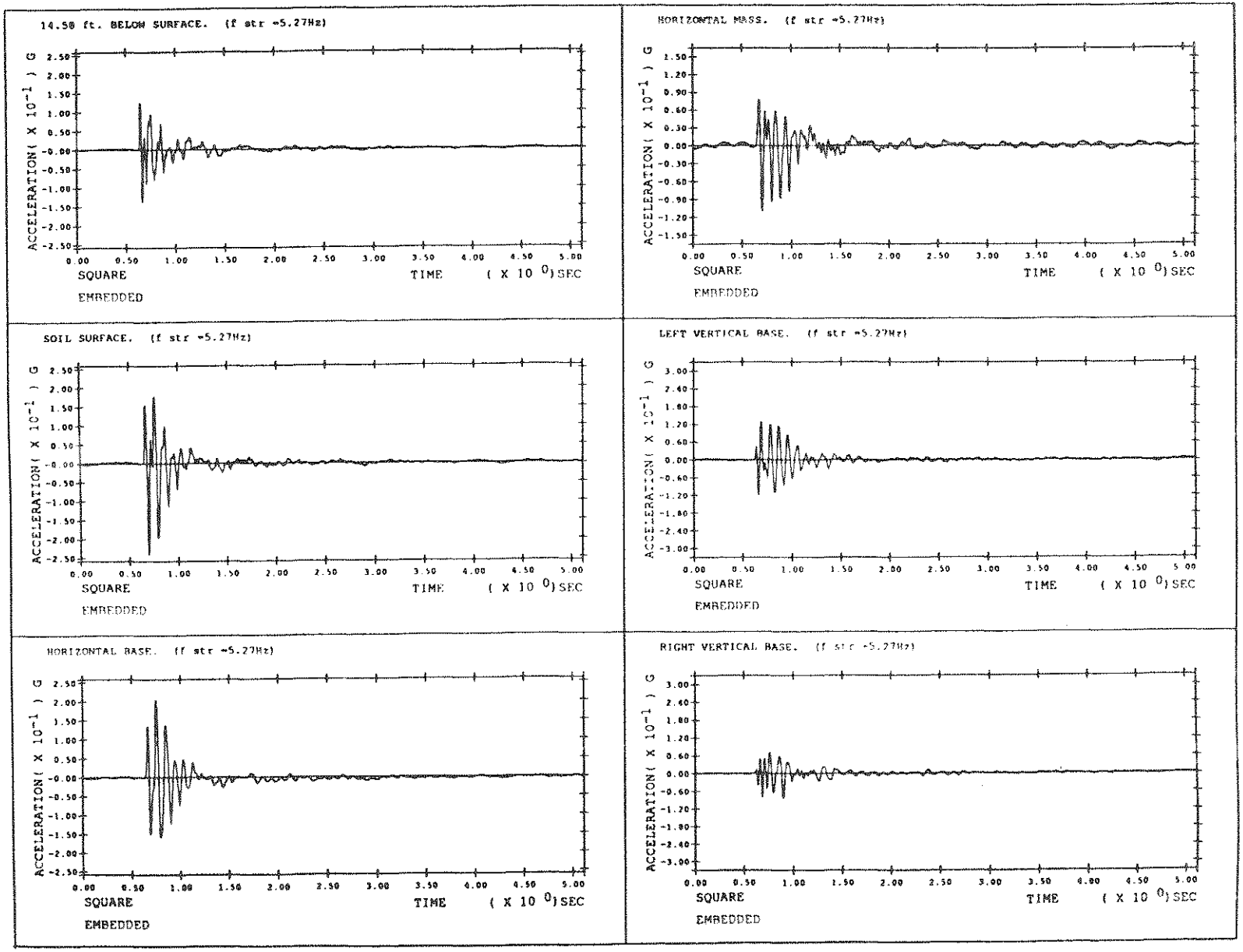

FIGURE 5-10 System with Embedded Square Footing (f_{str} = 5.27Hz)

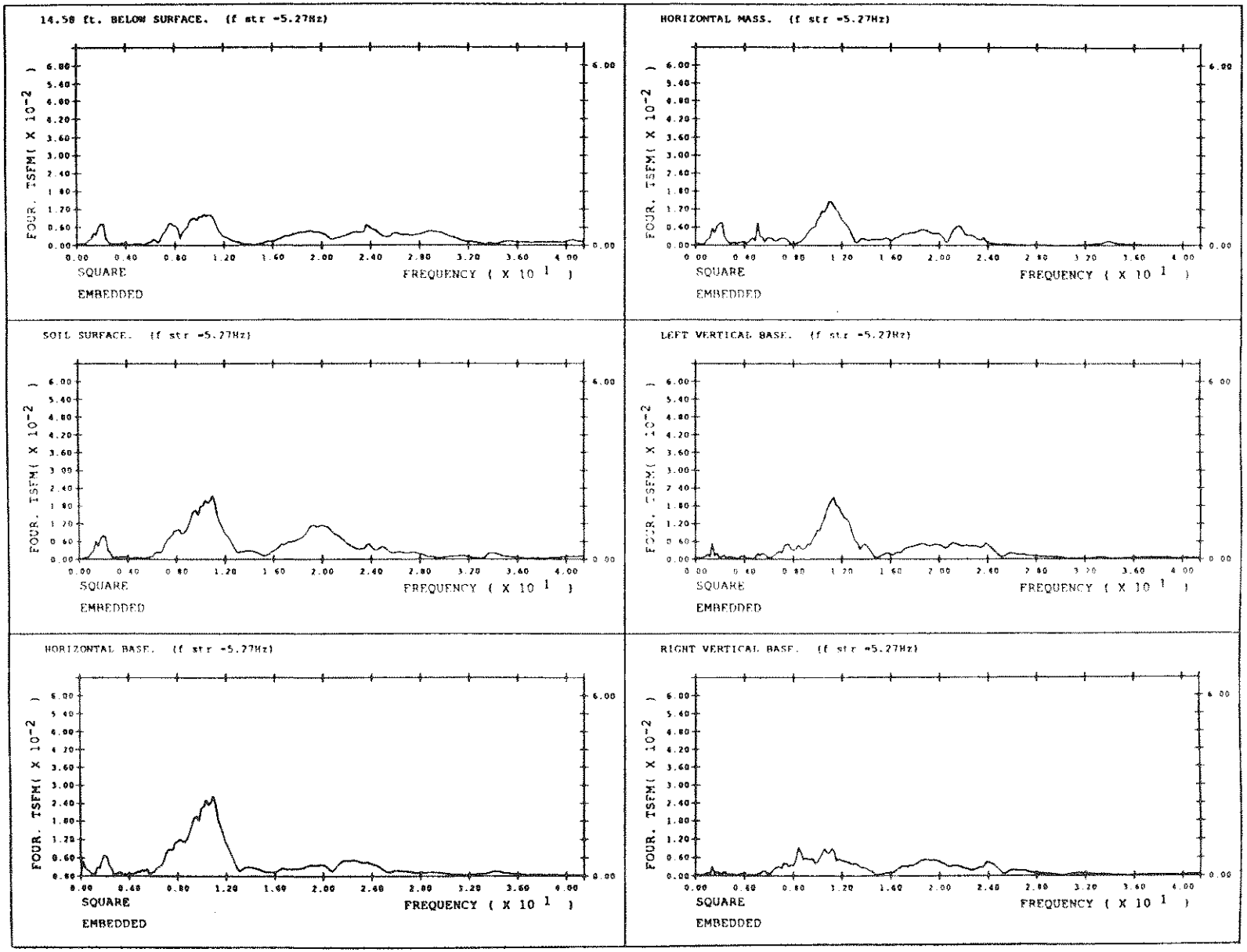

FIGURE 5-10 System with Embedded Square Footing (f_{str} = 5.27Hz) (cont'd)

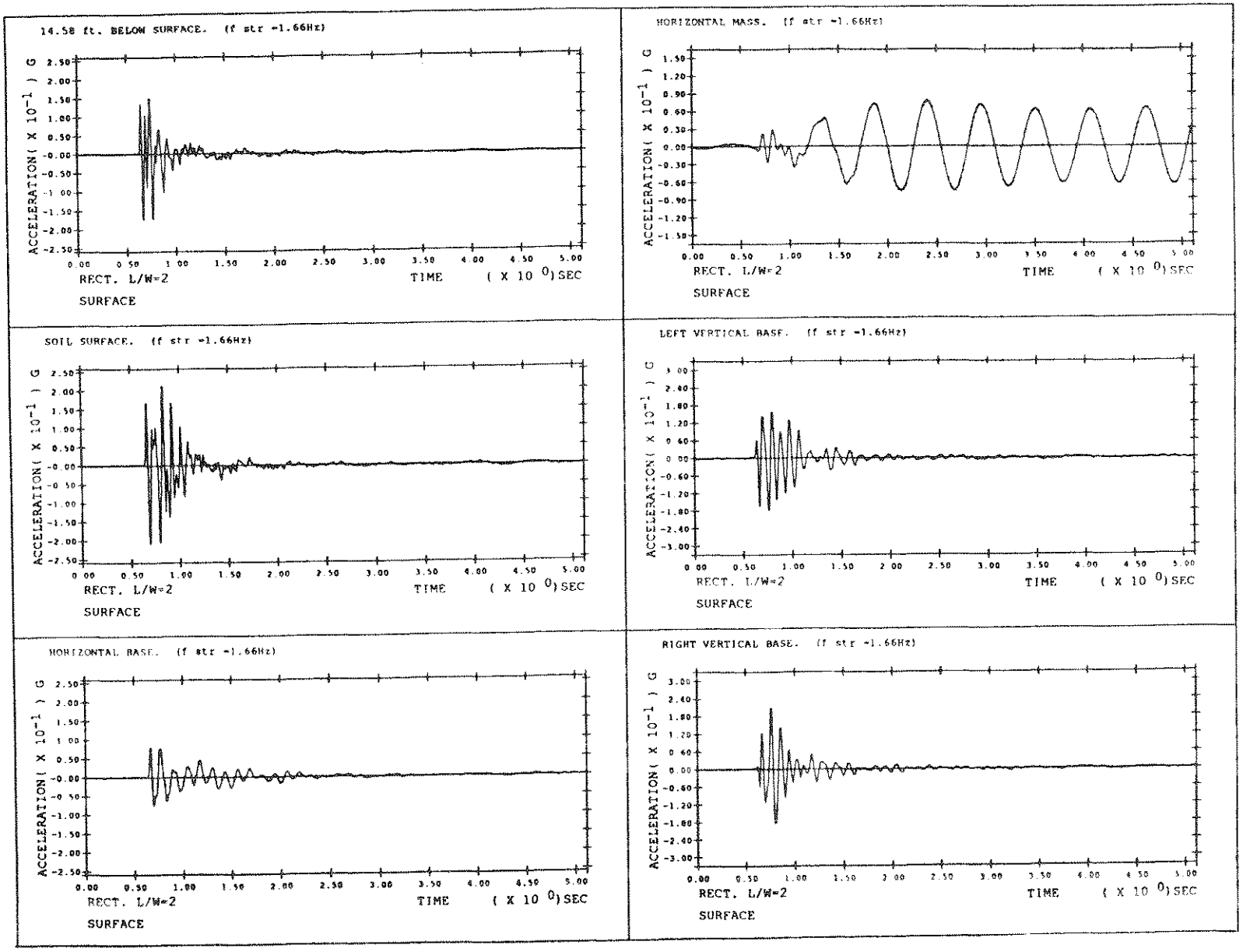

FIGURE 5-11 System with Surface Rectangular (L/W=2) Footing (f_{str} = 1.66Hz)

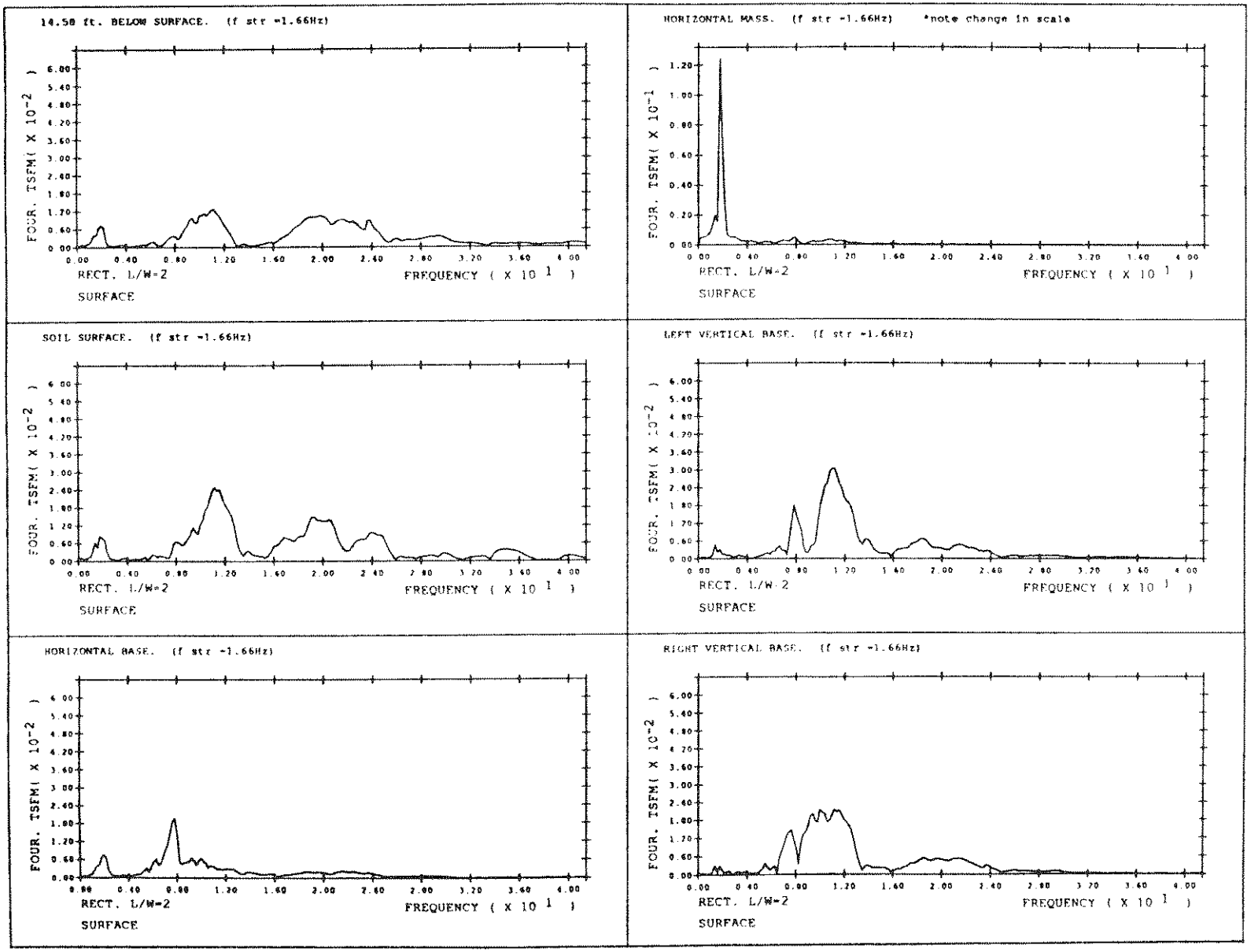

FIGURE 5-11 System with Surface Rectangular (L/W=2) Footing (f_{str} = 1.66Hz) (cont'd)

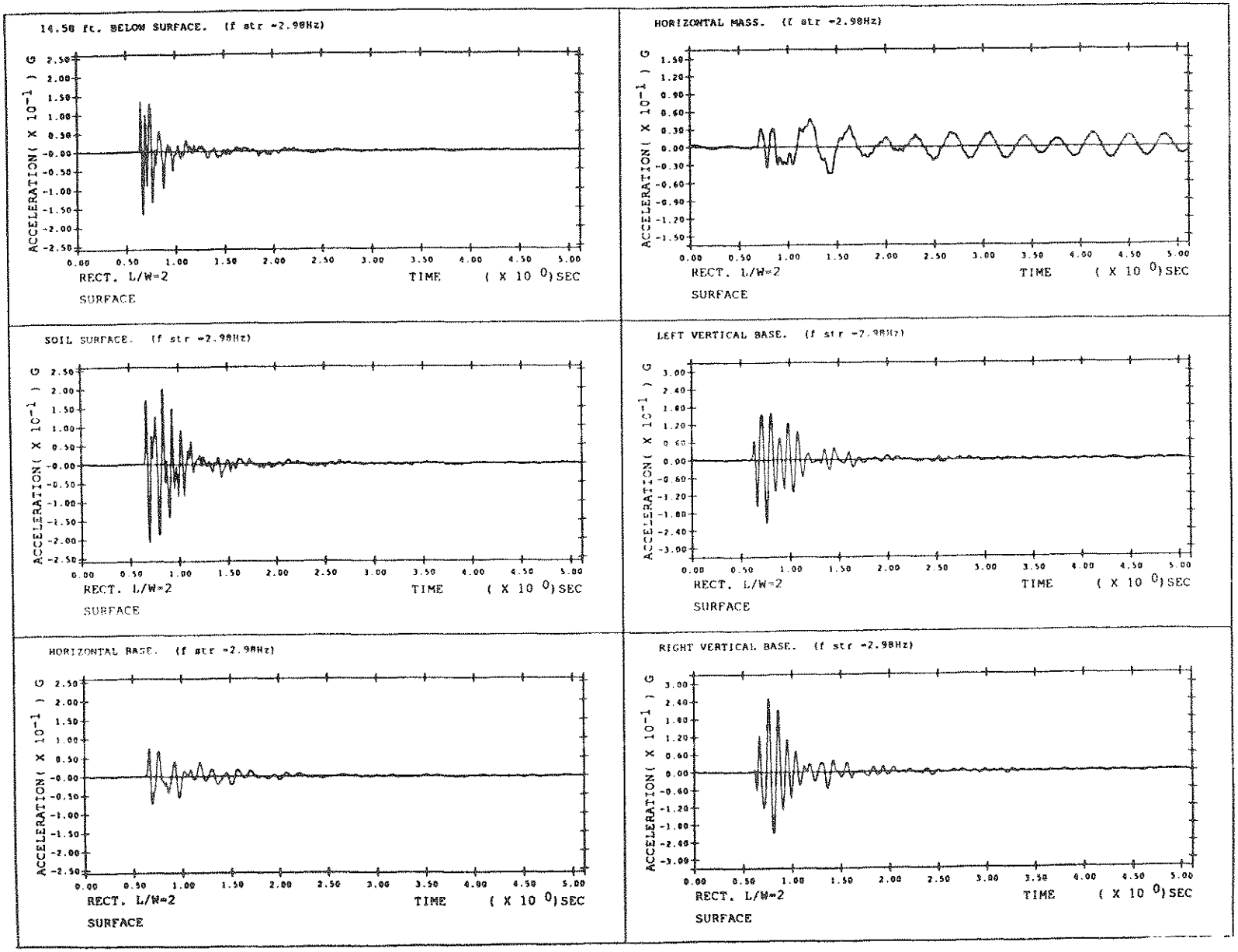

FIGURE 5-12 System with Surface Rectangular (L/W=2) Footing (f_{str} = 2.98Hz)

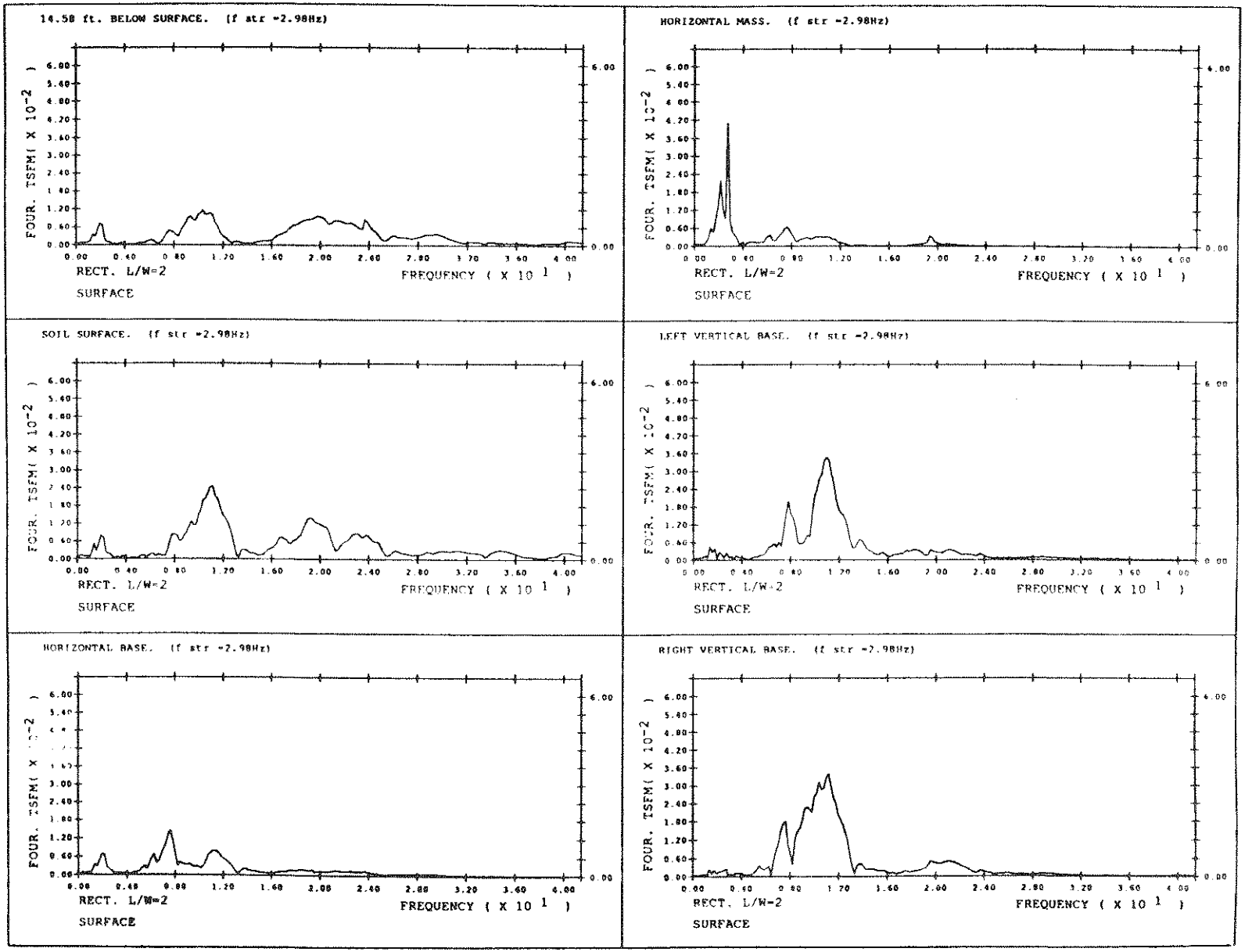

FIGURE 5-12 System with Surface Rectangular (L/W=2) Footing (f_{str} = 2.98Hz) (cont'd)

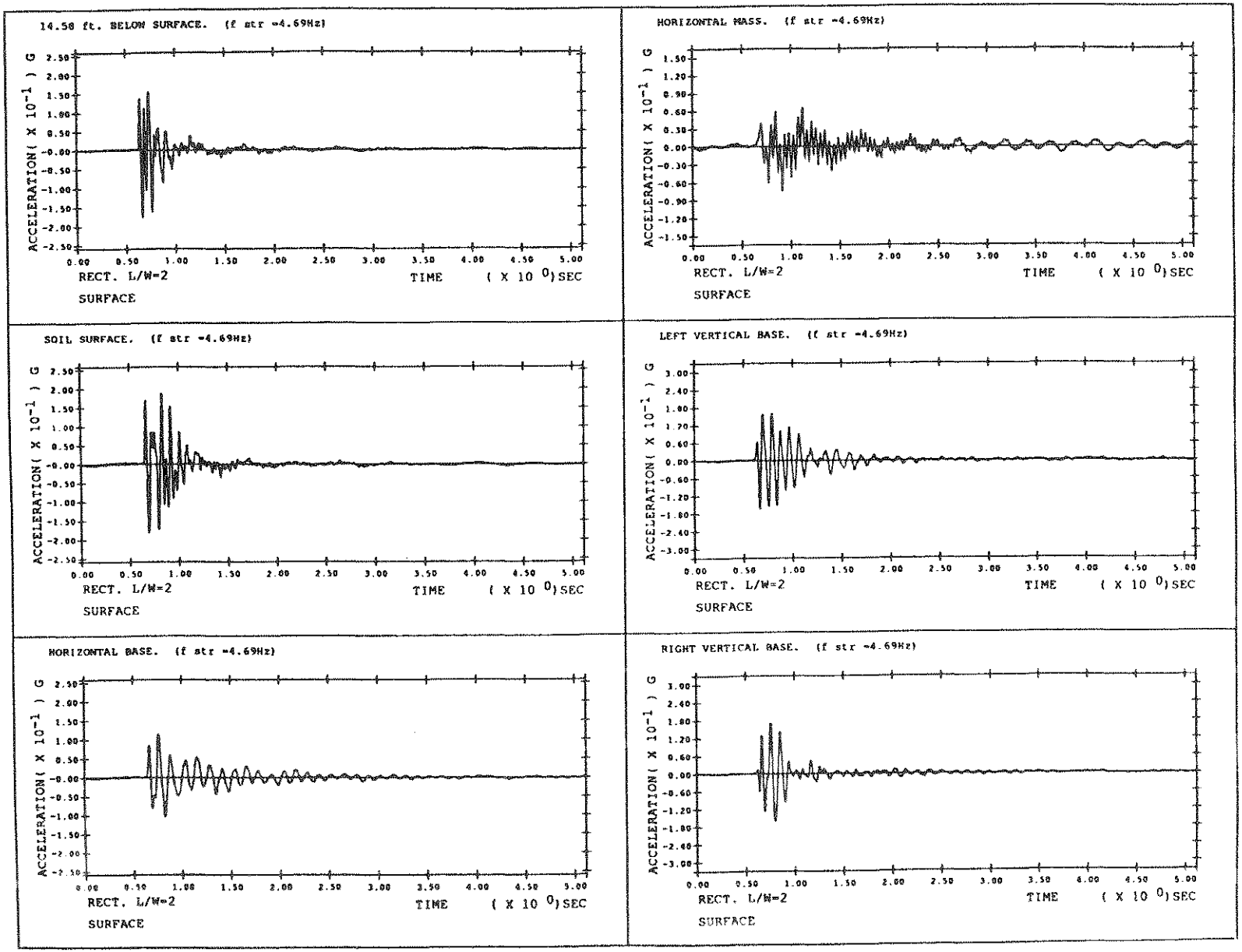

FIGURE 5-13 System with Surface Rectangular (L/W=2) Footing (f_{str} = 4.69Hz)

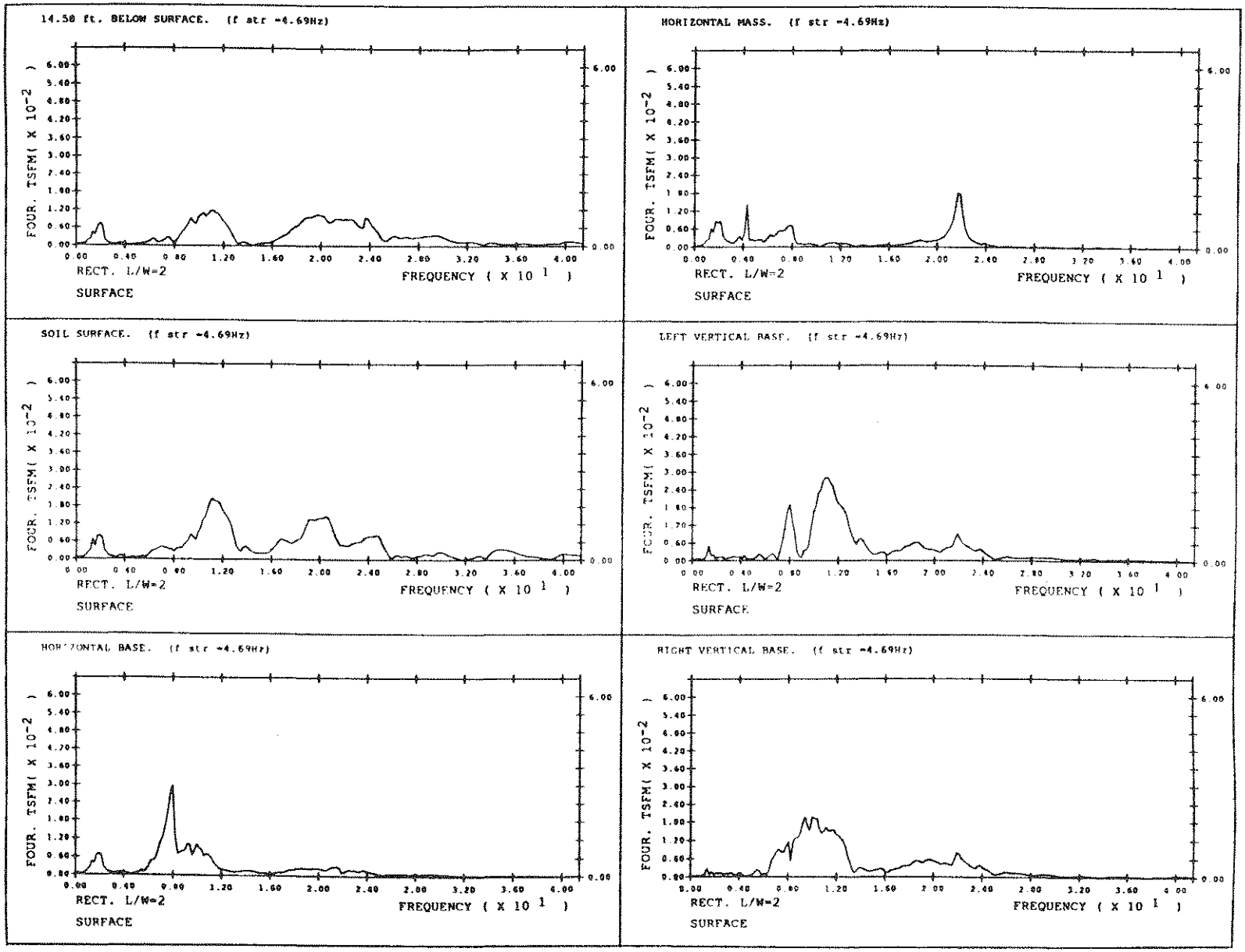

FIGURE 5-13 System with Surface Rectangular (L/W=2) Footing (f_{str} = 4.69Hz) (cont'd)

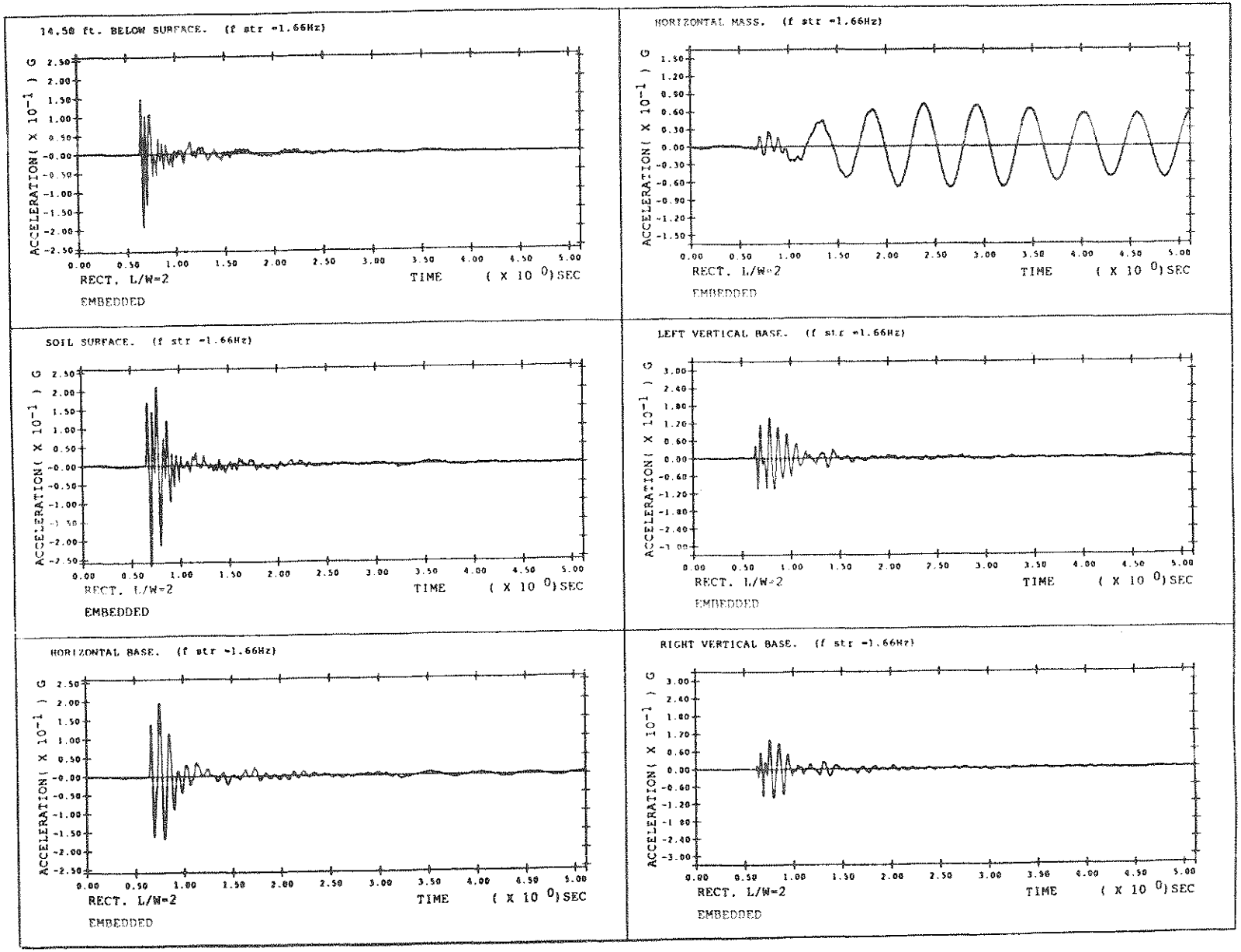

FIGURE 5-14 System with Embedded Rectangular (L/W=2) Footing (f_{str} = 1.66Hz)

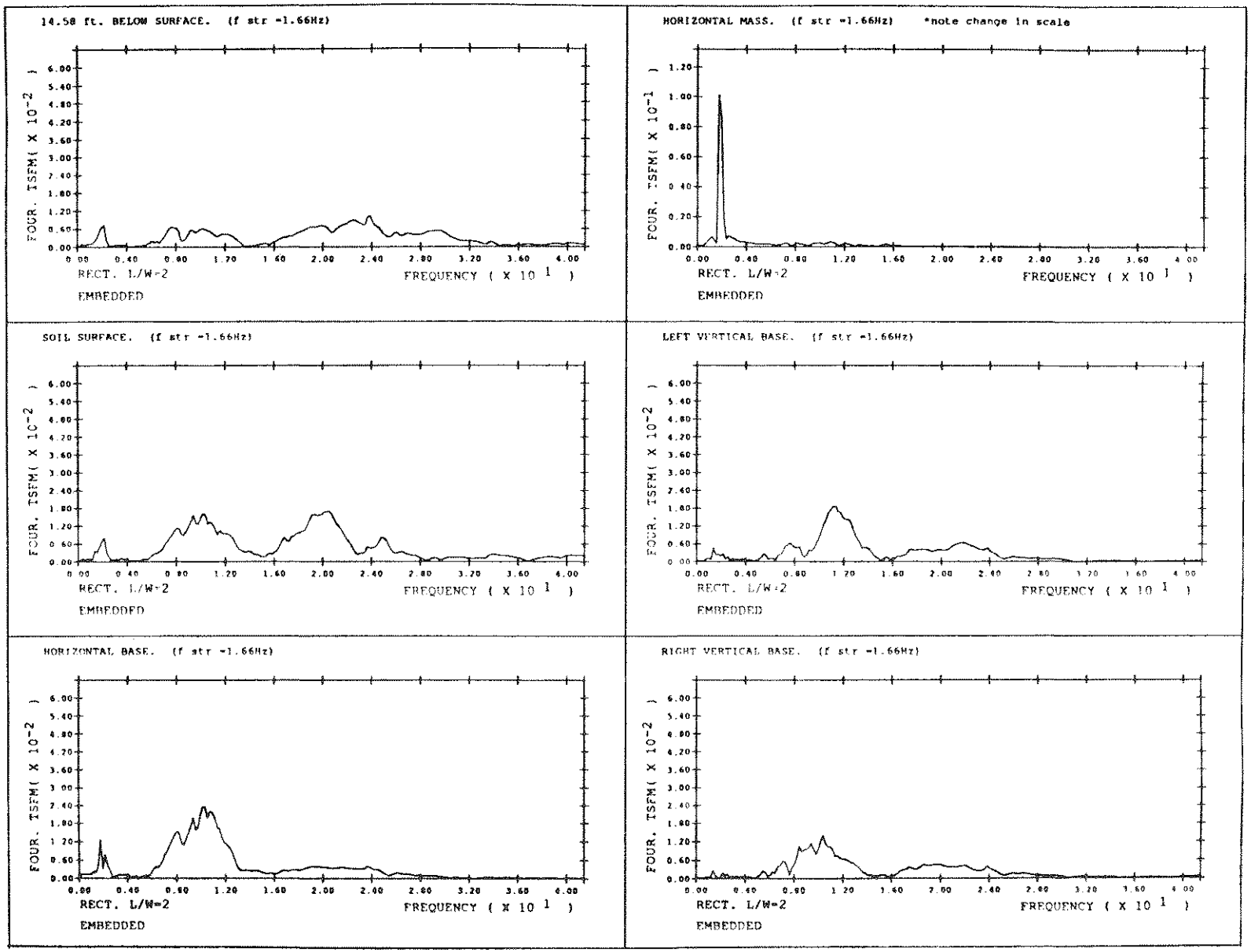

FIGURE 5-14 System with Embedded Rectangular (L/W=2) Footing (f_{str} = 1.66Hz) (cont'd)

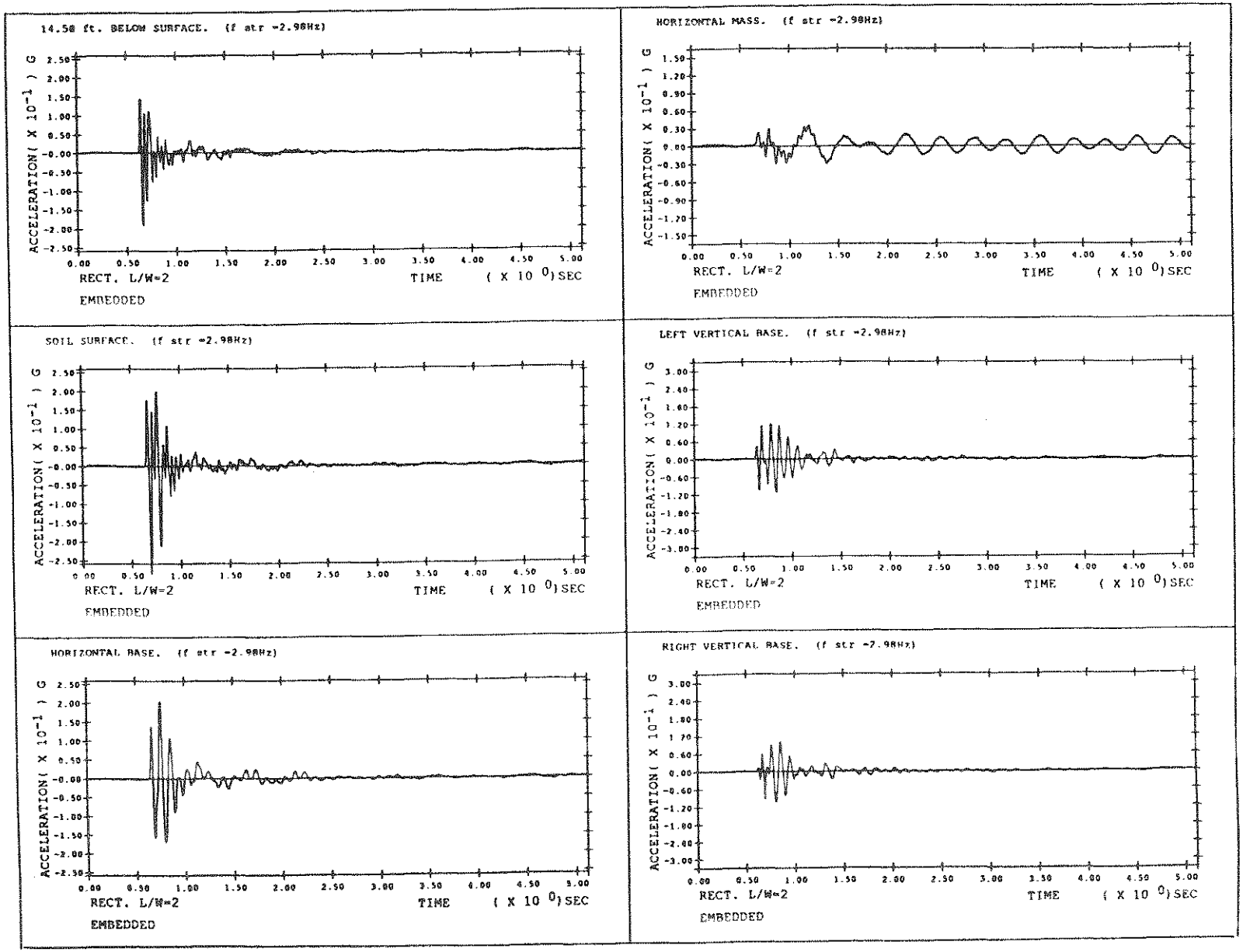

FIGURE 5-15 System with Embedded Rectangular (L/W=2) Footing (f_{str} = 2.98Hz)

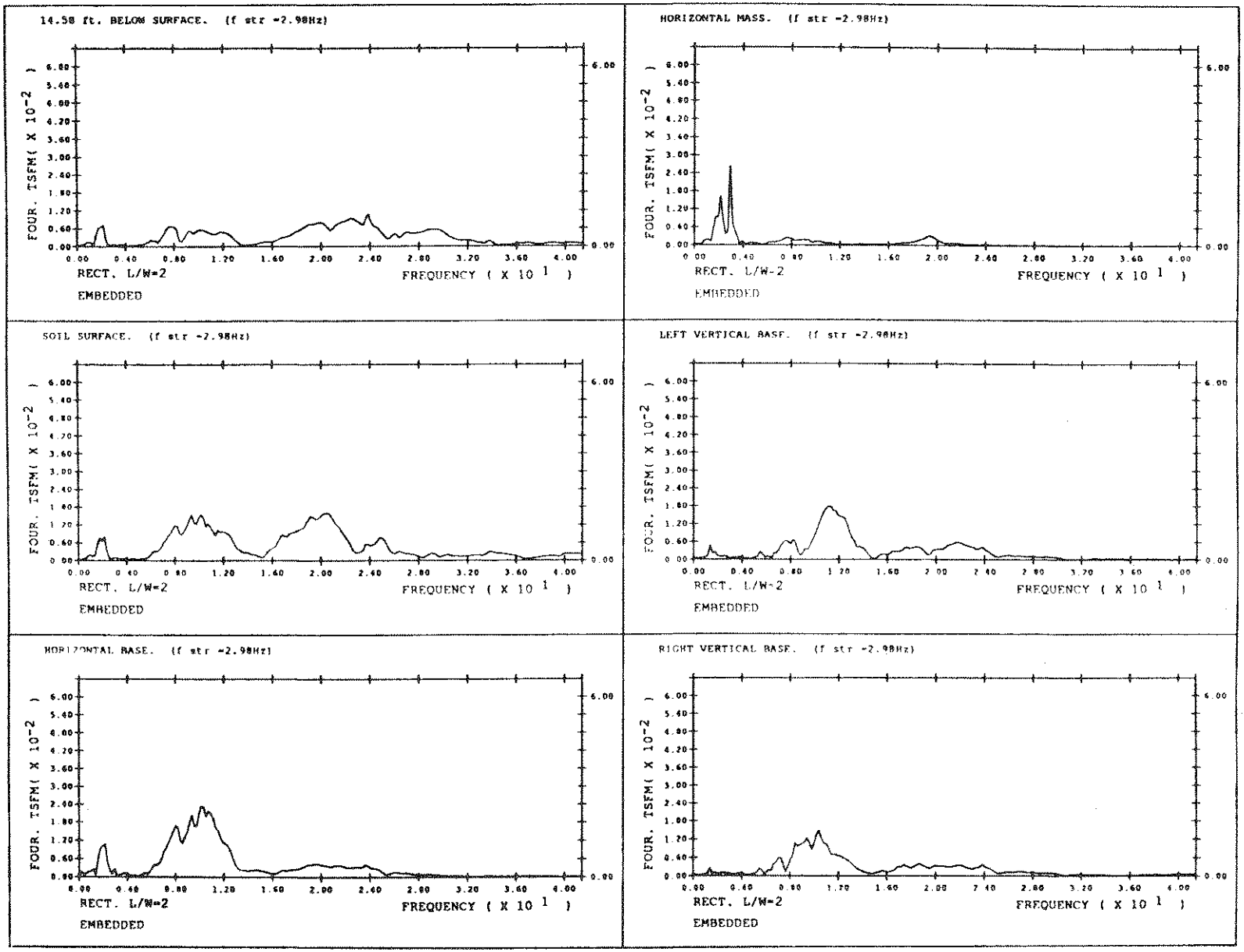

FIGURE 5-15 System with Embedded Rectangular (L/W=2) Footing (f_{str} = 2.98Hz) (cont'd)

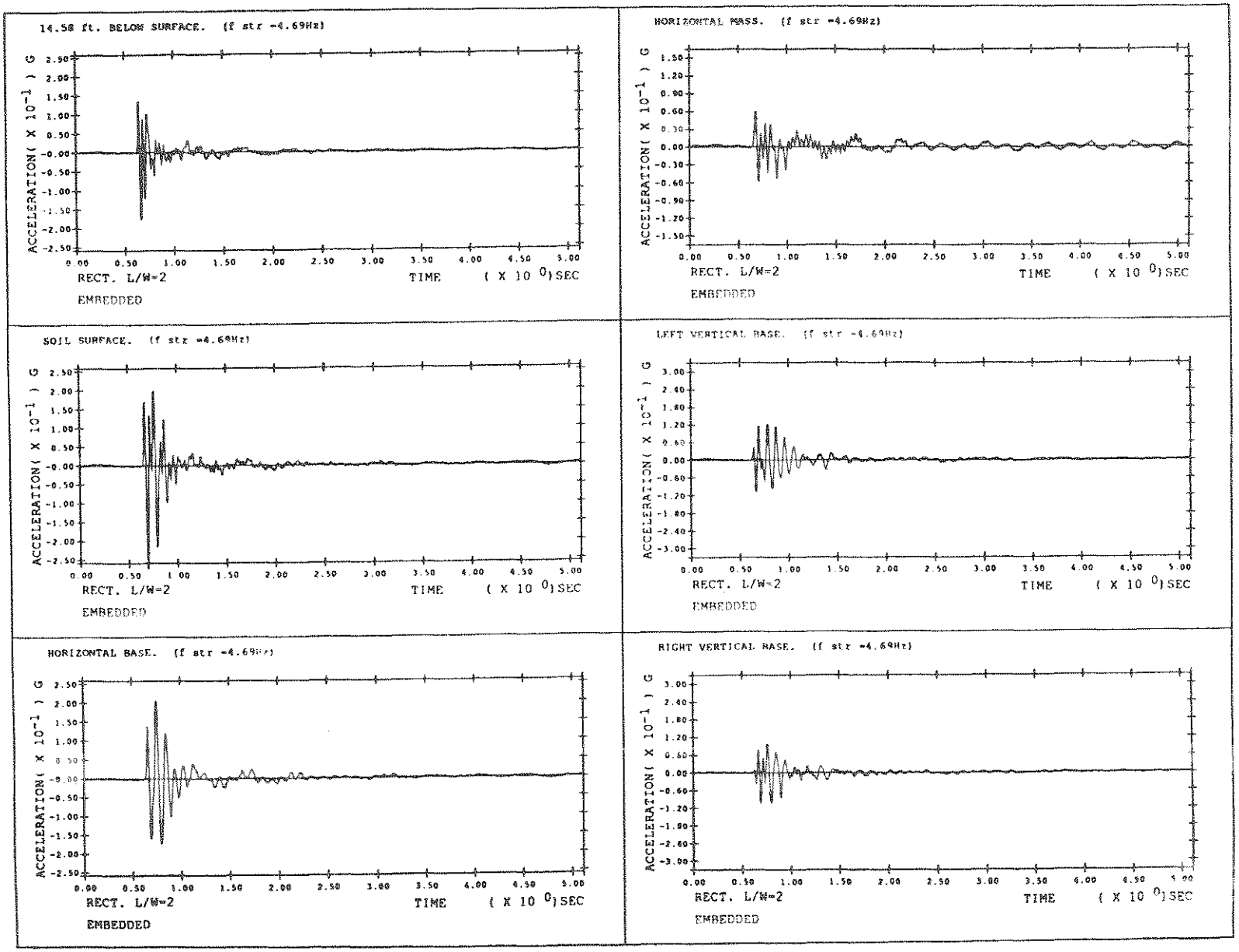

FIGURE 5-16 System with Embedded Rectangular (L/W=2) Footing (f_{str} = 4.69Hz)

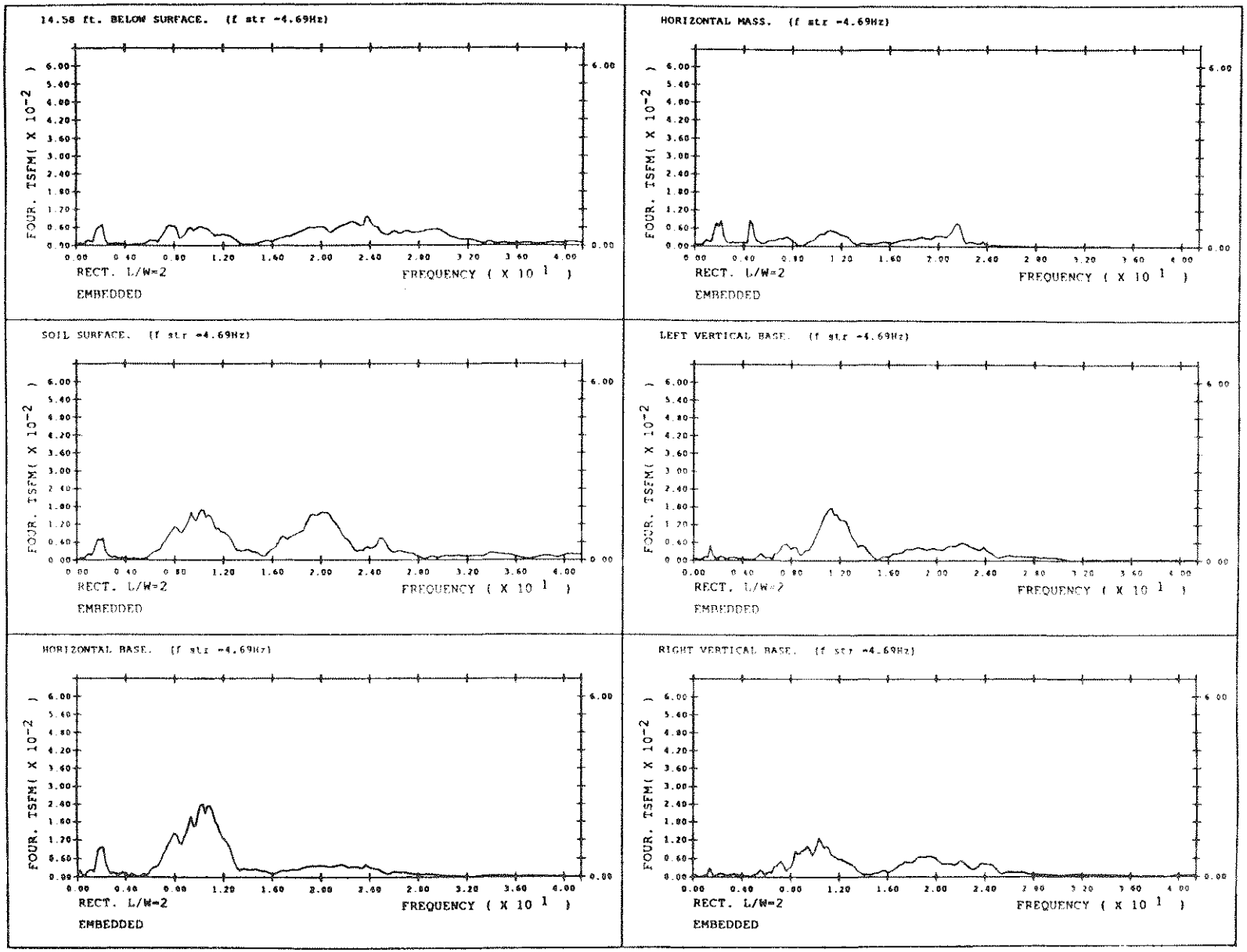

FIGURE 5-16 System with Embedded Rectangular (L/W=2) Footing (f_{str} = 4.69Hz) (cont'd)

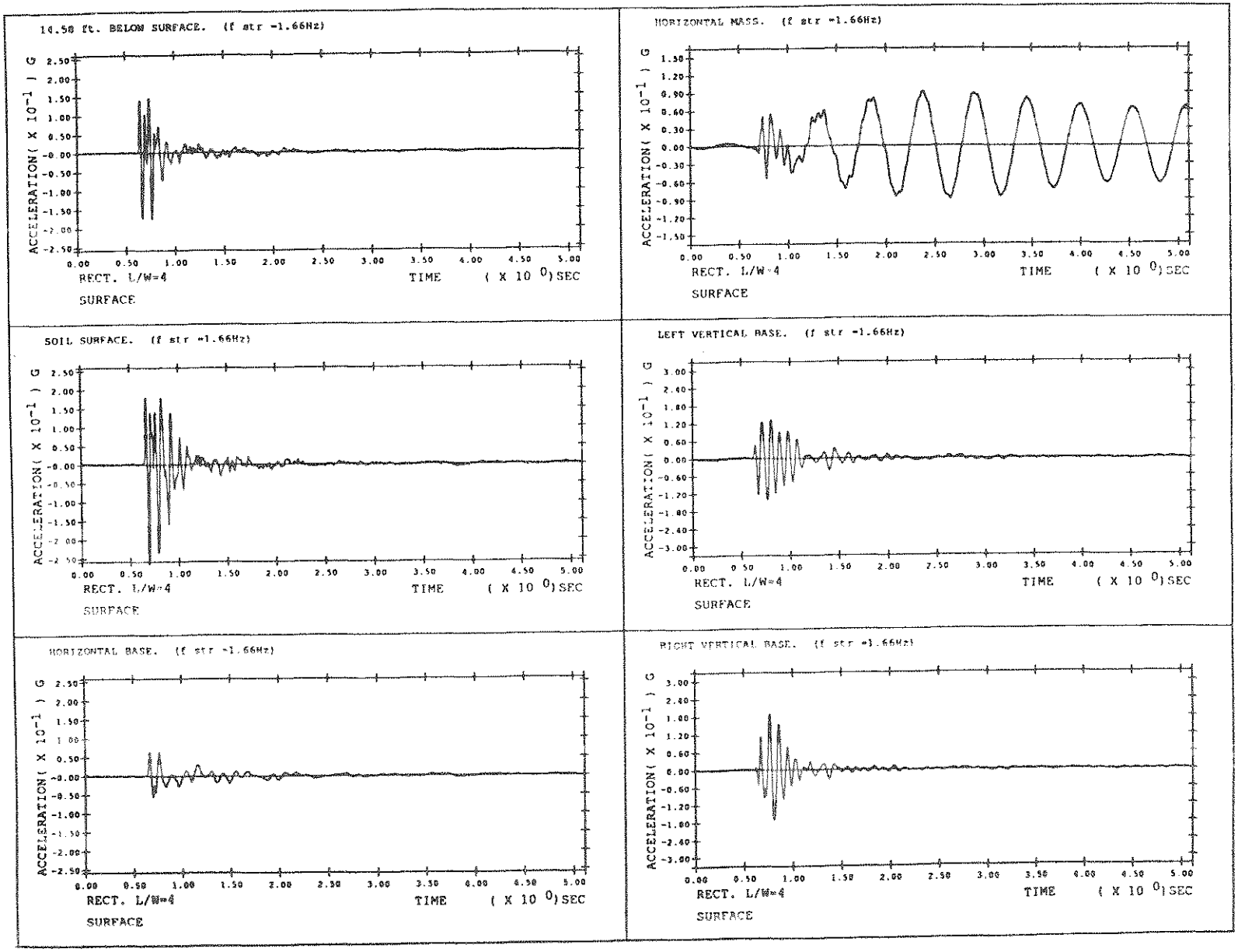

FIGURE 5-17 System with Surface Rectangular (L/W=4) Footing (f_{str} = 1.66Hz)

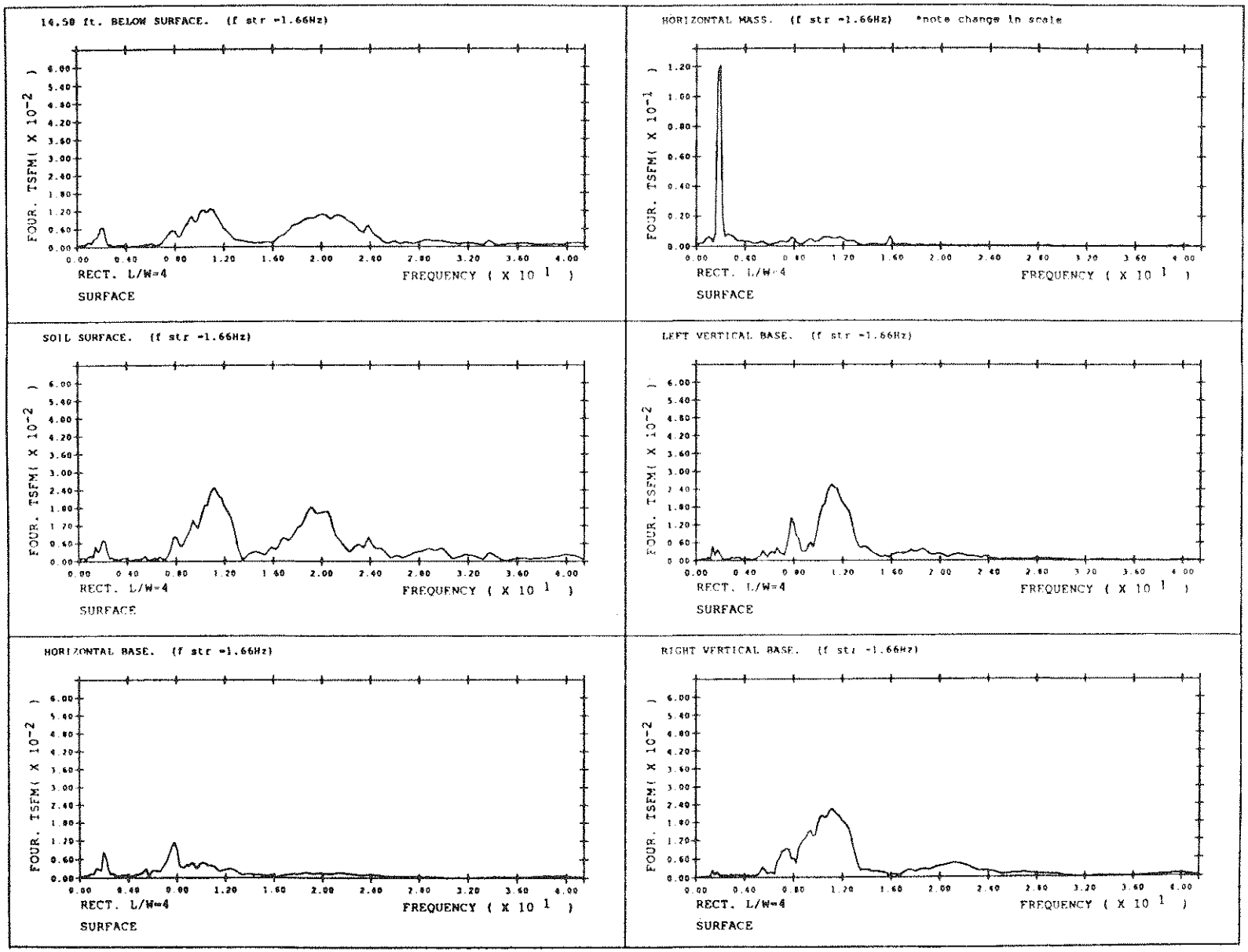

FIGURE 5-17 System with Surface Rectangular (L/W=4) Footing (f_{str} = 1.66Hz) (cont'd)

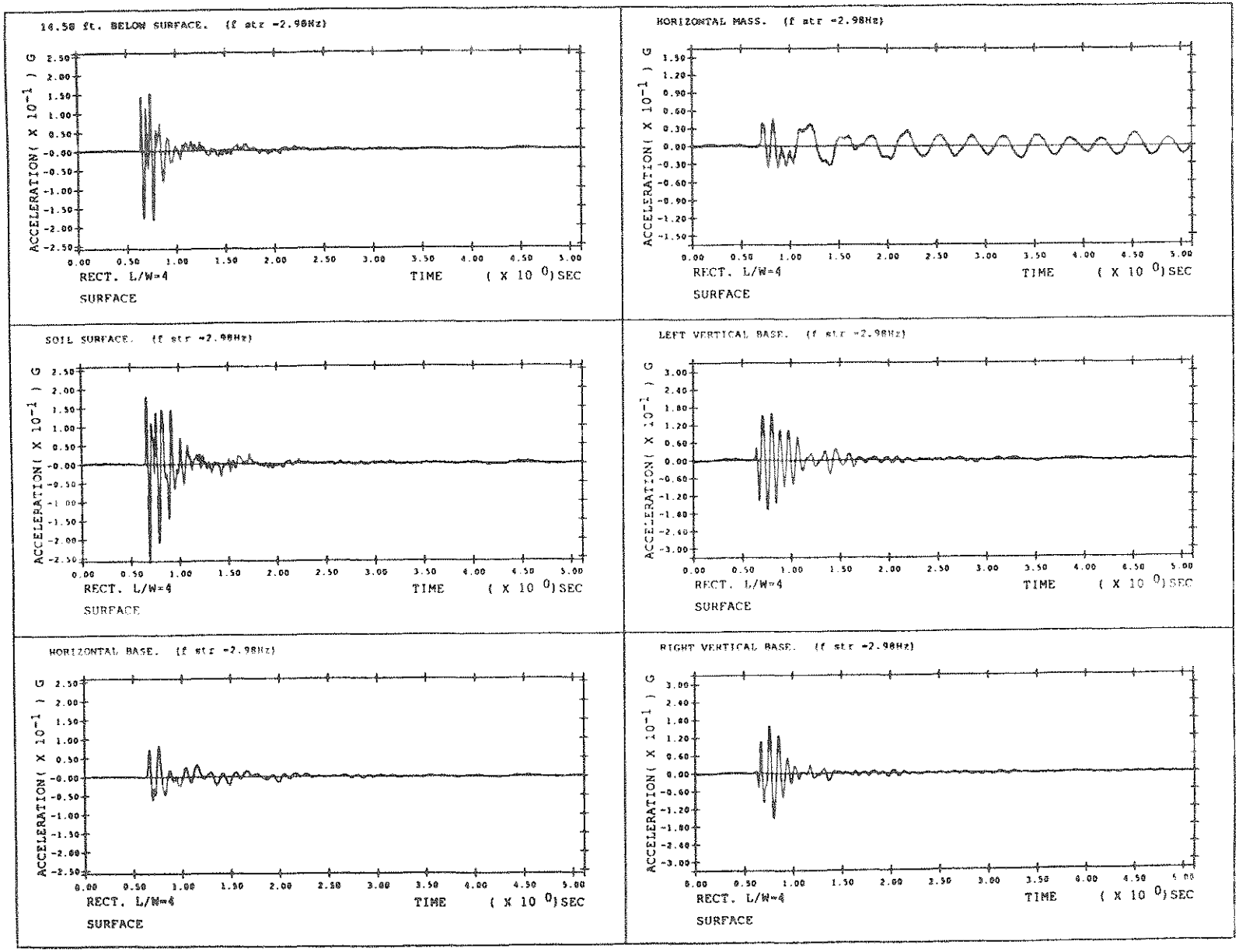

FIGURE 5-18 System with Surface Rectangular (L/W=4) Footing (f_{str} = 2.98Hz)

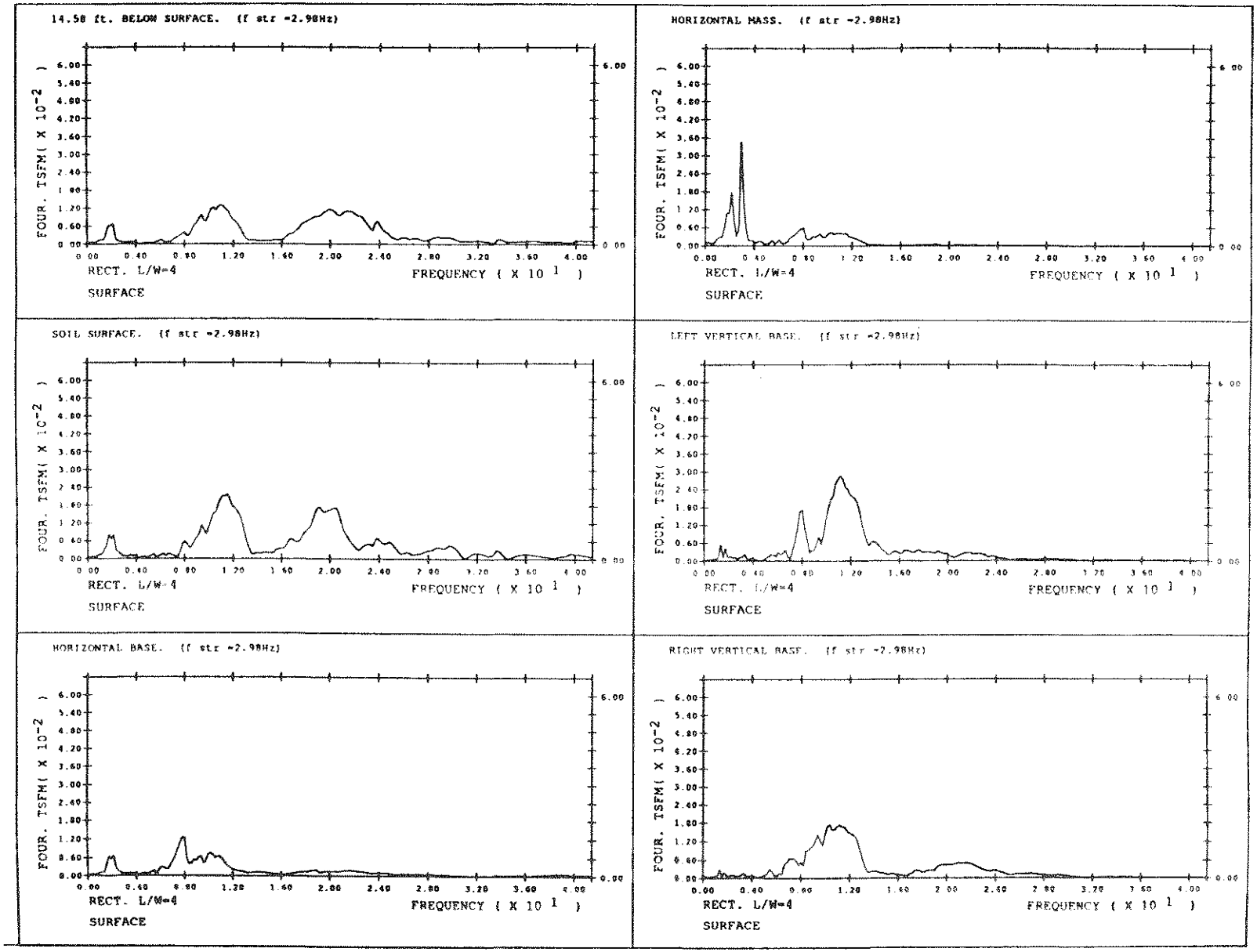

FIGURE 5-18 System with Surface Rectangular (L/W=4) Footing (f_{str} = 2.98Hz) (cont'd)

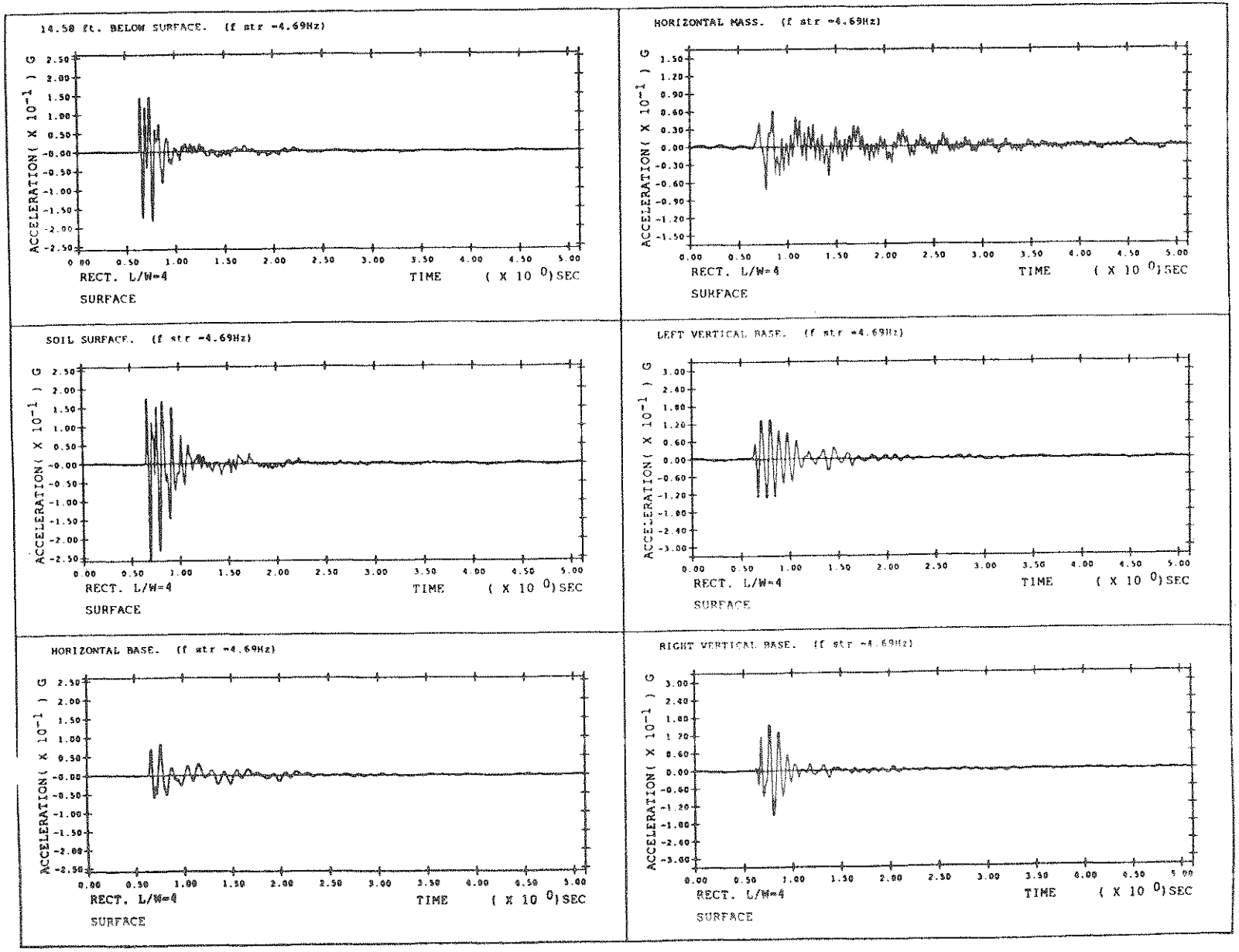

FIGURE 5-19 System with Surface Rectangular (L/W=4) Footing (f_{str} = 4.69Hz)

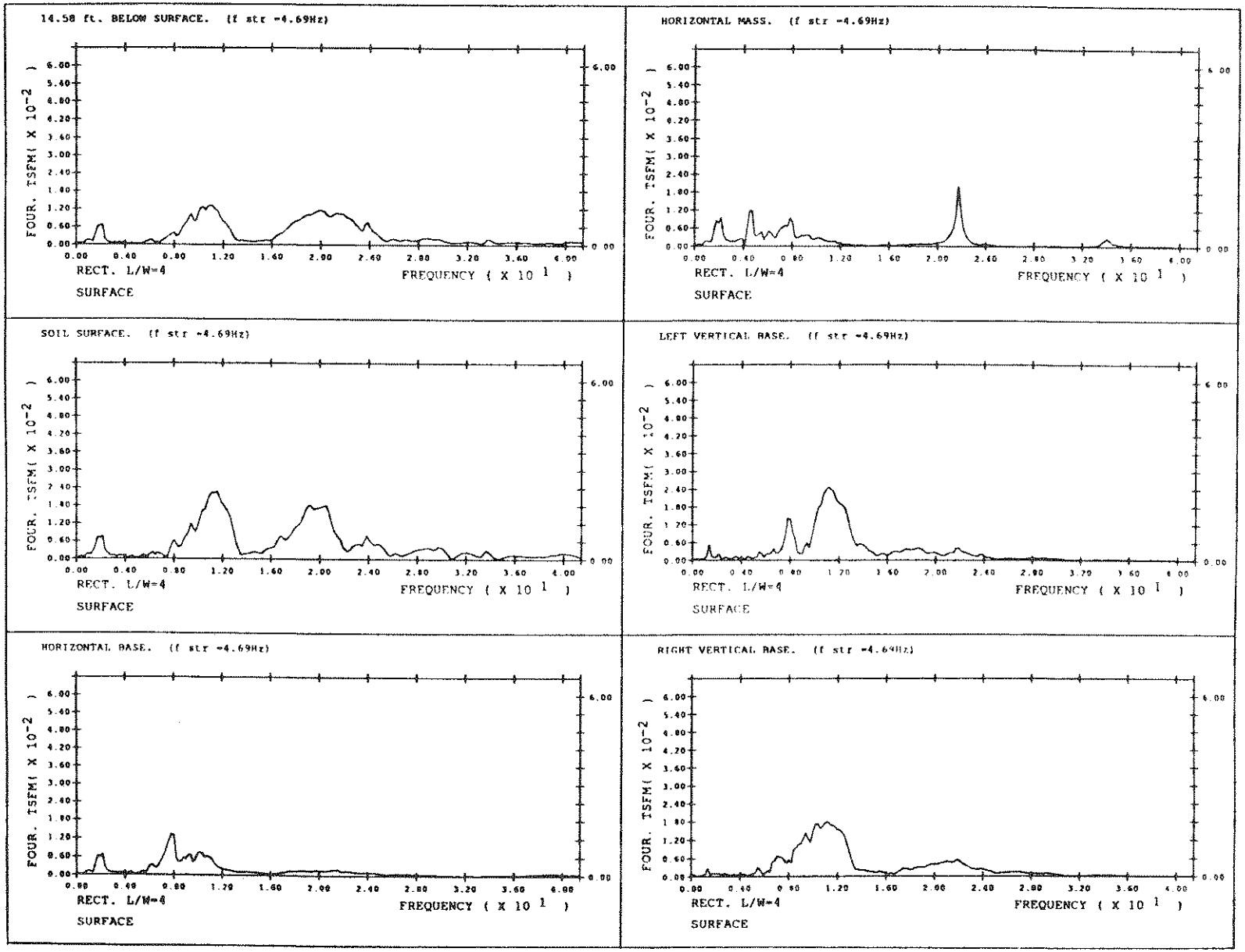

FIGURE 5-19 System with Surface Rectangular (L/W=4) Footing (f_{str} = 4.69Hz) (cont'd)

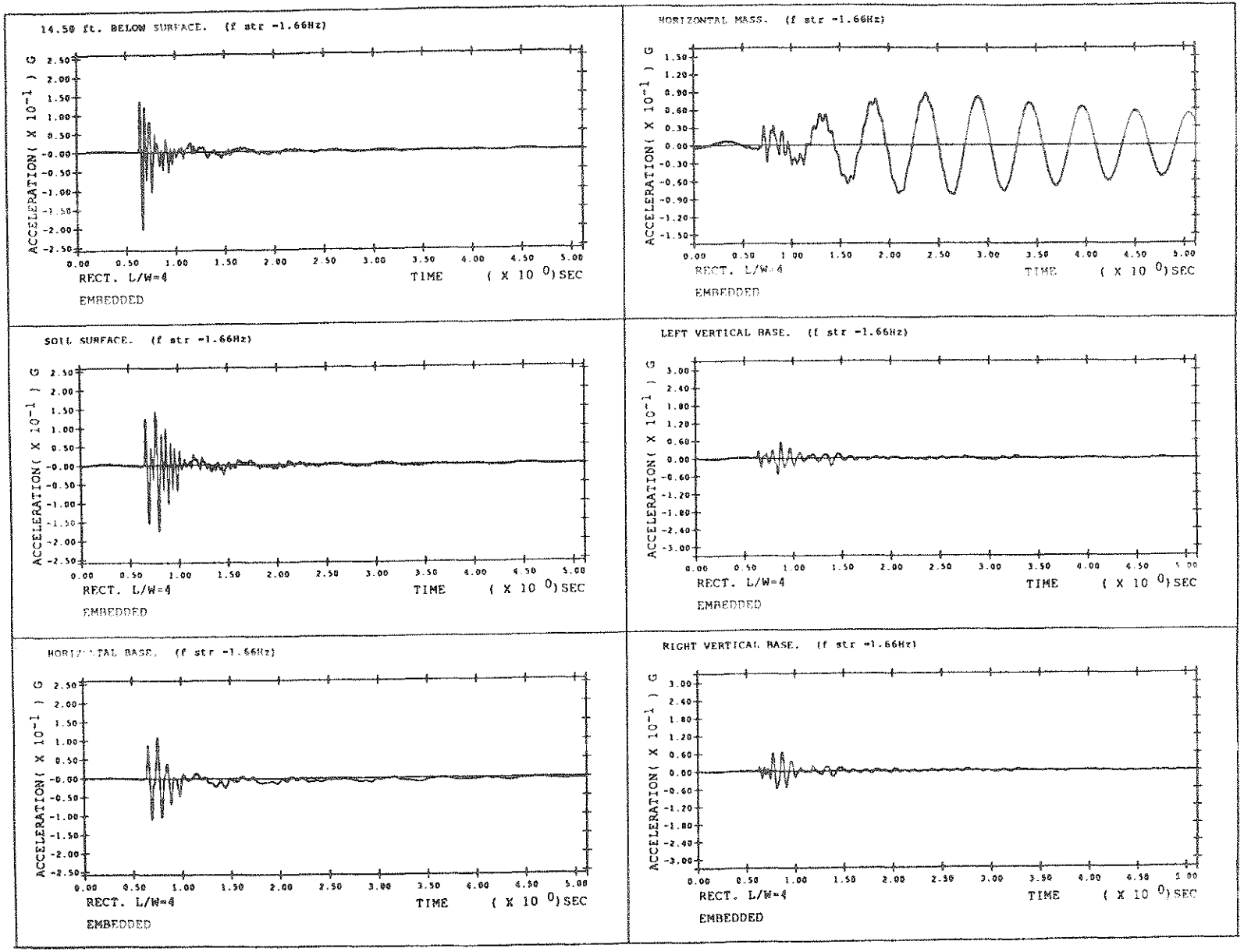

FIGURE 5-20 System with Embedded Rectangular (L/W=4) Footing (f_{str} = 1.66Hz)

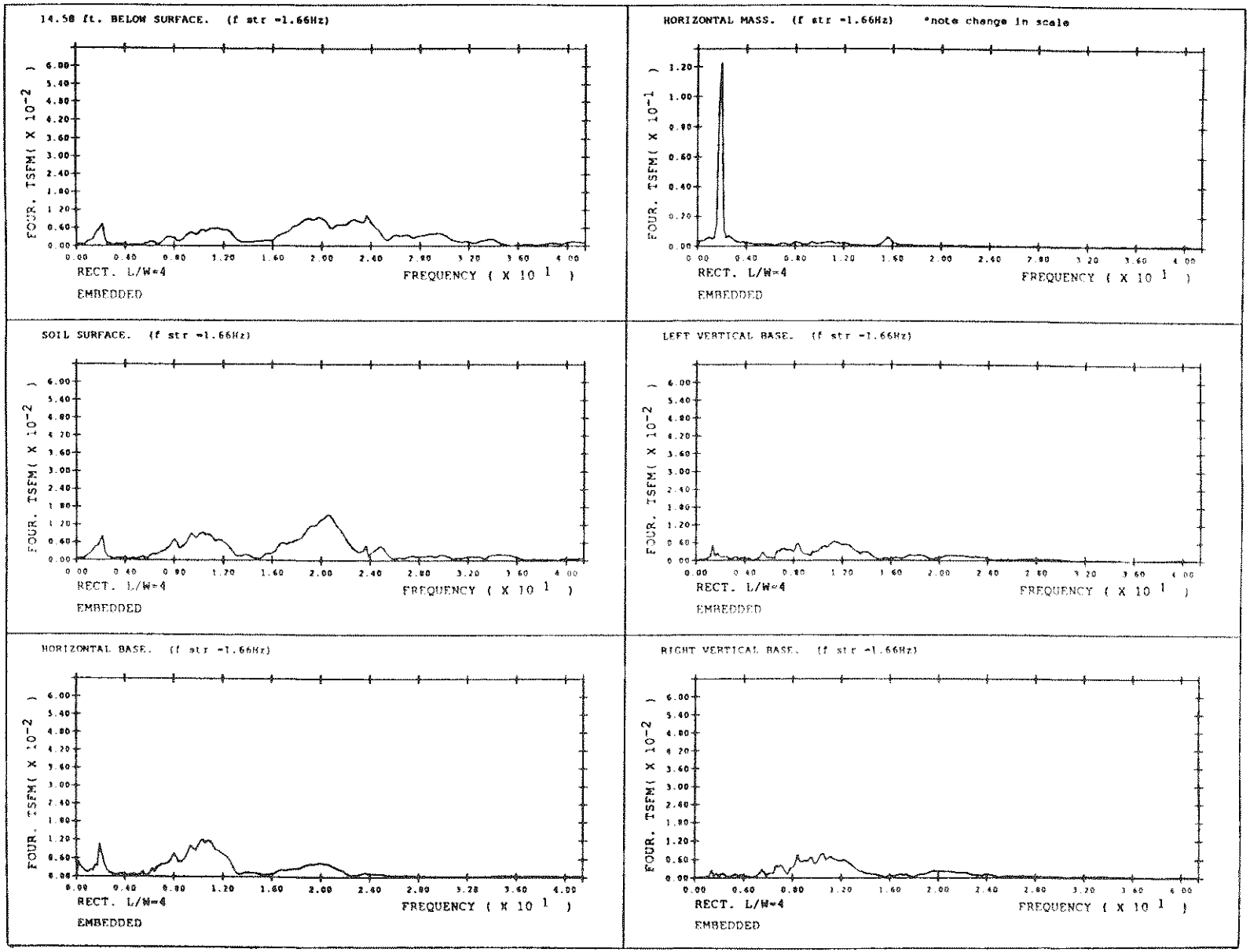

FIGURE 5-20 System with Embedded Rectangular (L/W=4) Footing (f_{str} = 1.66Hz) (cont'd)

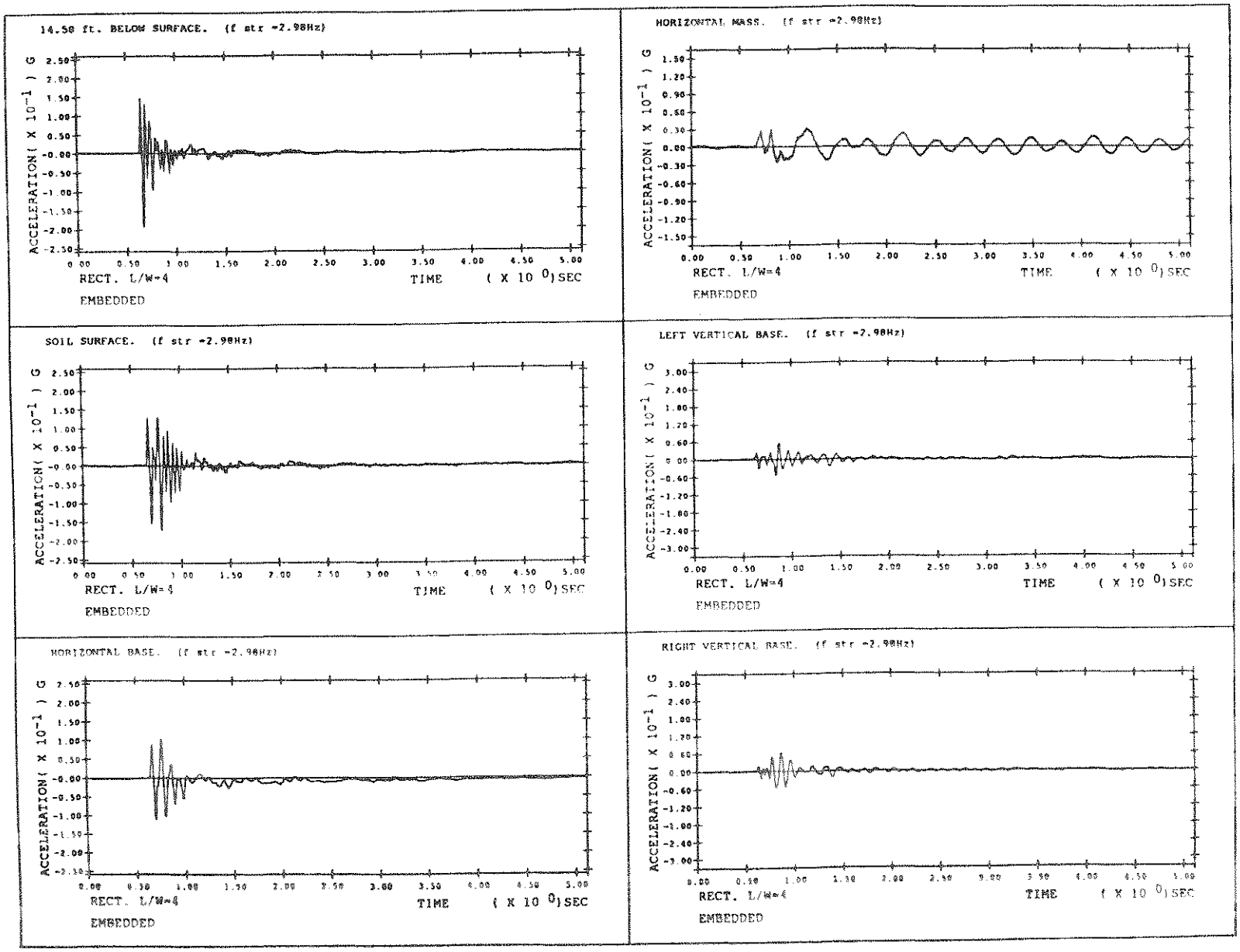

FIGURE 5-21 System with Embedded Rectangular (L/W=4) Footing (f_{str} = 2.98Hz)

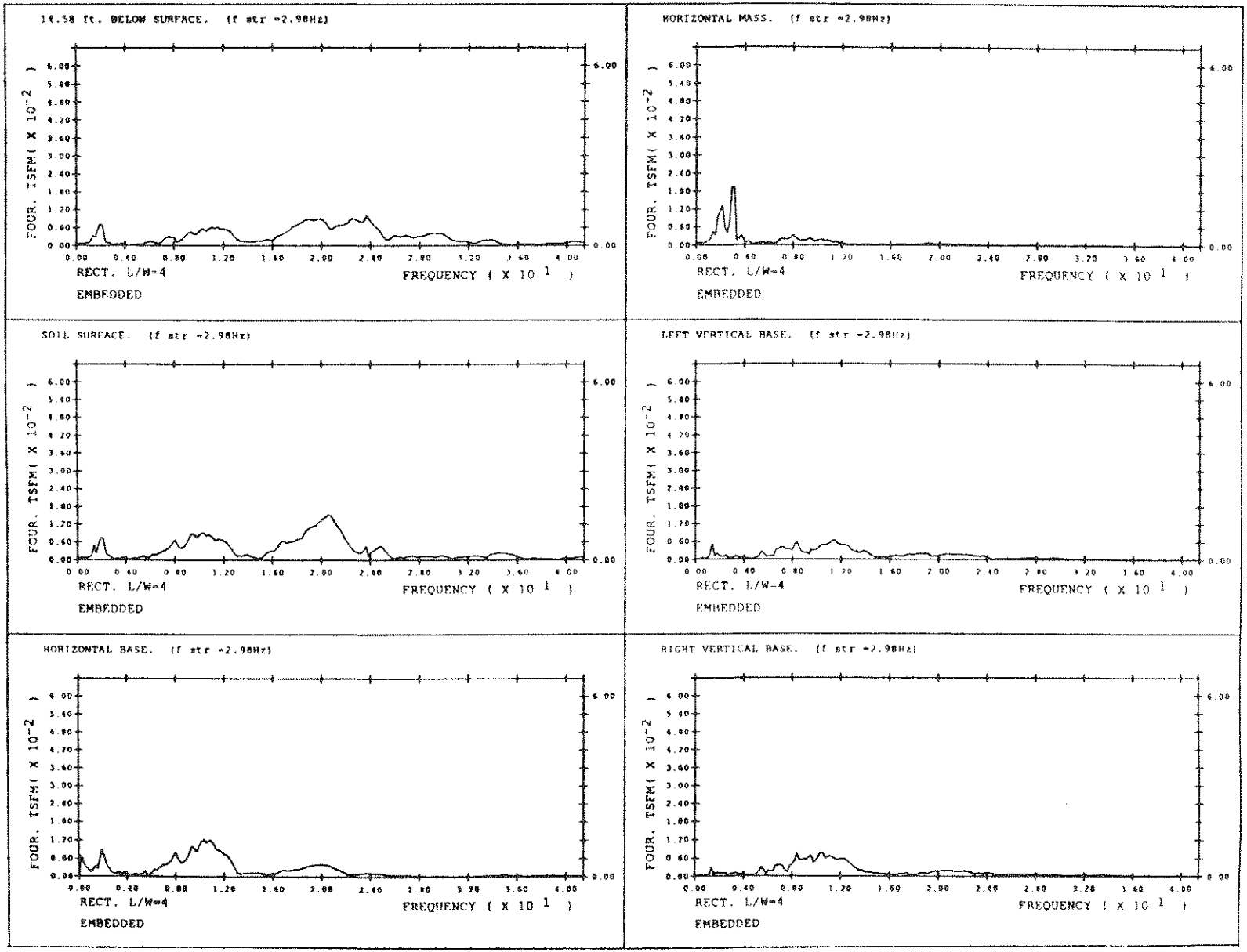

FIGURE 5-21 System with Embedded Rectangular (L/W=4) Footing (f_{str} = 2.98Hz) (cont'd)

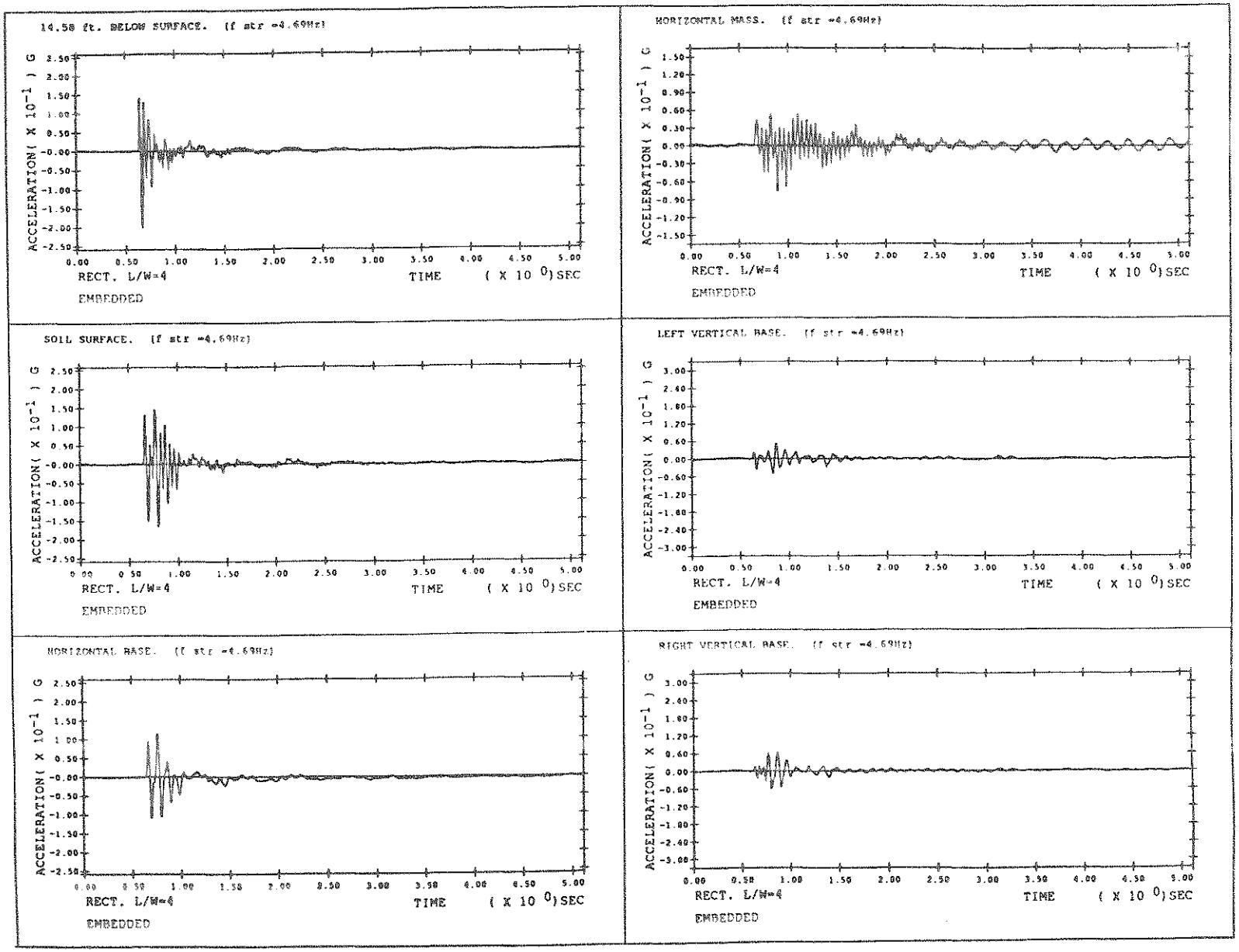

FIGURE 5-22 System with Embedded Rectangular (L/W=4) Footing (f_{str} = 4.69Hz)

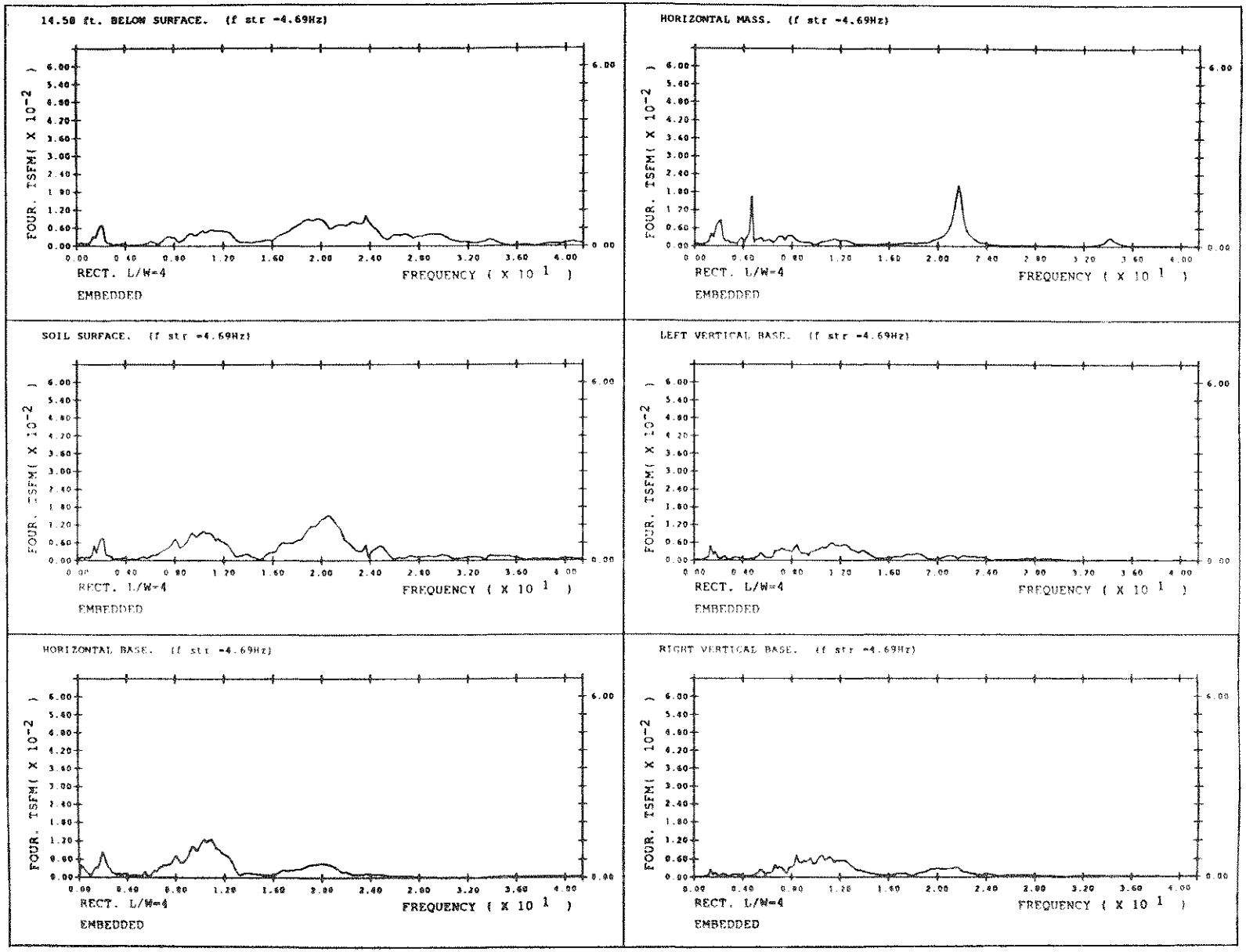

FIGURE 5-22 System with Embedded Rectangular (L/W=4) Footing (f_{str} = 4.69Hz) (cont'd)

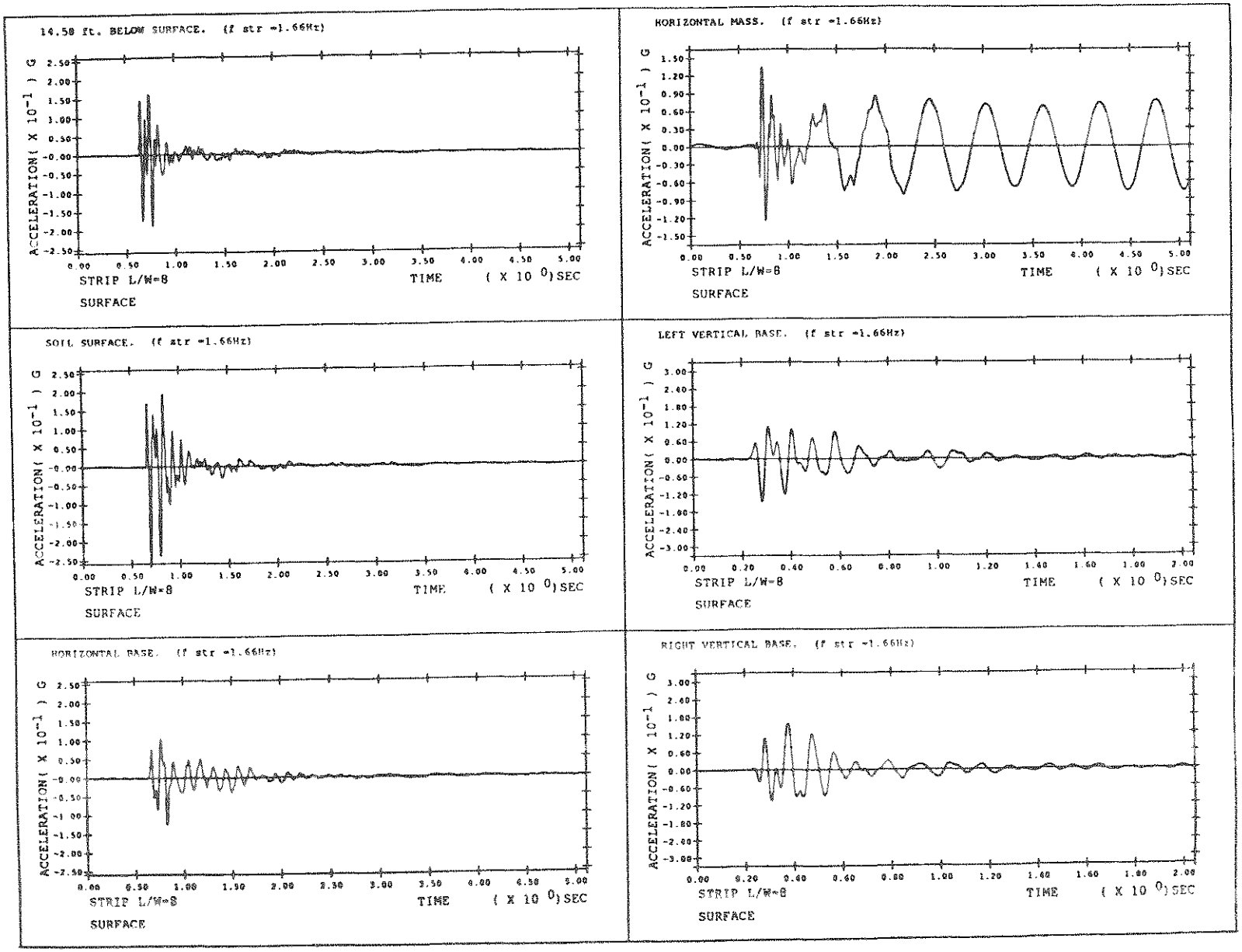

FIGURE 5-23 System with Surface Strip (L/W=8) Footing (f_{str} = 1.66Hz)

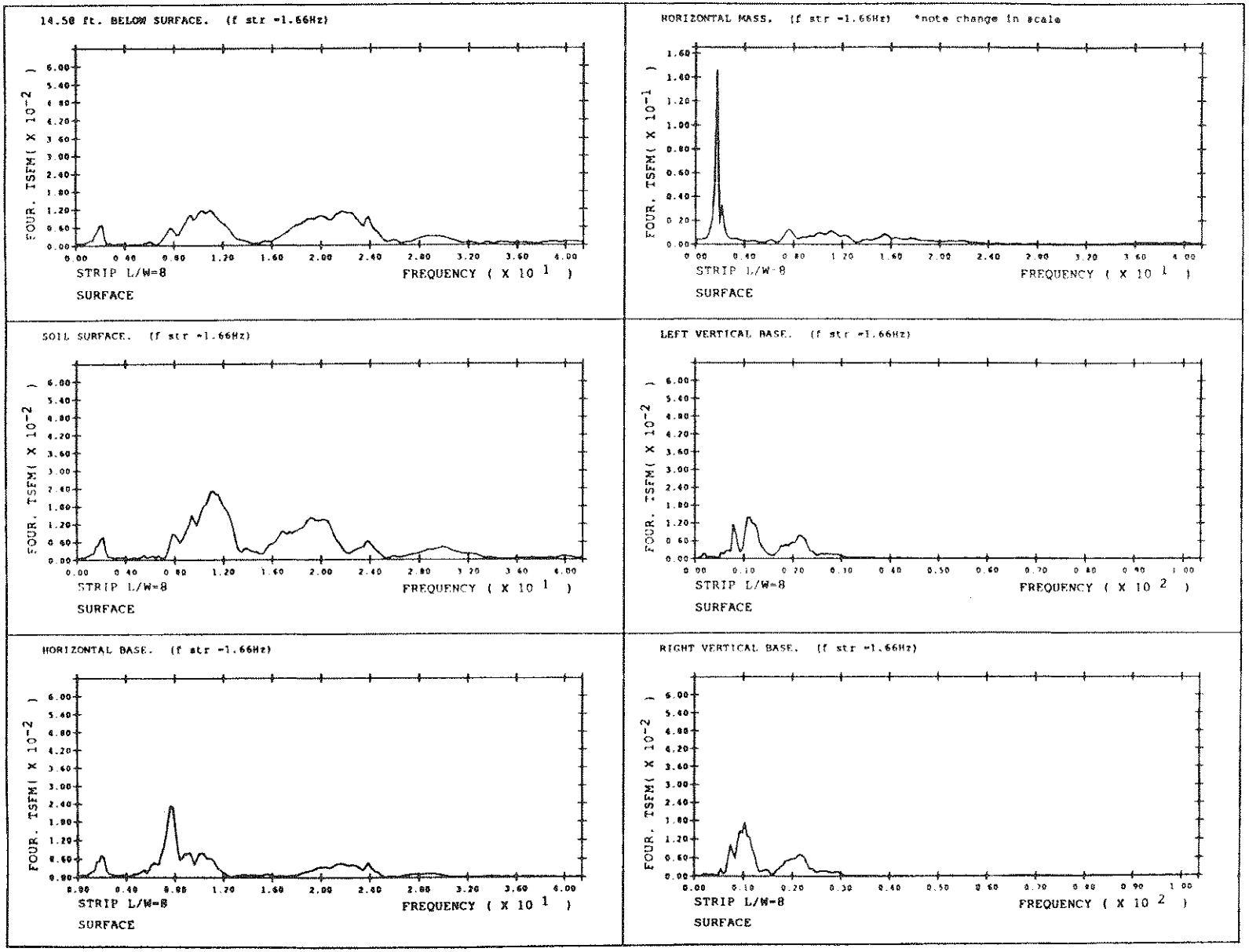

FIGURE 5-23 System with Surface Strip (L/W=8) Footing (f_{str} = 1.66Hz) (cont'd)

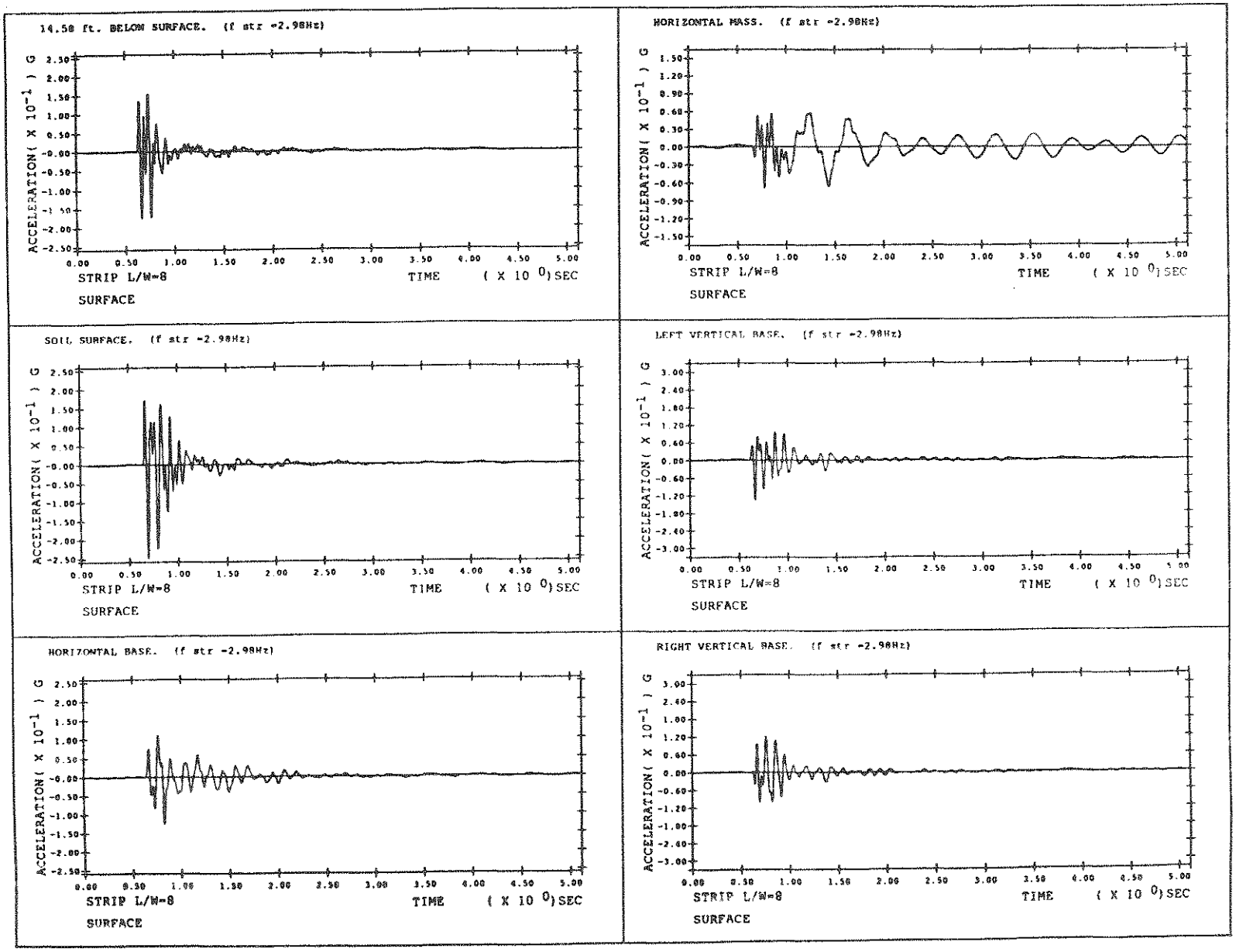

FIGURE 5-24 System with Surface Strip (L/W=8) Footing (f_{str} = 2.98Hz)

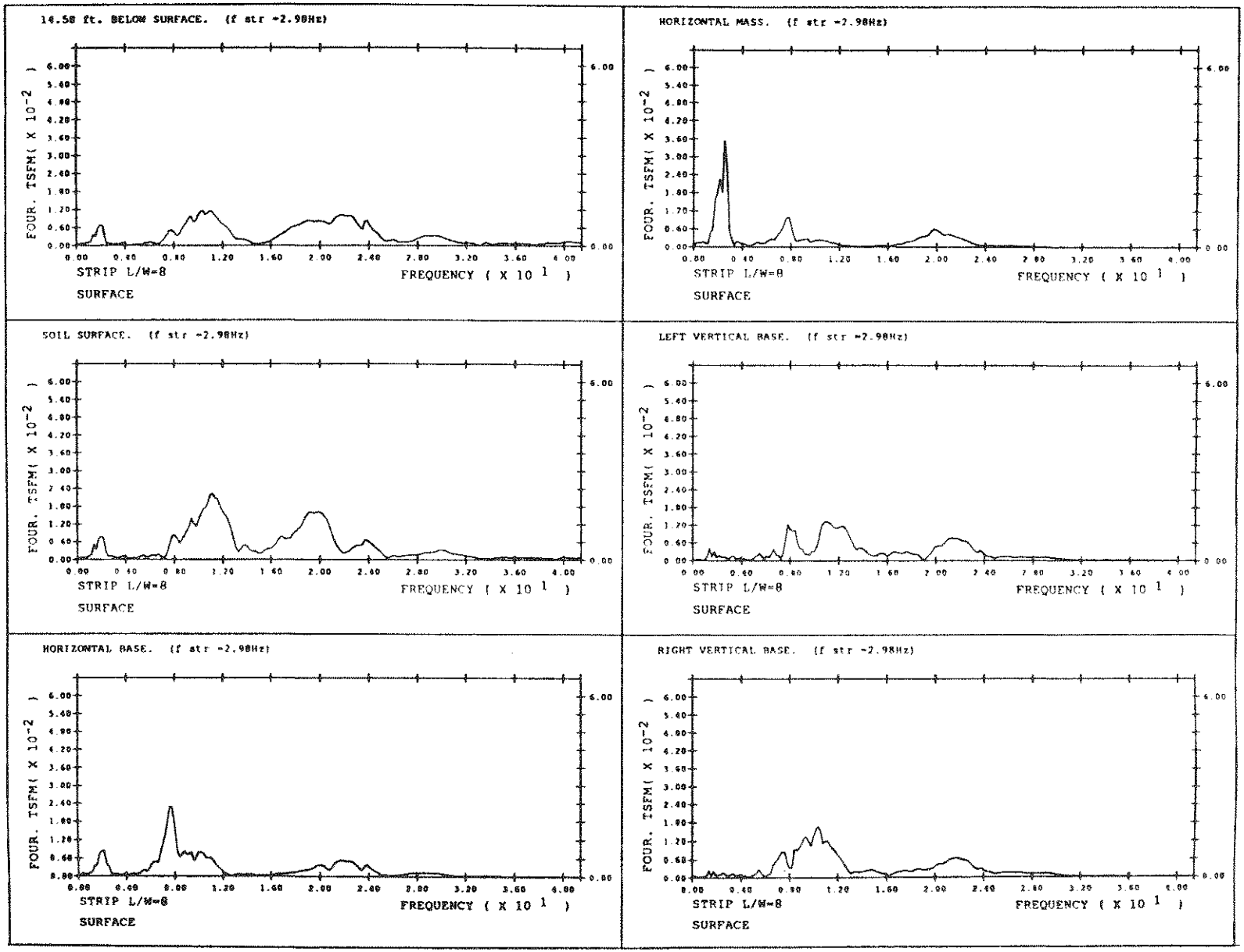

FIGURE 5-24 System with Surface Strip (L/W=8) Footing (f_{str} = 2.98Hz) (cont'd)

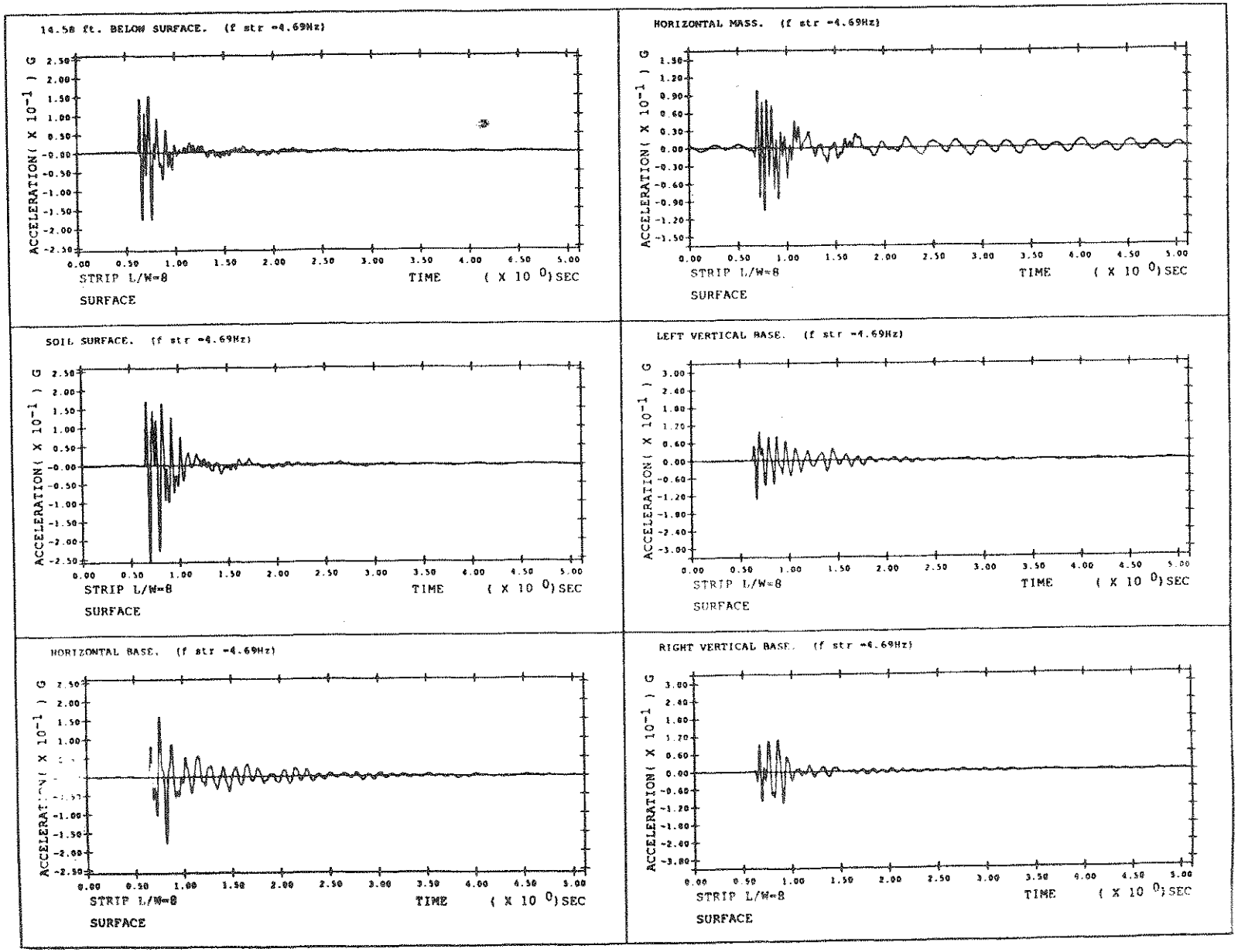

FIGURE 5-25 System with Surface Strip (L/W=8) Footing (f_{str} = 4.69Hz)

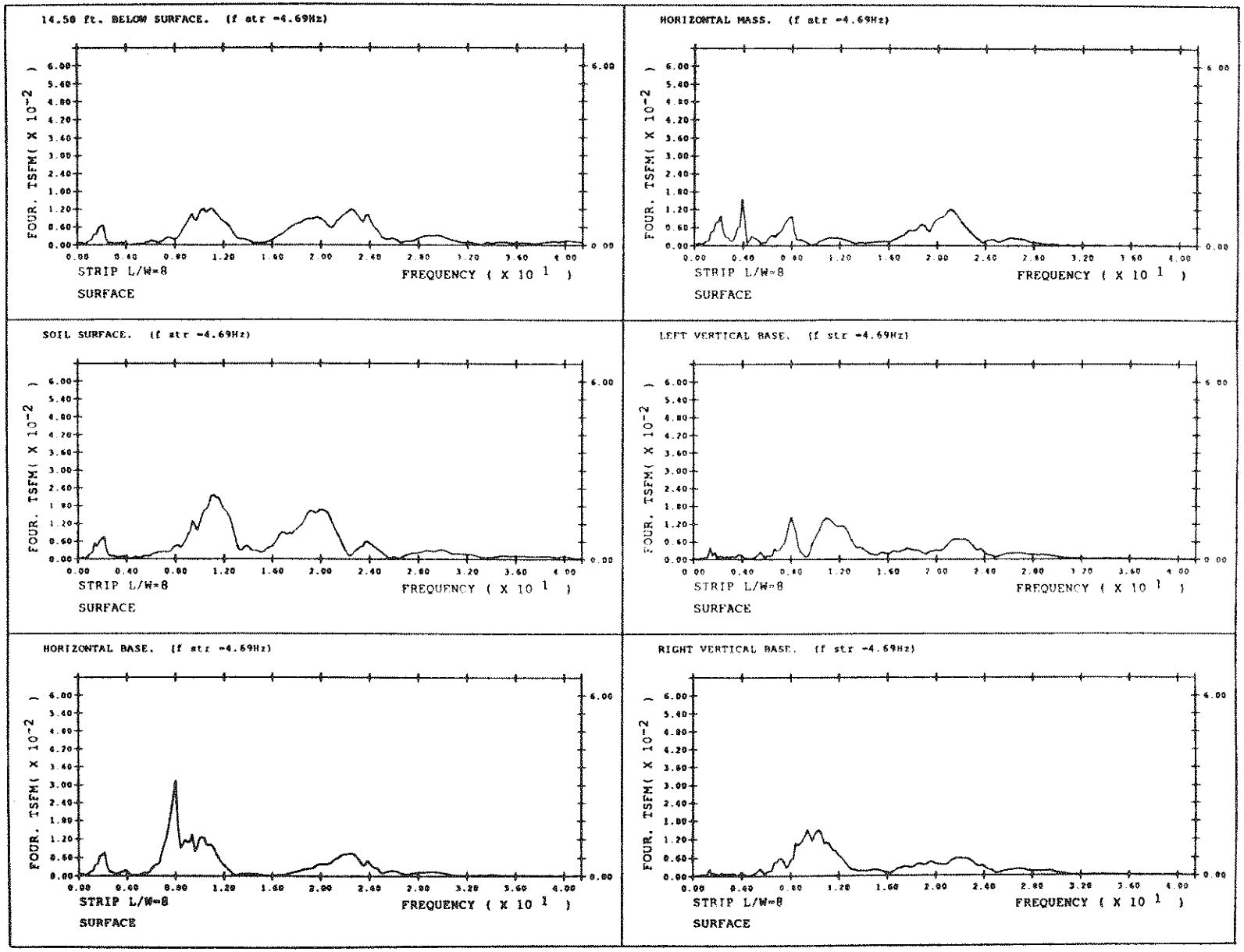

FIGURE 5-25 System with Surface Strip (L/W=8) Footing (f_{str} = 4.69Hz) (cont'd)

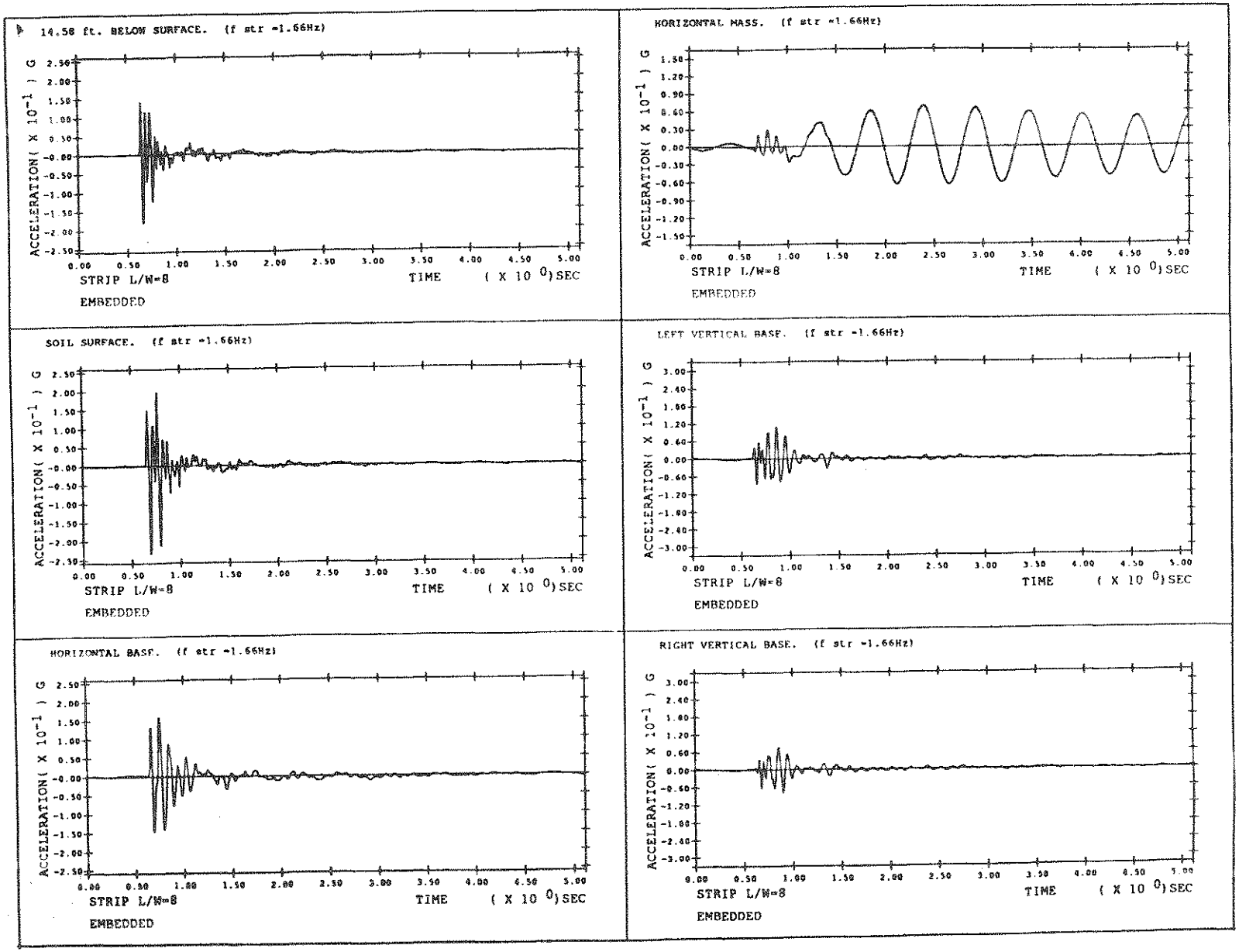

FIGURE 5-26 System with Embedded Strip (L/W=8) Footing (f_{str} = 1.66Hz)

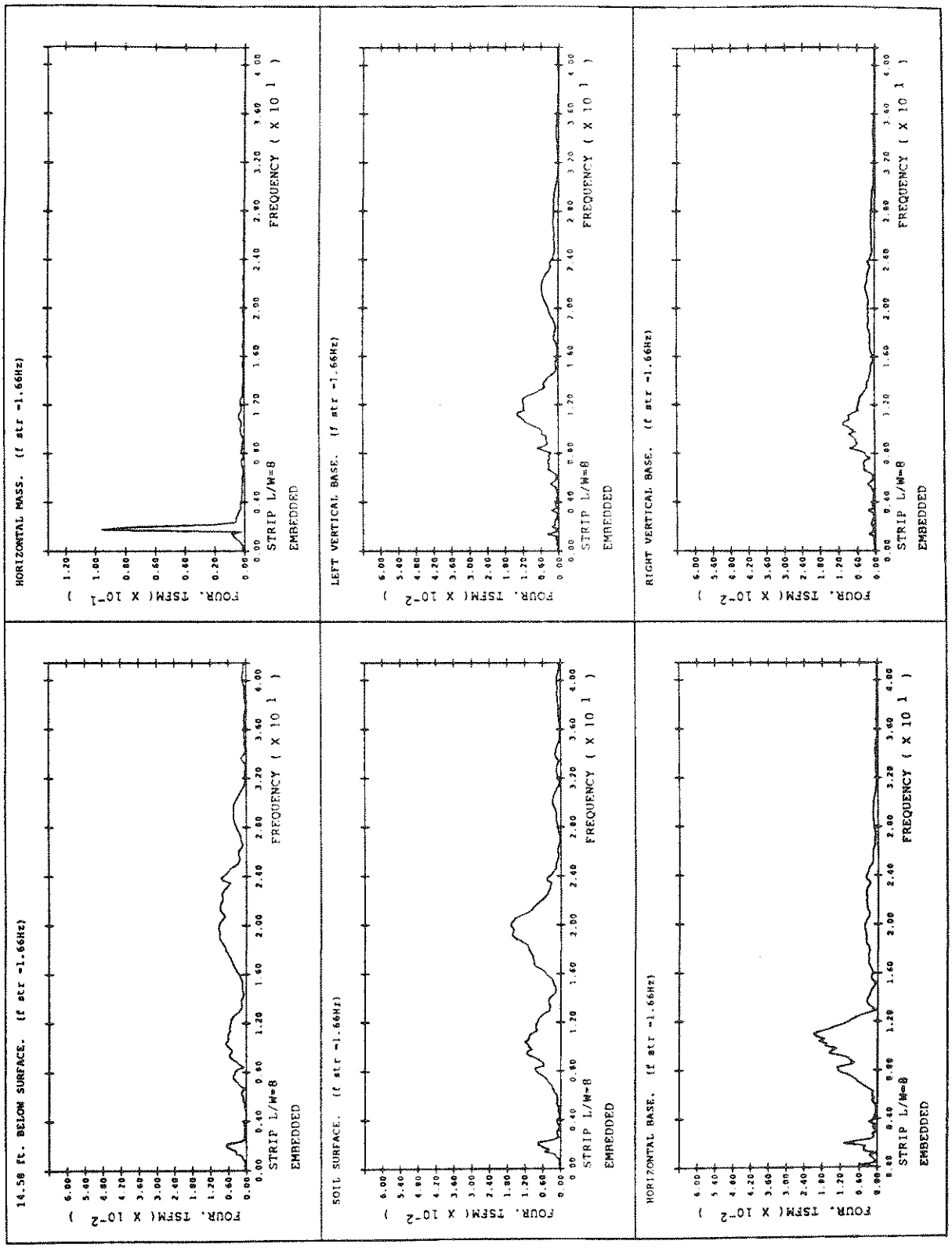

FIGURE 5-26 System with Embedded Strip (L/W=8) Footing (f_{str} = 1.66Hz) (cont'd)

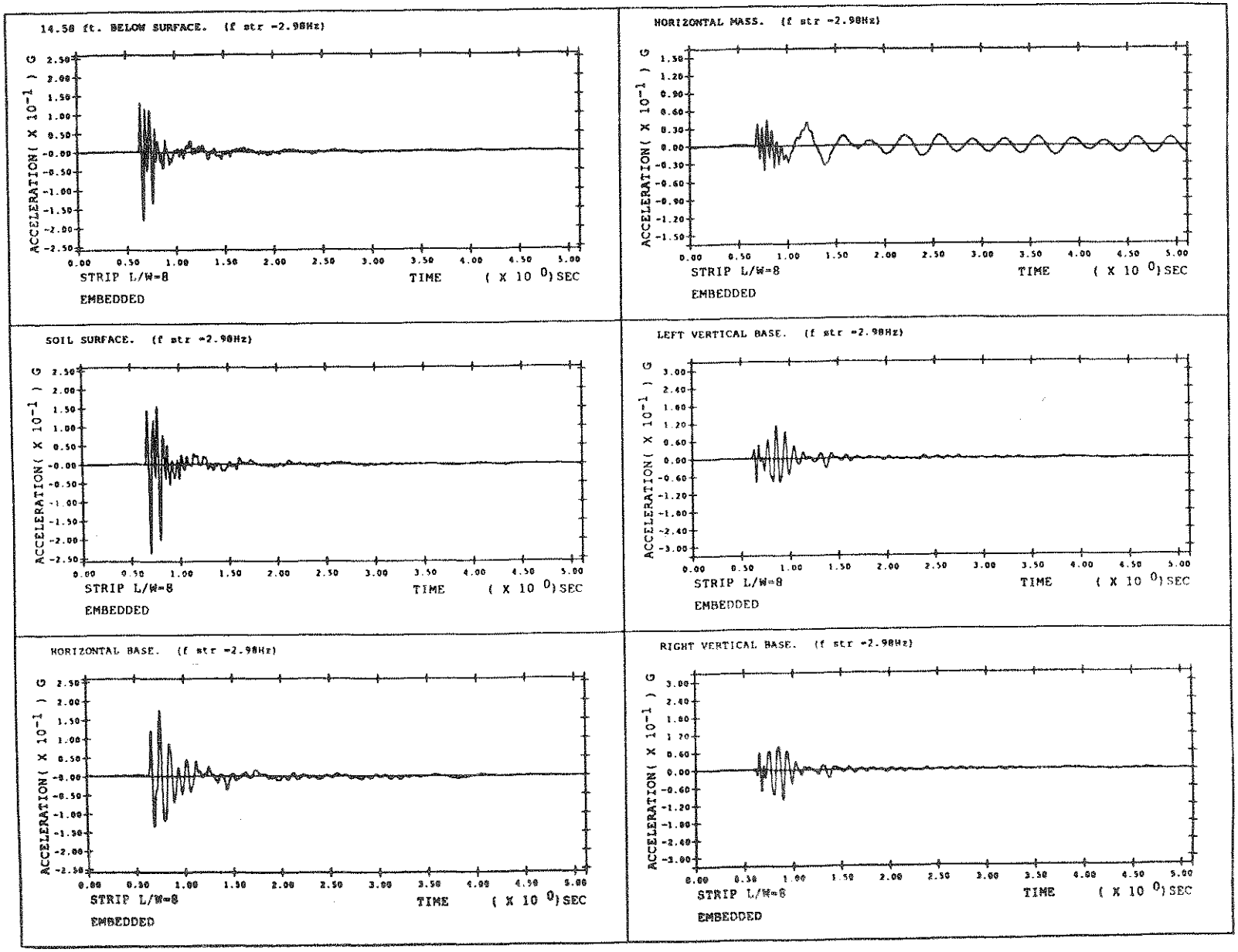

FIGURE 5-27 System with Embedded Strip (L/W=8) Footing (f_{str} = 2.98Hz)

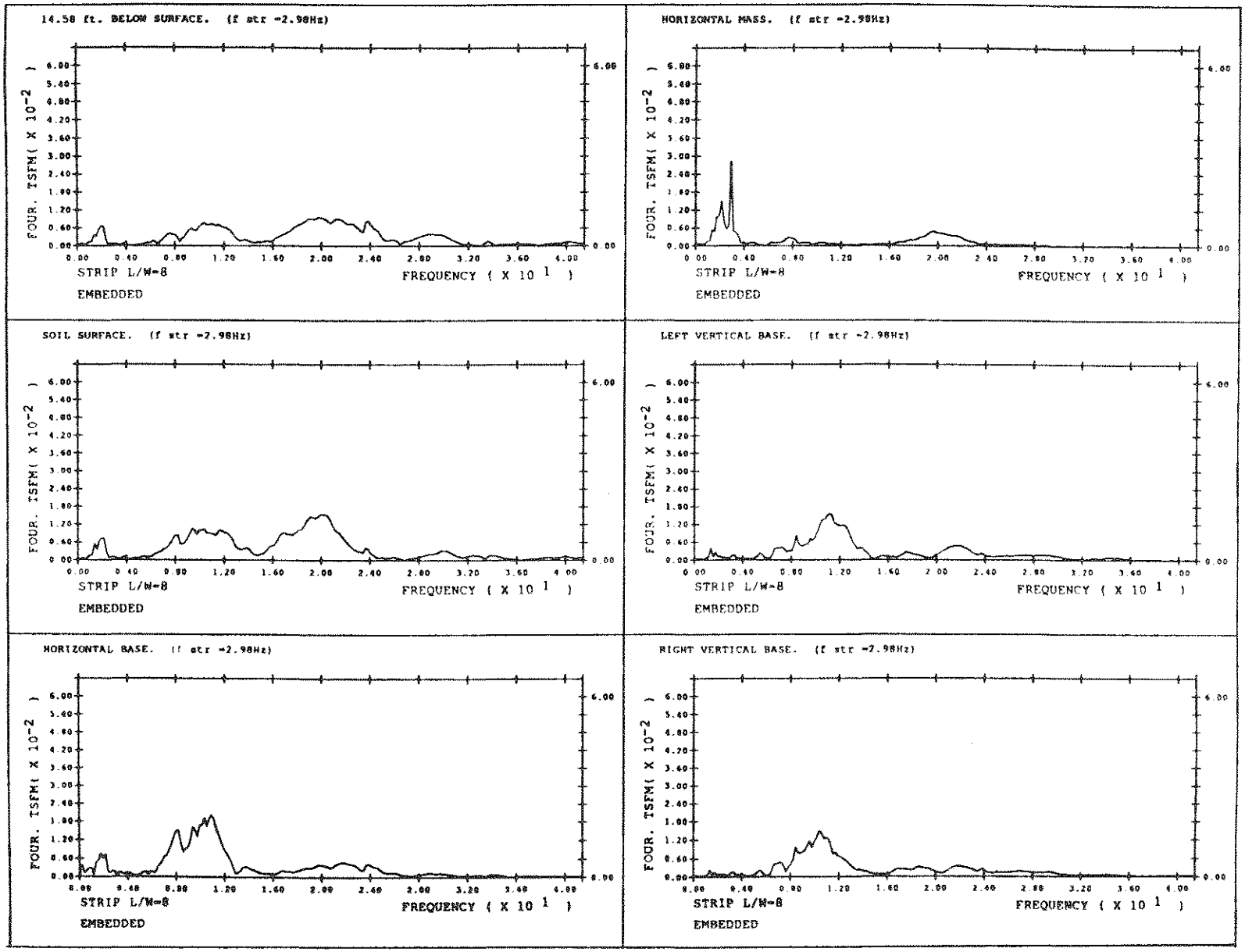

FIGURE 5-27 System with Embedded Strip (L/W=8) Footing (f_{str} = 2.98Hz) (cont'd)

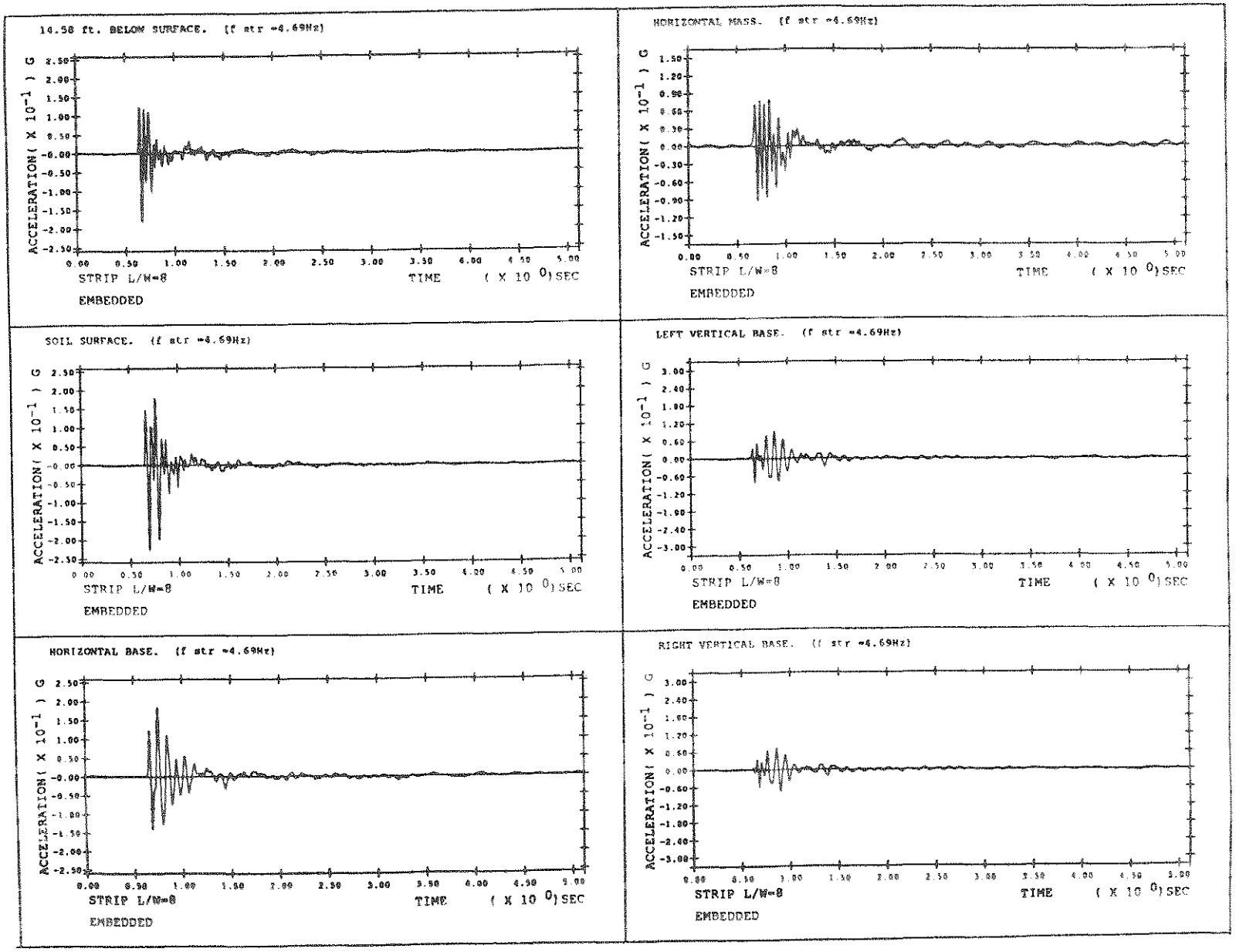

FIGURE 5-28 System with Embedded Strip (L/W=8) Footing (f_{str} = 4.69Hz)

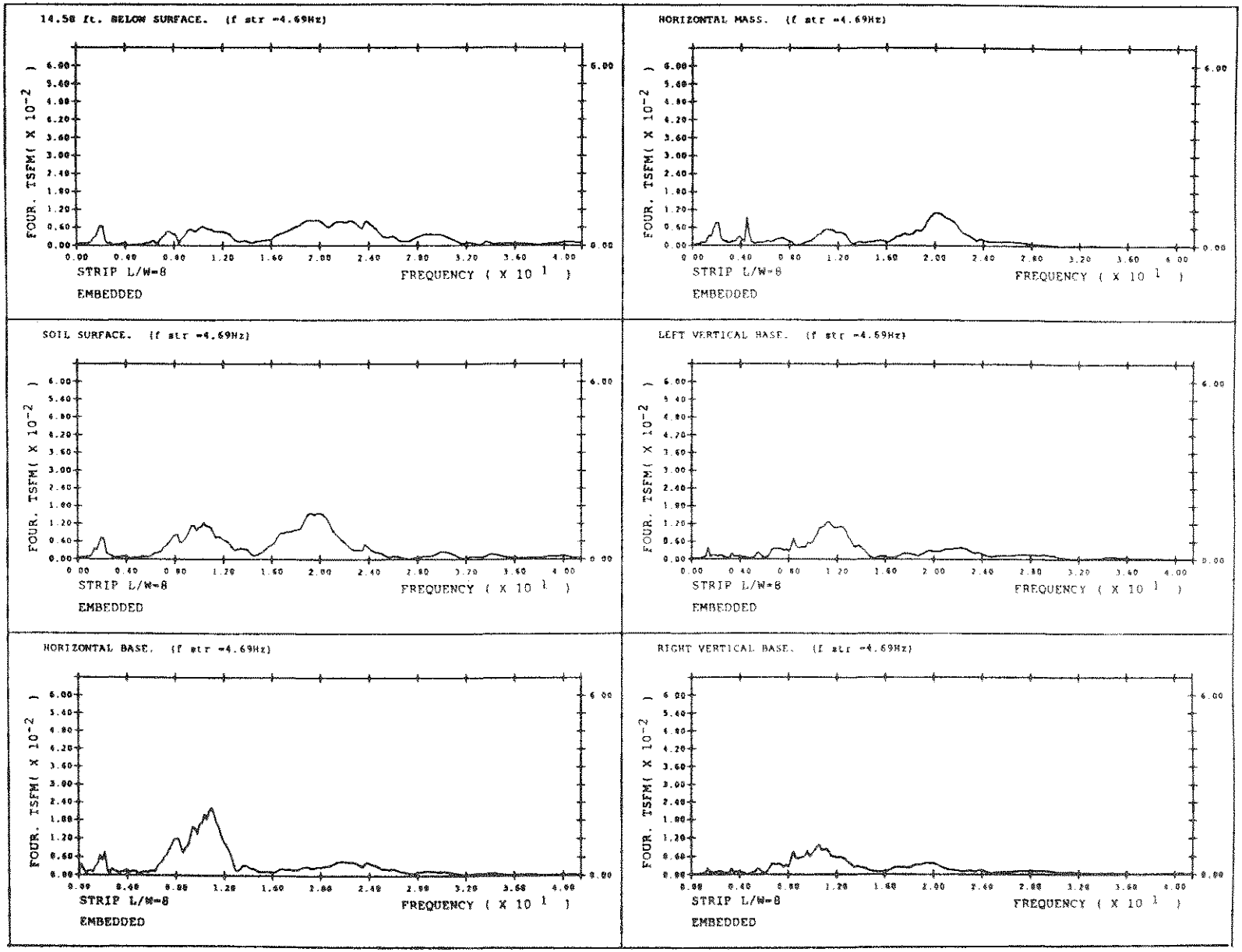

FIGURE 5-28 System with Embedded Strip (L/W=8) Footing (f_{str} = 4.69Hz) (cont'd)

SECTION 6

SUMMARY AND CONCLUSIONS

In this report the results of an extensive series of tests on radiation damping and soil-structure interaction performed in the centrifuge sre organized and presented. Surface and embedded structures with circular, square, rectangular and strip footings sre examined. In each case the natural frequency of the superstructure is varied but the higher order frequency associated with the motion of the base is kept constant. It is found that, regardless of the foundation shape or level of embedment, the amount of radiation damping depends on the natural frequency of the vibrating modes of the structure relative to the fundamental frequency of the soil layer. The amount of radiation damping at the top mass gradually increases as f_{str} is increased above f_{soil}. Radiation damping is always present in the horizontal motion of the base as the frequency associated with this degree of freedom is consistently greater than f_{soil}.

The base and top mass respond essentially independently except for the structure with the embedded circular footing. In this case when f_{str} is less than f_{soil}, the motion of the base exhibited a ringing at the same frequency as the ringing of the superstructure.

In general, embedment of the base does not affect the amount of radiation damping in the superstructure, but does affect its response to the strong motion part of the earthquake. Embedment causes an increase in the damping, stiffness and peak amplitude of the horizontal acceleration of the base, and a decrease in the peak amplitude of the vertical accelerations (and hence rocking) of the base.

Comparisons of stiffness and damping between surface and embedded structures can be made by observing changes in response frequency and response amplitude decay. Unfortunately, such direct comparisons are not valid between the structures of different footing shapes because the mass of the footing and the contact area between the footing and the soil are different for each case. It can be seen that the general

properties of radiation damping sre not affected by the foundation shape but any further conclusions must be based on numerical analysis. The response must in some way be normalized by the footing size before comparisons can be made. Such analysis is part of the future research plans.

The centrifuge experiments described in this report yield a large data pool which demonstrates the influence of f_{str}, the foundation embedment, and the foundation shape on radiation damping and soil-structure interaction for a structure on a layer of soil over bedrock during an earthquake. A good deal of insight is gained from the direct qualitative observations just described. The next step is to use this data pool to verify and improve existing analytical methods for predicting soil-structure interaction effects during earthquakes. This work is currently in progress at Princeton University and will be reported subsequently.

SECTION 7

REFERENCES

1. Weissman, K., Prevost, J.H., *Dynamic Soil-Structure Interaction: Centrifuge Modeling* , Research Report for The National Science Foundation, Princeton University May, 1987.

2. Clough, R.W., Penzien, J., *Dynamics of Structures*, McGraw-Hill, New York, 1975, pp. 47-48.

3. Das, B.M., *Fundamentals of Soil Dynamics*, Elsevier, New York, 1983, pp. 270-275.

4. Coe, Carlos, "On the Feasibility of Performing Dynamic Soil Tests in a Centrifuge," Ph.D. Thesis, Princeton University, Princeton, N.J., 1985.

5. Coe, C.J., Prevost, J.H., Scanlan, R.H., "Dynamic Stress Wave Reflections/Attenuation: Earthquake Simulation in Centrifuge soil models," *Earthquake Engineering and Structural Dynamics*, 1985, Vol. 13, pp 109-128.

NATIONAL CENTER FOR EARTHQUAKE ENGINEERING RESEARCH
LIST OF PUBLISHED TECHNICAL REPORTS

The National Center for Earthquake Engineering Research (NCEER) publishes technical reports on a variety of subjects related to earthquake engineering written by authors funded through NCEER. These reports are available from both NCEER's Publications Department and the National Technical Information Service (NTIS). Requests for reports should be directed to the Publications Department, National Center for Earthquake Engineering Research, State University of New York at Buffalo, Red Jacket Quadrangle, Buffalo, New York 14261. Reports can also be requested through NTIS, 5285 Port Royal Road, Springfield, Virginia 22161. NTIS accession numbers are shown in parenthesis, if available.

NCEER-87-0001 "First-Year Program in Research, Education and Technology Transfer," 3/5/87, (PB88-134275/AS).

NCEER-87-0002 "Experimental Evaluation of Instantaneous Optimal Algorithms for Structural Control," by R.C. Lin, T.T. Soong and A.M. Reinhorn, 4/20/87, (PB88-134341/AS).

NCEER-87-0003 "Experimentation Using the Earthquake Simulation Facilities at University at Buffalo," by A.M. Reinhorn and R.L. Ketter, to be published.

NCEER-87-0004 "The System Characteristics and Performance of a Shaking Table," by J.S. Hwang, K.C. Chang and G.C. Lee, 6/1/87, (PB88-134259/AS).

NCEER-87-0005 "A Finite Element Formulation for Nonlinear Viscoplastic Material Using a Q Model," by O. Gyebi and G. Dasgupta, 11/2/87, (PB88-213764/AS).

NCEER-87-0006 "Symbolic Manipulation Program (SMP) - Algebraic Codes for Two and Three Dimensional Finite Element Formulations," by X. Lee and G. Dasgupta, 11/9/87, (PB88-219522/AS).

NCEER-87-0007 "Instantaneous Optimal Control Laws for Tall Buildings Under Seismic Excitations," by J.N. Yang, A. Akbarpour and P. Ghaemmaghami, 6/10/87, (PB88-134333/AS).

NCEER-87-0008 "IDARC: Inelastic Damage Analysis of Reinforced Concrete-Frame Shear-Wall Structures," by Y.J. Park, A.M. Reinhorn and S.K. Kunnath, 7/20/87, (PB88-134325/AS).

NCEER-87-0009 "Liquefaction Potential for New York State: A Preliminary Report on Sites in Manhattan and Buffalo," by M. Budhu, V. Vijayakumar, R.F. Giese and L. Baumgras, 8/31/87, (PB88-163704/AS).

NCEER-87-0010 "Vertical and Torsional Vibration of Foundations in Inhomogeneous Media," by A.S. Veletsos and K.W. Dotson, 6/1/87, (PB88-134291/AS).

NCEER-87-0011 "Seismic Probabilistic Risk Assessment and Seismic Margins Studies for Nuclear Power Plants," by Howard H.M. Hwang, 6/15/87, (PB88-134267/AS).

NCEER-87-0012 "Parametric Studies of Frequency Response of Secondary Systems Under Ground-Acceleration Excitations," by Y. Yong and Y.K. Lin, 6/10/87, (PB88-134309/AS).

NCEER-87-0013 "Frequency Response of Secondary Systems Under Seismic Excitation," by J.A. HoLung, J. Cai and Y.K. Lin, 7/31/87, (PB88-134317/AS).

NCEER-87-0014 "Modelling Earthquake Ground Motions in Seismically Active Regions Using Parametric Time Series Methods," by G.W. Ellis and A.S. Cakmak, 8/25/87, (PB88-134283/AS).

NCEER-87-0015 "Detection and Assessment of Seismic Structural Damage," by E. DiPasquale and A.S. Cakmak, 8/25/87, (PB88-163712/AS).

NCEER-87-0016 "Pipeline Experiment at Parkfield, California," by J. Isenberg and E. Richardson, 9/15/87, (PB88-163720/AS).

NCEER-87-0017 "Digital Simulation of Seismic Ground Motion," by M. Shinozuka, G. Deodatis and T. Harada, 8/31/87, (PB88-155197/AS).

NCEER-87-0018 "Practical Considerations for Structural Control: System Uncertainty, System Time Delay and Truncation of Small Control Forces," by J. Yang and A. Akbarpour, 8/10/87, (PB88-163738/AS).

NCEER-87-0019 "Modal Analysis of Nonclassically Damped Structural Systems Using Canonical Transformation," by J.N. Yang, S. Sarkani and F.X. Long, 9/27/87, (PB88-187851/AS).

NCEER-87-0020 "A Nonstationary Solution in Random Vibration Theory," by J.R. Red-Horse and P.D. Spanos, 11/3/87, (PB88-163746/AS).

NCEER-87-0021 "Horizontal Impedances for Radially Inhomogeneous Viscoelastic Soil Layers," by A.S. Veletsos and K.W. Dotson, 10/15/87, (PB88-150859/AS).

NCEER-87-0022 "Seismic Damage Assessment of Reinforced Concrete Members," by Y.S. Chung, C. Meyer and M. Shinozuka, 10/9/87, (PB88-150867/AS).

NCEER-87-0023 "Active Structural Control in Civil Engineering," by T.T. Soong, 11/11/87, (PB88-187778/AS).

NCEER-87-0024 "Vertical and Torsional Impedances for Radially Inhomogeneous Viscoelastic Soil Layers," by K.W. Dotson and A.S. Veletsos, 12/87, (PB88-187786/AS).

NCEER-87-0025 "Proceedings from the Symposium on Seismic Hazards, Ground Motions, Soil-Liquefaction and Engineering Practice in Eastern North America, October 20-22, 1987, edited by K.H. Jacob, 12/87, (PB88-188115/AS).

NCEER-87-0026 "Report on the Whittier-Narrows, California, Earthquake of October 1, 1987," by J. Pantelic and A. Reinhorn, 11/87, (PB88-187752/AS).

NCEER-87-0027 "Design of a Modular Program for Transient Nonlinear Analysis of Large 3-D Building Structures," by S. Srivastav and J.F. Abel, 12/30/87, (PB88-187950/AS).

NCEER-87-0028 "Second-Year Program in Research, Education and Technology Transfer," 3/8/88, (PB88-219480/AS).

NCEER-88-0001 "Workshop on Seismic Computer Analysis and Design of Buildings With Interactive Graphics," by J.F. Abel and C.H. Conley, 1/18/88, (PB88-187760/AS).

NCEER-88-0002 "Optimal Control of Nonlinear Flexible Structures," by J.N. Yang, F.X. Long and D. Wong, 1/22/88, (PB88-213772/AS).

NCEER-88-0003 "Substructuring Techniques in the Time Domain for Primary-Secondary Structural Systems," by G. D. Manolis and G. Juhn, 2/10/88, (PB88-213780/AS).

NCEER-88-0004 "Iterative Seismic Analysis of Primary-Secondary Systems," by A. Singhal, L.D. Lutes and P. Spanos, 2/23/88, (PB88-213798/AS).

NCEER-88-0005 "Stochastic Finite Element Expansion for Random Media," by P. D. Spanos and R. Ghanem, 3/14/88, (PB88-213806/AS).

NCEER-88-0006 "Combining Structural Optimization and Structural Control," by F. Y. Cheng and C. P. Pantelides, 1/10/88, (PB88-213814/AS).

NCEER-88-0007 "Seismic Performance Assessment of Code-Designed Structures," by H.H-M. Hwang, J-W. Jaw and H-J. Shau, 3/20/88, (PB88-219423/AS).

NCEER-88-0008 "Reliability Analysis of Code-Designed Structures Under Natural Hazards," by H.H-M. Hwang, H. Ushiba and M. Shinozuka, 2/29/88.

NCEER-88-0009 "Seismic Fragility Analysis of Shear Wall Structures," by J-W Jaw and H.H-M. Hwang, 4/30/88.

NCEER-88-0010 "Base Isolation of a Multi-Story Building Under a Harmonic Ground Motion - A Comparison of Performances of Various Systems," by F-G Fan, G. Ahmadi and I.G. Tadjbakhsh, 5/17/88.

NCEER-88-0011 "Seismic Floor Response Spectra for a Combined System by Green's Functions," by F.M. Lavelle, A. Bergman and P.D. Spanos, 5/1/88.

NCEER-88-0012 "A New Solution Technique for Randomly Excited Hysteretic Structures," by G.Q. Cai and Y.K. Lin, 5/16/88.

NCEER-88-0013 "A Study of Radiation Damping and Soil-Structure Interaction Effects in the Centrifuge," by K. Weissman, supervised by J.H. Prevost, 5/24/88.

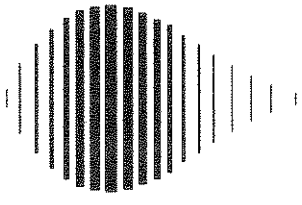

National Center for Earthquake Engineering Research
State University of New York at Buffalo